LINEAR VISCOELASTICITY
OF
ENTANGLEMENT NETWORKS

LINEAR VISCOELASTICITY

OF

ENTANGLEMENT NETWORKS

PROEFSCHRIFT

TER VERKRIJGING VAN DE GRAAD VAN DOCTOR IN DE TECHNISCHE WETENSCHAPPEN AAN DE TECHNISCHE HOGESCHOOL TE DELFT OP GEZAG VAN DE RECTOR MAGNIFICUS IR. H. J. DE WIJS, HOOGLERAAR IN DE AFDELING DER MIJNBOUWKUNDE, VOOR EEN COMMISSIE UIT DE SENAAT TE VERDEDIGEN OP WOENSDAG 15 SEPTEMBER 1965, DES NAMIDDAGS TE 4 UUR.

DOOR

ALFRED JOHAN CHÖMPFF

SCHEIKUNDIG INGENIEUR

GEBOREN TE MALANG (IND.)

DELFTSCHE UITGEVERS MAATSCHAPPIJ N.V. – DELFT – 1965

DIT PROEFSCHRIFT IS GOEDGEKEURD DOOR DE PROMOTOR
PROF. DR. W. PRINS

AAN MIJN OUDERS
AAN MIJN VROUW

Acknowledgement.

The work described in this thesis was made possible by the financial support of the Royal Shell Laboratory, Amsterdam, to whom the author hereby expresses his gratitude.

During the last year of the work described in this thesis Dr. George Lamb, on leave from the Central Research Laboratory, Allied Chemical Corp., has been a most appreciated coworker. Especial thanks are due to him for his help in writing the thesis in English.

E R R A T A

page:	line:	stands:	read:
14	5	Rousse	Rouse
18	Eq.(2-17)	--	p = 1,2,3,.....N
23	2	Eq.(2-19)	Eq.(2-17)
24	4	rootes	roots
24	9	rootes	roots
24	32	floates	floats
26	footnote	whom the author	to whom the author
31	28	choise	choice
9	10	$\partial\sigma/\partial t$	$\partial\gamma/\partial t$

CONTENTS

1 Introduction 3

1-1 General considerations. 3
1-2 Linear viscoelasticity-Phenomenological treatment. 5
1-3 Relaxation spectra. 8

2 Molecular theory. 14

2-1 Theory of Rouse. 14
2-2 Modification of the single chain problem 21
2-3 Modification for crosslinked networks 27
2-4 Modification for temporary or entanglement networks. 31
2-5 Summary of Chapter 2 40

3 Preparation and characterization of the polymers. 43

3-1 Anionic polymerization. 43
3-2 Experimental procedure. 45
3-3 Characterization of PMA polymers. 51

4 The rheometer. 57

4-1 General construction of the rheometer. 57
4-2 Deformation of the sample. 60
4-3 The piezoelectric devices. 63
4-4 Operating limits. 69
4-5 Calibration of the pick-up 72
4-6 Mechanical coupling between the driver and the pick-up. 73
4-7 Additional details. 75
4-8 Electronic components. 77
4-9 Low temperature bath. 78

5 Experiments and results. 80

5-1 Examples of computations of H[m-1]. 80
5-2 Calculations with poly-n-octyl methacrylate (POMA) 81
5-3 Conclusions from the results for POMA 89
5-4 Measurements with poly-methyl acrylate (PMA) 90
5-5 Conclusions from the results for PMA 96

Summary. 98

List of symbols. 101

Appendix. 106

Detailed drawing of the rheometer. 109

CHAPTER 1

INTRODUCTION

1-1 General considerations.

In the literature dealing with the mechanical behavior of polymers and polymer solutions, several theories can be found, which attempt to describe this behavior on a molecular basis[1-5]. In most cases, these theories concentrate on a rather narrow field of interest. Frequently, they yield contradictory conclusions.

The work described in this thesis represents the first step in a series of projects which, when completed, should lead to a comprehensive molecular theory of the mechanical behavior of polymers. This should include not only rubber-elastic properties but also time-dependent or rheological behavior.

Pure rubbery behavior is best approached in gels diluted with inert solvents[6]. Molecular theories of the rheological behavior of polymers have also usually been developed for dilute polymer solutions[7-8], although they are very often also applicable to concentrated solutions. It is reasonable therefore to begin by studying polymer solutions and dilute networks.

Characterization of a network involves determination of the chemical and physical (entanglements) crosslinks. Chemical crosslinks can in principle, be determined by analytical methods[9-10]. Physical crosslinks are generally mechanical couplings caused by chain entanglements, often called temporary crosslinks. The entanglements can be determined from their rheological effect[3].

If a rheometer were designed which could measure first the properties of an entanglement network, then those of the same sample after chemical crosslinking in situ, the effects of the chemical and entanglement crosslinks could be separated. Experiments of this type would thus provide a deeper insight into the topology of polymer networks. The dearth of knowledge

in this field, reflected in several controversies in current polymer network theories, provides the main impetus for research in this area.

Molecular theories are still restricted to linear viscoelastic behavior of linear, randomly coiling polymer chains. Furthermore, the existing molecular theories must still be extended to the long-time regions where entanglements affect the viscoelastic properties[11-13].

Since the polymers are to be in dilute form, the viscoelastic measurements must be made dynamically (e.g. with sinusoidal deformations) at low temperatures. Moreover, the measurements at low temperatures will be useful only if interference from secondary (or β-) transition regions is avoided. Thus molecules with side chains, which are considerably restricted in their rotation around the side chain axis for steric reasons , should not be used[14]. The polymer should also crosslink readily and be easily soluble in common solvents. A polymer which fits all these requirements is poly-methyl acrylate (PMA).

The phenomena which accompany the presence of entanglements are always associated with a region of very long relaxation times. In this region the total contour length of the molecule has a dominant influence. For this reason, existing molecular theories always describe the mechanical behavior of polymer molecules with a uniform chain length. Unfortunately absolutely monodisperse polymer cannot be prepared. The molecular weight distribution, however, can approach monodispersity quite closely if appropriate polymerization techniques are used[15]. An attempt was made therefore to prepare the polymer by the anionic, or "living polymer" polymerization technique of Szwarc[16]. Under favorable conditions this yields a Poisson distribution of molecular weights.

The fulfillment of each of the above requirements represents a sizeable project in itself. Not all of these have been completed in the work to be described in this thesis. Most importantly, the work has been restricted to a study of entanglement networks.

In Chapter 2, a molecular theory is presented which permits a quantitative description of the relaxation spectrum of entanglement networks. This theory is based on an extension of the molecular model of Rouse[7].

A similar line of research has been followed independently by Duiser and Staverman[17] and several conclusions reached in Chapter 2 of this thesis are based on their results.

Chapter 3 describes the preparation and characterization of the anionically polymerized polymer. At the same time a radically polymerized polymer of about the same molecular weight was also characterized.

A completely new rheometer, designed to measure dynamically the viscoelastic properties of polymer solutions and gels is described in Chapter 4. The design incorporates recently developed piezoelectric titanate ceramics, which permit a rather compact construction.

The results of the theory are compared with experiments in Chapter 5, which consists of two parts. In the first part, the theoretical relaxation spectrum is checked against the detailed measurements on a poly-n-octyl methacrylate fraction published by Ferry and co-workers. The second part gives the results of measurements on a solution of PMA in toluene performed with the rheometer described in Chapter 4.

1-2 Linear viscoelasticity - Phenomenological treatment.

In the following treatment only shear deformations are considered, as shown in Figure 1-1.

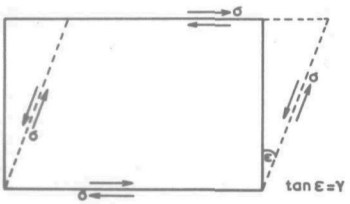

Fig. 1-1. Simple shear deformation.

If stress σ and strain γ are time dependent, the time-dependent shear modulus $G(t)$ is given the general definition

$$\sigma(t) = G(t) \cdot \gamma(t) \qquad (1\text{-}1)$$

In a stress relaxation experiment, a sudden constant strain γ_0 is applied so that

$$\gamma(0) = 0 \quad \text{and} \quad \gamma(t) = \gamma_0$$

Then

$$\sigma(t) = G(t) \cdot \gamma_0 \qquad (1\text{-}2)$$

where $G(t)$ is a continuously decreasing function

$$G(t) = G_g \left[1 - \Phi(t) \right] \qquad (1\text{-}3)$$

Here G_g is the glassy modulus, defined by $G(0) = G_g$ and the "relaxation function" $\Phi(t)$ is approximately described by an exponential function

$$\Phi(t) = \beta \left[1 - \exp(-\alpha t) \right] \tag{1-4}$$

where α and β are constants and β approaches 1. Clearly, $\Phi(0) = 0$ and $\Phi(\infty) = \beta$.

If γ changes continuously with time, as in a dynamic experiment, Equation (1-1) is generalized by Boltzmann's superposition principle which states that the total stress due to a number of strains applied at different times is equal to the linear summation of all the stresses related to those strains at their respective elapsed times. In mathematical form:

$$\sigma(t) = \Delta\gamma_0 \, G(t) + \Delta\gamma_1 \, G(t-t_1) + \Delta\gamma_2 \, G(t-t_2) + \ldots\ldots \tag{1-5}$$

or

$$\sigma(t) = \sum_{s_i=0}^{s_i=t} G(t-s_i) \, \Delta\gamma_i(s_i) \tag{1-6}$$

For a continuously varying strain Equation (1-6) becomes

$$\sigma(t) = \int_{-\infty}^{t} G(t-s) \, \frac{\partial \gamma(s)}{\partial s} \, ds \tag{1-7}$$

and substitution of Equation (1-3) in Equation (1-7) yields

$$\sigma(t) = G_g \left[\gamma(t) - \int_{-\infty}^{t} \Phi(t-s) \, \frac{\partial \gamma(s)}{\partial s} \, ds \right] \tag{1-8}$$

which on integration by parts gives

$$\sigma(t) = G_g \left[\gamma(t) - \int_{-\infty}^{t} \gamma(s) \, \varphi(t-s) ds \right] \tag{1-9}$$

where $\varphi(t) = \partial\Phi(t)/\partial t$

Putting s' for (t-s)

$$\sigma(t) = G_g \left[\gamma(t) - \int_{0}^{\infty} \gamma(t-s') \, \varphi(s') ds' \right] \tag{1-10}$$

where the primes will be omitted in the following sections.

If the strain is sinusoidal

$$\gamma^* = \gamma_0 \exp(i\omega t) \tag{1-11}$$

then

$$\sigma^* = G_g \gamma^* - G_g \int_0^\infty \gamma_o \exp\left[i\omega(t-s)\right] \varphi(s)ds$$

$$= G_g \gamma^* \left[1 - \int_0^\infty \exp(-i\omega s)\, \varphi(s)ds \right] \qquad (1\text{-}12)$$

Equation (1-12) may be written

$$\sigma^* = G_g \gamma^* \left[1 - \int_0^\infty \varphi(t) \cos \omega t.dt + i \int_0^\infty \varphi(t) \sin \omega t.dt \right]$$

$$= G_g \gamma_o \left[\cos\omega t + i \sin \omega t \right] x$$

$$\left[1 - \int_0^\infty \varphi(t).\cos\omega t.dt + i \int_0^\infty \varphi(t).\sin\omega t.dt \right] \qquad (1\text{-}13)$$

Writing out the real parts of Equations (1-11) and (1-13)

$$\text{Re } \gamma^* = \gamma(\omega t) = \gamma_o \cos\omega t$$

$$\text{Re } \sigma^* = \sigma(\omega t) = G_g \gamma_o \left[\cos\omega t \left\{ 1 - \int_0^\infty \varphi(t).\cos\omega t.dt \right\} - \sin\omega t \left\{ \int_0^\infty \varphi(t).\sin\omega t.dt \right\} \right] \qquad (1\text{-}14)$$

The integrals in Equation (1-14) are functions of ω only, so that Equation (1-14) gives the two components of $\sigma(\omega t)$, one in phase, the other $\pi/2$ out of phase with $\gamma(\omega t)$. Since $\sin\omega t = \cos(\omega t - \pi/2)$, the last term in Equation (1-14) is the component which leads $\gamma(\omega t)$ by $\pi/2$.

This result can be written in a shorter notation

$$\gamma(\omega t) = \gamma_o \cos\omega t$$

$$\sigma(\omega t) = \sigma_o \cos(\omega t + \delta)$$

$$= \sigma_o (\cos\omega t \cos\delta - \sin\omega t \sin\delta)$$

$$= \gamma_o \left[G'(\omega)\cos\omega t - G''(\omega) \sin\omega t \right] \qquad (1\text{-}15)$$

which defines $G'(\omega) = (\sigma_o/\gamma_o).\cos\delta$

$G''(\omega) = (\sigma_o/\gamma_o).\sin\delta$

$\tan\delta = G''(\omega)/G'(\omega)$

The "loss-tangent", $\tan\delta$, is a measure for the ratio of the dissipated and stored energy per cycle. G' and G" are the real and imaginary components of the complex modulus G*, as shown in Figure 1-2

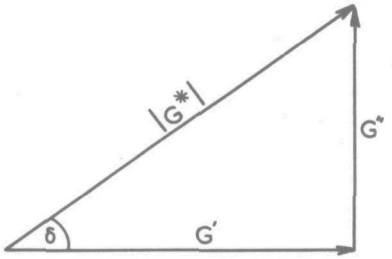

Fig.1-2.

From Equation (1-13) or (1-14), G'(ω) and G"(ω) are derived thus:

$$G^*(i\omega) = \frac{\sigma^*}{\gamma^*} = G_g\left[1 - \int_0^\infty \varphi(t).\cos\omega t.dt\right] + i\, G_g \int_0^\infty \varphi(t).\sin\omega t.dt$$

$$= G'(\omega) + i\, G''(\omega) \qquad (1\text{-}16)$$

whence

$$G'(\omega) = G_g + \int_0^\infty \left[\partial G(t)/\partial t\right].\cos\omega t.dt \qquad (1\text{-}17)$$

$$G''(\omega) = -\int_0^\infty [\partial G(t)/\partial t].\sin\omega t.dt \qquad (1\text{-}18)$$

Equations (1-17) and (1-18) are the relations between the dynamic moduli and the transient modulus.

1-3 Relaxation Spectra.

Usually, the value of β in Equation (1-4) is between 0.999 and 1. For an uncrosslinked polymer, $\beta = 1$, which means that the polymer shows flow properties. Then Equation (1-3) reduces to

$$G(t) = G_g \exp(-\alpha t) \qquad (1\text{-}19)$$

Substituting this in Equations (1-17) and (1-18) yields

$$G'(\omega) = G_g - \alpha G_g \int_0^\infty \exp(-\alpha t).\cos\omega t.dt \qquad (1\text{-}20)$$

$$= G_g\left[1 - \alpha \mathcal{L}\{\cos\omega t\}\right] = G_g.\frac{\omega^2/\alpha^2}{1 + \omega^2/\alpha^2}$$

where $\mathcal{L}\{f(x)\}$ is the Laplace transform of f(x)

$$G''(\omega) = G_g\,\alpha\int_0^\infty \exp(-\alpha t).\sin\omega t.dt$$

$$= G_g\,\alpha\omega\mathcal{L}\left\{\frac{\sin\omega t}{\omega}\right\} = G_g.\frac{\omega/\alpha}{1+\omega^2/\alpha^2} \qquad (1\text{-}21)$$

Equations (1-19), (1-20) and (1-21) are identical with equations derived for a Maxwell element (a spring and a dashpot in series), where $1/\alpha = \tau$, the relaxation time of the element. This becomes clear from the differential equation for the deformation of a Maxwell element with a spring constant G_i and a dashpot viscosity η_i.

For stress relaxation conditions

$$\frac{1}{G_i}.\frac{\partial\sigma}{\partial t} + \frac{\sigma}{\eta_i} = \frac{\partial\sigma}{\partial t} = 0$$

This gives $G(t) = G_i \exp(-t/\tau_i)$ (1-22)

where $\tau_i = \eta_i/G_i$

For dynamic loading conditions, substitution of

$$\gamma^* = \gamma_o \exp(i\omega t) \quad \text{and} \quad \sigma^* = \sigma_o^* \exp(i\omega t)$$

in

$$\dot\gamma = (\dot\sigma/G_i) + (\sigma/\eta_i)$$

yields

$$G^* = \frac{\sigma^*}{\gamma^*} = G_i.\frac{i\omega\tau_i}{1+i\omega\tau_i} = G_i\left[\frac{\omega^2\tau_i^2}{1+\omega^2\tau_i^2} + \frac{i\omega\tau_i}{1+\omega^2\tau_i^2}\right] \qquad (1\text{-}23)$$

It is rather unreasonable to expect a real polymer to behave as a system with only one relaxation time, because of the many possible modes of motion which a polymer chain can undergo. In fact, it is found that the experimental curves are not matched exactly by these equations.

To obtain a better mathematical description of the experimental curve a series solution is required. The most convenient series to choose is

$$G(t) = \sum_{i=1}^{N} G_i \exp(-t/\tau_i) \qquad (1\text{-}24)$$

$$G'(\omega) = \sum_{i=1}^{N} G_i \omega^2\tau_i^2/(1 + \omega^2\tau_i^2) \qquad (1\text{-}25)$$

$$G''(\omega) = \sum_{i=1}^{N} G_i\omega\tau_i/(1 + \omega^2\tau_i^2) \qquad (1\text{-}26)$$

which can also be represented by a series of Maxwell elements in parallel, as shown in Figure 1-3, where the summation is also carried out from i = 1 to i = N.

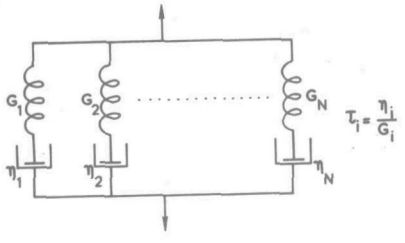

Fig. 1-3. Generalised Maxwell model

A two-dimensional representation of the 2N constants G_i and τ_i takes the form of a discrete line spectrum (the relaxation spectrum). The height of each line is equal to G_i and the position on the abscissa is given by τ_i. With a high density of lines, Equation (1-24) approaches the form of a Laplace transform. If instead of a summation an integration is written, the relaxation spectrum can then be calculated by inverting the Laplace transform, provided the modulus G(t) is first expressed as a continuous analytical function.

Experimental results are in fact obtained in the form of a continuous function and it is therefore necessary to re-write the above equations for an infinite number of terms. If Equation (1-24) is replaced by

$$G(t) = G_e + \int_0^{\infty} F(\tau) \exp(-t/\tau).d\tau \qquad (1\text{-}27)$$

where G_e represents the spring constant of an element with infinite relaxation time (if present), this procedure then assigns an infinite array of relaxation times to the polymer network. Then, by definition

$$\sum_{\tau}^{\tau+\Delta\tau} G_i = F(\tau).\Delta\tau \qquad (1\text{-}28)$$

In the case where the interval is chosen sufficiently small or where all the lines have equal height, Equation (1-28) can be written

$$F(\tau) = G_i di/d\tau \qquad (1\text{-}29)$$

Then $F(\tau)$ is equal to G_i multiplied by the number of lines in a unit interval of $\Delta\tau = 1$. Equation (1-29) is of special importance in Chapter 2 because molecular theories yield discrete spectra.

$F(\tau)$ is the linear relaxation spectrum, which, for practical reasons, is converted to a logarithmic relaxation spectrum, defined by $H(\tau) = F(\tau).\tau$ or $F(\tau).d\tau = H(\tau)d\ \ln\tau$ Then, Equations (1-24), (1-25) and (1-26) are converted to

$$G(t) = G_e + \int_{-\infty}^{\infty} H(\tau)\ \exp(-t/\tau)d\ \ln\tau \qquad (1\text{-}30)$$

$$G'(\omega) = G_e + \int_{-\infty}^{\infty} H(\tau)\ \omega^2\tau^2/(1 + \omega^2\tau^2).d\ \ln\tau \qquad (1\text{-}31)$$

$$G''(\omega) = \int_{-\infty}^{\infty} H(\tau)\ \omega\tau\ /(1 + \omega^2\tau^2).d\ \ln\tau \qquad (1\text{-}32)$$

The glassy modulus G_g can be obtained from Equation (1-31) by letting ω approach infinity.

$$G_g = G_e + \int_{-\infty}^{\infty} H(\tau)d\ \ln\tau \qquad (1\text{-}33)$$

The definition of the complex viscosity η^* is similar to that of the complex modulus in Equation (1-16)

$$\eta^*(i\omega) = \sigma^*/\dot{\gamma}^*$$

By putting

$$\gamma^* = \gamma_o \exp(i\omega t) \quad \text{so that} \quad \dot{\gamma}^* = i\omega\gamma^*$$

clearly

$$\eta^*(i\omega) = G^*(i\omega)/i\omega = (G''/\omega) - (i\ G'/\omega) = \eta'(\omega) - i\,\eta''(\omega) \qquad (1\text{-}34)$$

From Equation (1-32) the real part of the complex viscosity is obtainable as

$$G''(\omega)/\omega = \eta'(\omega) = \int_{-\infty}^{\infty} H(\tau).\tau/(1 + \omega^2\tau^2).\, d\ln\tau \qquad (1\text{-}35)$$

The steady-flow viscosity follows readily by letting ω approach zero.

$$\eta_e = \int_0^{\infty} H(\tau).d\tau \qquad (1\text{-}36a)$$

for a continuous spectrum , or

$$\eta_e = \sum_{i=1}^{N} G_i\tau_i \qquad (1\text{-}36b)$$

in the case of a discrete spectrum .

If all the lines in the discrete relaxation spectrum have equal heights of dimension N/m^2, then $H(\tau)$ is equal to this height multiplied by the number of lines per unit interval $\Delta \ln\tau = 1$.

Usually, H is plotted, not against $\ln\tau$ but against $\log\tau$. Then $Fd\tau = H.d\ln\tau = 2.303.H.d\log\tau$. (1-37)

Thus, if the abscissa is chosen to be $\log\tau$, the ordinate must be not H, but 2.303 H, in order to let 2.303 H be equal to the product of the height and the number of lines in a unit interval $\Delta\log\tau = 1$.

References (Chapter 1)

1) A.J. Staverman; in Encyclopedia of Physics, Vol. XIII, ed. S. Flügge, Springer-Verlag, Berlin (1962) p. 432-451.
2) L.R.G. Treloar; in Die Physik der Hochpolymeren, Vol. IV, ed. H.A. Stuart, Springer-Verlag, Berlin (1956) p. 295-372.
3) J.D. Ferry; Viscoelastic Properties of Polymers, John Wiley & Sons Inc., New York (1961) p. 151 ff.
4) N.W. Tschoegl; J.Chem.Phys. 39, 149 (1963), and 40, 473 (1964).
5) A.V. Tobolsky & J.J. Aklonis; J.Phys.Chem. 68, 1970 (1964).
6) B. Mukherji & W. Prins; J.Polymer Sci., Part A, 2,4367 (1964). W. Prins; in Physics of Non-Crystalline Solids, ed. J.A.Prins, North Holland Publ.Comp., Amsterdam (1965) p. 360-375.
7) P.E. Rouse, Jr.; J.Chem.Phys. 21, 1272 (1953).
8) B.H. Zimm; J.Chem.Phys. 24, 269 (1956).
9) B. Mukherji; Ph.D. thesis, Syracuse, N.Y. (1963).
10) A.M. Rijke; Ph.D. thesis Leiden, The Netherlands (1961).
11) R.S. Marvin; in Viscoelasticity-Phenomenological Aspects, ed. J.T. Bergen, Academic Press, New York (1960) p. 27-54.
12) F. Bueche; J.Chem.Phys. 25, 599 (1956).
13) J.D. Ferry; R.F. Landel & M.L. Williams; J.Applied Phys. 26, 359 (1955).
14) J. Heyboer; in Physics of Non-Crystalline Solids, ed.J.A.Prins, North Holland Publ.Comp., Amsterdam (1965) p.231-254.
15) P.J. Flory; Principles of Polymer Chemistry, Cornell University Press (1953) p. 336 ff.
16) M. Szwarc, M. Levy & R. Milkovich; J.Am.Chem.Soc. 78, 2656 (1956).
17) J.A. Duiser & A.J. Staverman; in Physics of Non-Crystalline Solids, ed. J.A. Prins, North Holland Publ.Comp., Amsterdam (1965) p.376-387.

CHAPTER 2

MOLECULAR THEORY

In this chapter a theory is developed for the viscoelastic behavior of entangled linear polymer molecules. The theory is a modification of the theory of Rousse[1]. The molecular model on which Rouse's theory is based does not always give as close an agreement with experiment[2-3] as models proposed later[4-8], but is easier to modify for the effect of temporary crosslinks due to chain entanglements and for the effect of permanent chemical crosslinks. The reason is that a very important part of the mechanical behavior in Rouse's theory is incorporated in a "mobility coefficient matrix" which accounts for the mobility at several points in the chain. It is possible to modify Rouse's theory by suitably changing this matrix.

2-1 Theory of Rouse.

As in Zimm's theory[4] the derivation considers only a single molecule. Originally, the Rouse treatment was intended for the explanation of the dynamic viscoelastic behavior of dilute polymer solutions. The results, however, are also applicable to transient loading problems and experiments also show that the results are a good approximation for more concentrated solutions, provided the molecular weight is low so that no entanglements occur. A monodisperse polymer is essential for the treatment.

A free-draining molecule of randomly coiling, freely jointed segments is considered, as postulated by Debye[9]. The solution containing the molecule is assumed to be sheared by harmonic motion in the x-direction of a z = constant plane. The angular frequency of the motion is ω. One end of the molecule is chosen as the origin of this coordinate system. The velocity gradient $\dot{\gamma}$ is assumed to be undisturbed by the presence of the molecule, even at the center of the coil.

The molecule is thought of as being composed of N equal submolecules of a length, which is rather arbitrary, but is so chosen that the end-to-end distance of a submolecule follows a Gaussian probability distribution function. It is generally accepted that in flexible organic polymer chains the minimum length of the backbone chain of a submolecule is about 50 chain atoms, or more. The purely viscous resistance of the medium is imagined to be concentrated at the junctions of the submolecules, while the submolecules themselves are supposed to act like ideal elastic entropy springs.

A submolecule with a length which fulfils the above conditions has a R.M.S. end-to-end distance given by $\langle r_s^2 \rangle^{\frac{1}{2}} = a\sqrt{q}$, where q is the number of monomer units in the submolecule and a is the length of a freely jointed segment. The spring constant for a submolecule is then given by rubber elasticity theory as $3kT/qa^2$ or $2kT\beta^2$. Clearly, the R.M.S. end-to-end distance of the whole molecule is $\langle r_o^2 \rangle^{\frac{1}{2}} = a\sqrt{Z}$, where the degree of polymerization $Z = Nq$.

Each submolecule has its own Cartesian coordinate system $x_j y_j z_j$ parallel to the original system x, y, z. The configuration of the entire molecule is then described by 3N coordinates. At equilibrium the probability of finding the chain in the 3N dimensional volume-element $d\phi_i$ at x_i, y_i, z_i $\ldots\ldots z_N$ is

$$\Psi_i d\phi_i = \left(\beta^2/\pi\right)^{3N/2} \exp\left[-\beta^2 \sum_{j=1}^{N} (x_j^2+y_j^2+z_j^2)\right] dx_1 \ldots\ldots dz_N \qquad (2\text{-}1)$$

where $\beta^2 = 3/\left(2\langle r_s^2 \rangle\right)$. Perturbation of this distribution by a velocity gradient $\dot{\gamma}$, acting on ν molecules in volume V, changes the number of molecules in $d\phi_i$. At equilibrium, the number n_i of molecules in $d\phi_i$ is $n_i = \nu \Psi_i d\phi_i$. In the perturbed state, this number is s_i.

Assuming that Wall's[10] relation

$$\Delta F = - kT \sum_i s_i \ln(n_i/s_i) \qquad (2\text{-}2)$$

is valid at non-equilibrium conditions and that the number s_i can be expressed in a convergent series

$$s_i = n_i(1 + \dot{\gamma} f + \dot{\gamma}^2 g + \dot{\gamma}^3 h + ...)$$

the chemical potential $\mu_i = \partial \Delta F / \partial s_i = \mu$ is found to be

$$\mu = kT\left[1 + \ln(1 + \dot{\gamma} f)\right] \qquad (2\text{-}3)$$

where the higher powers in the series have been omitted, because the perturbation is assumed to be small.

It should be noted that the concept of a chemical potential is applied here to a non-equilibrium situation. This is only valid at small deviation from equilibrium[1]. This restriction makes the Rouse treatment applicable only to linear viscoelasticity, where strains are infinitesimally small.

Motion of the end of the jth submolecule (jth junction) is dependent on two quantities: the influence of the velocity gradient on the position of the junctions and the configurational diffusion of the junctions towards their equilibrium positions. Thus the velocity of the jth junction

$$(\dot{x}_j)_{tot} = (\dot{x}_j)_{\dot{\gamma}} + (\dot{x}_j)_D \qquad (2\text{-}4)$$

where

$$(\dot{x}_j)_{\dot{\gamma}} = \dot{\gamma} z_j \qquad (2\text{-}5)$$

and $(\dot{x}_j)_D$ is the back diffusion term during deformation.

By analogy with Fick's first law for regular particle diffusion, or more generally, from irreversible thermodynamics, the driving force for the configurational diffusion is $\partial \mu / \partial x_j$.

The configurational diffusion of the molecule, whose configuration lies in $d\emptyset_i$, along the x_j coordinate, can occur by displacement in the x direction of the (j-1)th or the jth junction, represented by

$$(\dot{x}_j)_{j-1} = -B\left[\frac{\partial \mu}{\partial x_j} - \frac{\partial \mu}{\partial x_{j-1}}\right] \qquad (2\text{-}6)$$

and

$$(\dot{x}_j)_j = - B \left[\frac{\partial \mu}{\partial x_j} - \frac{\partial \mu}{\partial x_{j+1}} \right] \quad \text{respectively} \tag{2-7}$$

The mobility B is inversely proportional to the length chosen for the submolecule. All junctions except the (j-1)th in Equation (2-6) and the jth in Equation (2-7) are assumed to remain fixed.

The sum of these velocities is equal to the last term in Equation (2-4)

$$(\dot{x}_j)_D = - B \left[- \frac{\partial \mu}{\partial x_{j-1}} + 2 \frac{\partial \mu}{\partial x_j} - \frac{\partial \mu}{\partial x_{j+1}} \right] \tag{2-8}$$

The equation of motion of the polymer molecule in the various x directions in 3N space is then

$$\underline{\dot{x}} = \dot{\gamma} \, \underline{z} - B \, \underline{A}_{33} \, \underline{\nabla}_x \mu \tag{2-9}$$

where $\underline{\dot{x}} = \{ \dot{x}_1, \dot{x}_2, \dot{x}_3 \ldots\ldots \dot{x}_N \}$ (2-10)

$\underline{z} = \{ z_1, z_2, z_3 \ldots\ldots z_N \}$ (2-11)

$\underline{\nabla}_x = \{ \frac{\partial}{\partial x_1}, \frac{\partial}{\partial x_2}, \frac{\partial}{\partial x_3} \ldots\ldots \frac{\partial}{\partial x_N} \}$ (2-12)

(2-10), (2-11) and (2-12) are column vectors and $\underline{A}_{33}$ is the square N^{th} order matrix

$$\underline{A}_{33} = \begin{bmatrix} 3 & -1 & & & & & \\ -1 & 2 & -1 & & & & \\ & -1 & 2 & -1 & & & \\ & & \ddots & \ddots & \ddots & & \\ & & & -1 & 2 & -1 & \\ & & & & -1 & 2 & -1 \\ & & & & & -1 & 3 \end{bmatrix} \tag{2-13}$$

Similarly for the y and z directions:

$$\dot{\underline{y}} = - B \underline{A}_{33} \underline{\nabla}_y \mu \tag{2-14}$$

$$\dot{\underline{z}} = - B \underline{A}_{33} \underline{\nabla}_z \mu \tag{2-15}$$

As pointed out by Duiser and Staverman[11], the mobility of the submolecules at the ends of the chains must be taken as at least twice the average mobility of the submolecules in the middle. This accounts for the three's at the corners of the matrix, rather than two's as in the original Rouse treatment.

Each $(\dot{x}_j)_D$ depends on three differentials of μ with respect to x_{j-1}, x_j and x_{j+1}. In order to solve the problem, a transformation must be carried out to new coordinates u_p v_p and w_p, such that $(\dot{u}_p)_D$ is a function of $(\partial \mu / \partial u_p)$ alone. This is done by an orthogonal transformation of the matrix $\underline{A}_{33}$ into a matrix $\underline{\Lambda}$ by the operation

$$R^{-1} \underline{A}_{33} \underline{R} = \underline{\Lambda} = [\lambda_p \delta_{pq}] \tag{2-16}$$

and the new coordinates are related to the original coordinates by

$$\begin{aligned} \underline{u} &= \underline{R}^{-1} \underline{x} \\ \underline{v} &= \underline{R}^{-1} \underline{y} \\ \underline{w} &= \underline{R}^{-1} \underline{z} \end{aligned} \tag{2-16a}$$

The orthogonal matrix $\underline{R}$ need not be determined, λ_p are the eigenvalues of $\underline{A}_{33}$ and δ_{pq} is the Kronecker delta. The solution of the eigenvalues, which will be discussed later, is

$$\lambda_p = 4 \sin^2(p\pi / 2N) \tag{2-17}$$

Equations (2-9), (2-14) and (2-15) then are transformed into

$$\dot{\underline{u}} = \dot{\gamma} \underline{w} - B \underline{\Lambda} \{ \underline{\nabla}_u \mu \} \tag{2-18}$$

$$\dot{\underline{v}} = - B \underline{\Lambda} \{ \underline{\nabla}_v \mu \} \tag{2-19}$$

$$\dot{\underline{w}} = - B \underline{\Lambda} \{ \underline{\nabla}_w \mu \} \tag{2-20}$$

At equilibrium, the density of points in configuration space is

$$\rho_o = n_i / d\emptyset_i = \nu \Psi \tag{2-21}$$

In the disturbed state, at time t, it is

$$\rho = s_i / d\emptyset_i = \nu \Psi (1 + \dot{\gamma} f) \tag{2-22}$$

By solving the equation of continuity

$$\dot{\rho} = i\omega \dot{\gamma} \nu \Psi f = - \sum_{p=1}^{N} \frac{\partial(\rho \dot{u}_p)}{\partial u_p} + \frac{\partial(\rho \dot{v}_p)}{\partial v_p} + \frac{\partial(\rho \dot{w}_p)}{\partial w_p} \tag{2-23}$$

the function f is found by Rouse to be

$$f = \frac{3}{\langle r_s^2 \rangle} \sum_{p=1}^{N} u_p w_p \tau_p / (1 + i\omega\tau_p) \tag{2-24a}$$

where $$\tau_p = \langle r_s^2 \rangle / (6BkT \lambda_p) \tag{2-24b}$$

Equation (2-24) is only a particular, time independent solution of the set of Equations (2-23) and τ_p are the relaxation times of the polymer coil.

This permits calculation of the average rate of input of free energy per molecule (P_1) whose representative points lie in $d\emptyset_i$: which is the scalar product of the velocity of the liquid ($\underline{V}_L$) and of the gradient of the thermodynamic potential ($\underline{\nabla} \mu$), both in the transformed 3N coordinates.

$$P_1 = \underline{V}_L \cdot \underline{\nabla}\mu$$

$\underline{V}_L$ has 3N components: $\dot{\underline{u}}_L$, $\dot{\underline{v}}_L$ and $\dot{\underline{w}}_L$ of which $\dot{\underline{v}}_L$ and $\dot{\underline{w}}_L$ are zero, while $\dot{\underline{u}}_L = \dot{\gamma} \underline{w}$ or $\dot{u}_p = \dot{\gamma} w_p = \dot{\gamma}_o w_p \cos \omega t$.

$\underline{\nabla}\mu$ also has three components of which only the $\underline{u}$-component $\underline{\nabla}_u \mu$ is effective. Then P_1 is found to be

$$P_1 = \dot{\gamma}_o^2 \, kT \sum_{p=1}^{N} \frac{w_p^2(\cos^2\omega t + \omega\tau_p \sin\omega t.\cos\omega t)}{2BkT\,\lambda_p(1 + \omega^2\tau_p^2)} \qquad (2\text{-}25a)$$

The number of molecules whose points lie in $d\phi_i$ is $n\Psi(1 + \dot{\gamma} f)d\phi_i$. To obtain the average rate of input of free energy per unit volume, this number is multiplied by P_1 and the product integrated over the whole configuration space. The result is

$$P = \dot{\gamma}_o^2 \, n\,kT \sum_{p=1}^{N} \frac{\tau_p\cos^2\omega t + \omega\tau_p^2 \sin\omega t.\cos\omega t}{(1 + \omega^2\tau_p^2)} \qquad (2\text{-}25b)$$

The value of P can also be calculated from phenomenological considerations. If the strain $\gamma = \gamma_o \sin\omega t$, then

$$\dot{\gamma} = \omega\gamma_o \cos\omega t = \dot{\gamma}_o \cos\omega t$$

and the stress σ can be written in terms of the complex viscosity as

$$\sigma = \dot{\gamma}_o(\eta' \cos\omega t + \eta'' \sin\omega t)$$

Then $$P = \dot{\gamma}\sigma = \dot{\gamma}_o^2(\eta' \cos^2\omega t + \eta'' \sin\omega t \cos\omega t) \qquad (2\text{-}25c)$$

Comparing terms in Equations (2-25c) and (2-25b) yields the components of the complex viscosity η' and η'', which are easily transformed into the components of the complex modulus

$$G' = n\,kT \sum_{p=1}^{N} \omega^2\tau_p^2/(1 + \omega^2\tau_p^2) \qquad (2\text{-}26)$$

$$G'' = \omega\eta_s + nkT \sum_{p=1}^{N} \omega\tau_p/(1 + \omega^2\tau_p^2) \qquad (2\text{-}27)$$

where n is the number of molecules per unit volume ($n = \frac{N}{V}$).

This expression is similar to that derived from a parallel series of Maxwell elements where the elastic constants are all equal to nkT and the relaxation times are those given in Equation (2-24b).

For relaxation times where $p < N/5$, the sine in Equation (2-17) can be replaced by its argument, so that τ_p becomes

$$\tau_p = Z \left\langle r_o^2 \right\rangle \zeta_o / (6\pi^2 p^2 kT) \qquad (2\text{-}28)$$

where ζ_o is the monomeric friction coefficient, defined by

$$Z \zeta_o = N/B$$

The relaxation spectrum representing this viscoelastic behavior is a discrete line spectrum, where all the lines have a height nkT. The first relaxation time (p = 1) is the longest.

A further approximation can be made for relaxation times shorter than the first three[12] (i.e. for p > 3). In this region, as shown in Chapter 1, the relaxation spectrum is

$$H\, d(\ln \tau) = F d\tau = G_i (\partial i/\partial \tau) d\tau$$

and will now yield

$$H\, d(\ln \tau) = - nkT. (\partial p/\partial \tau) d\tau \qquad (2\text{-}29)$$

where the negative sign arises because p runs from right to left. Inserting Equation (2-28), in (2-29) gives

$$H = (\tfrac{1}{2} \left\langle r_o^2 \right\rangle^{\frac{1}{2}} n/\pi)(Z \zeta_o kT/6)^{\frac{1}{2}} \tau^{-\frac{1}{2}} \qquad (2\text{-}30)$$

It should be noted that H represents the density of lines, times nkT, along the relaxation time axis. The moduli G' and G" follow from Equation (2-30)

$$G' = \int_{-\infty}^{\infty} H\omega^2\tau^2/(1+\omega^2\tau^2) d \ln \tau = (\tfrac{1}{4} \left\langle r_o^2 \right\rangle^{\frac{1}{2}} n)(Z \zeta_o kT/3)^{\frac{1}{2}} \omega^{\frac{1}{2}} \qquad (2\text{-}31)$$

and G" is found to be equal to the R.H.S. of Equation (2-31). Because of the approximations involved, these values of G' and G" apply only to the region where $3 < p < N/5$.

2-2 Modification of the single chain problem.

As a first step in the derivation of a more extensive theory a single chain is again considered, but with the ends having a fixed position in space. These fixed ends can be seen as hypothetical crosslinks. For real crosslinks this model is not valid, but it provides a useful start. In the following section,

motion of the crosslinks is taken into account.

The matrix for such a chain with zero mobility at its ends and containing N submolecules, is

$$\underline{A}_{11} = \begin{bmatrix} 1 & -1 & & & & & \\ -1 & 2 & -1 & & & & \\ & -1 & 2 & -1 & & & \\ & & \ddots & \ddots & \ddots & & \\ & & & -1 & 2 & -1 & \\ & & & & -1 & 2 & -1 \\ & & & & & -1 & 1 \end{bmatrix} \qquad (2\text{-}32)$$

The eigenvalues of this matrix and of the matrix $\underline{A}_{33}$ of the free chain in Equation (2-13) can be calculated by substituting* $2 - \lambda = z + \frac{1}{z}$ in the characteristic equation:

$$| \underline{A}_{1i} - \lambda \underline{I} | = 0 \qquad (2\text{-}33)$$

where z is a complex quantity and $\underline{I}$ is a unit matrix.

In this substitution, it must be noted that, since $2 - \lambda$ is always real, the imaginary parts of z and 1/z must cancel. Writing $z = P + iQ$ and $1/z = (P - iQ)/(P^2 + Q^2)$, this means that $P^2 + Q^2 = 1$. Thus z always lies on the unit circle, unless $Q = 0$. λ therefore varies between +4 and 0.

This substitution yields:

$$| \underline{A}_{33} - \lambda \underline{I} | = A_{33}(z) = \frac{(z^{2N} - 1)(z + 1)}{z^N (z - 1)} = 0 \qquad (2\text{-}34)$$

* The author is grateful to Professor H.J.A. Duparc, Mathematics Department, T.H., Delft, for suggesting this substitution.

whence $\lambda_p = 2 - 2\mathrm{Cos}(p\pi/N) \qquad (p = 1,2 \ldots\ldots N)$ (2-35)

which proves Equation (2-19).

With the same substitution

$$A_{11}(z) = \frac{(z^{2N} - 1)(z - 1)}{z^N(z + 1)} = 0 \tag{2-36}$$

whence $\lambda_p = 2 - 2\mathrm{Cos}\{(p-1)\pi/N\} \quad (p = 1,2 \ldots\ldots N)$ (2-37)

Equation (2-37) gives a first relaxation time at infinity since τ_p is proportional to $1/\lambda_p$ and for $p = 1$, $\lambda_p = 0$.

Consider as an example five hypothetical fixed crosslinks in a free chain with 36 submolecules, the crosslinks being equally spaced at intervals of 6 submolecules. Then the 36th order $\underline{A}_{33}$ matrix of the free chain is converted into four 6th order $\underline{A}_{11}$ matrices and two 6th order $\underline{A}_{31}$ matrices.

The eigenvalues of $\underline{A}_{31}$ are found with the same substitution as above.

$$A_{31}(z) = (z^{2N} + 1)/z^N = 0$$

whence

$$\lambda_p = 2 - 2\cos\{(p - \tfrac{1}{2})\pi/N\} \qquad (p = 1,2 \ldots\ldots N)$$

Fig. 2-1

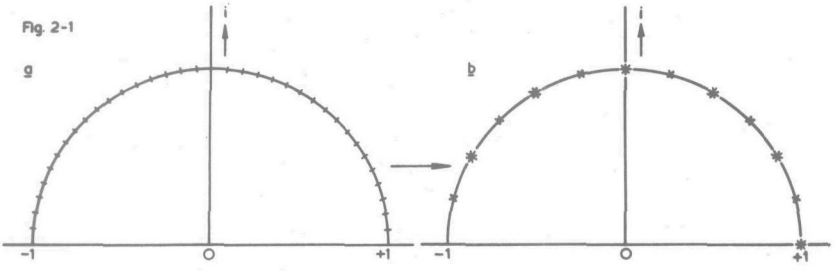

z values of $\underline{A}_{33}$ (36 th. order)

z values of $4\underline{A}_{11}$ (6 th. order) ✱
and $2\underline{A}_{31}$ (6 th. order) ×

The change is illustrated in Figure 2-1. The 36 different roots of $A_{33}(z) = 0$ are evenly distributed over the unit circle in Figure 2-1a. In Figure 2-1b the four interior sub-chains yield six groups of z values, which are the rootes of four identical equations $A_{11}(z) = 0$. Thus each asterisk represents a four-fold root. One of these groups lies at +1, which means that there are four relaxation times at infinity. The two exterior sub-chains yield six groups of z values, which are the rootes of two identical equations $A_{31}(z) = 0$.

In the relaxation spectrum of permanently crosslinked rubbers, a group of relaxation times is indeed found at infinity, whereas in the spectrum of rubbers with temporary crosslinks (entanglements) such a group lies not at infinity but closer to the glass transition region.

The question therefore arises, whether an entanglement point can be regarded as an intermediate state between a free and a fixed junction between submolecules. This intermediate state can be represented by assigning a higher friction coefficient to these points. This principle has already been applied, but only in mechanical models, by Bueche and Marvin[13-14].

It is qualitatively clear from Figure 2-1 that such intermediate states must give rise to a group of z values very close to the point z = +1 corresponding to a group of very high relaxation times. A representation of this type requires two additional parameters: a factor δ reducing the mobility B at an entanglement point, and the number of entanglements (m-1) in one molecule. This modification of the Rouse model affects only the mobility coefficient matrix and consequently the eigenvalues. The rest of the treatment is unchanged.

It must be noted, however, that this model accounts only for cooperative motions of neighbouring entanglements on the same molecule which floates in a continuum, and not for cooperative motions of other surrounding molecules.

Assigning a reduced mobility δB to the jth junction between submolecules yields instead of Equations (2-6) and (2-7):

$$(\dot{x}_j)_{j-1} = - B\left[\frac{\partial \mu}{\partial x_j} - \frac{\partial \mu}{\partial x_{j-1}} \right] \qquad (2\text{-}38)$$

and $$(\dot{x}_j)_j = -\delta B\left[\frac{\partial \mu}{\partial x_j} - \frac{\partial \mu}{\partial x_{j+1}}\right] \qquad (2\text{-}39)$$

Dividing the molecule into m sections by repeating this m-1 times yields a matrix of the form

$$\underline{A} = \begin{bmatrix} 3 & -1 & & & & & & & \\ -1 & 2 & -1 & & & & & & \\ & -1 & 1+\delta & -\delta & & & & & \\ & & -\delta & 1+\delta & -1 & & & & \\ & & & -1 & 1+\delta & -\delta & & & \\ & & & & -\delta & 1+\delta & -1 & & \\ & & & & & -1 & 1+\delta & -\delta & \\ & & & & & & -\delta & & \\ & & & & & & & -1 & 2 & -1 \\ & & & & & & & & -1 & 3 \end{bmatrix} \qquad (2\text{-}40)$$

The relaxation spectrum of this molecule will be given the symbol H[m-1]. This relaxation spectrum is still a discrete line spectrum, where all the lines have a height kT.

If $\delta = 0$, m-2 relaxation times are infinite, resulting in an equilibrium shear modulus per molecule of

$$G_e = (m-2)kT$$

If δ is small, the m-2 relaxation times are finite, but large. The number of relaxation times in this group will be the same no matter how the entanglements are distributed along the molecule.

It has been found possible to express this complicated matrix $\underline{A}$ in a workable form so as to permit calculation of the eigenvalues*.

Experiment, however, always gives a continuous relaxation

* The assistance of Dr. J. Ponstein, Shell Laboratory, Amsterdam, is gratefully acknowledged.

spectrum, so that the density of relaxation times is more important than the relaxation times themselves. This affords a short-cut** to the calculation of the continuous relaxation spectrum $H[m-1]$ by application of a property of the Sturm sequence[15]. Random distribution of entanglement points over the entire molecule can now also be easily introduced.

The method is based on the fact that, given a tri-diagonal determinant in the characteristic equation

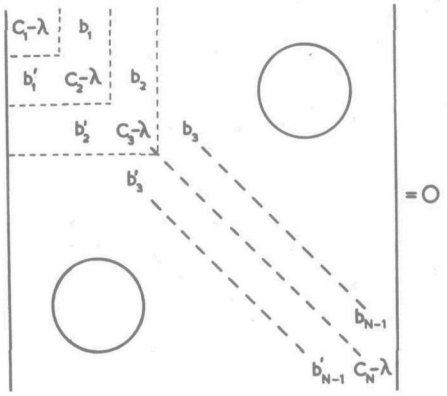

(2-41)

the subdeterminants (H_{11}, H_{22} .....) indicated by dotted lines form the following sequence:

$$
\begin{aligned}
H_{oo} &= +1 \\
H_{11} &= (c_1 - \lambda)H_{oo} \\
H_{22} &= (c_2 - \lambda)H_{11} - b_1' b_1 H_{oo} \\
H_{33} &= (c_3 - \lambda)H_{22} - b_2' b_2 H_{11} \\
&\vdots \\
H_{ii} &= (c_i - \lambda)H_{i-1,i-1} - b_{i-1}' b_{i-1} H_{i-2,i-2}
\end{aligned}
\qquad (2\text{-}42)
$$

A theorem exists which proves that if a certain value of λ is substituted into this "Sturm sequence", the number of agreements (a_1) in sign between consecutive members of the sequence is equal to the number of eigenvalues greater than that λ. If a $H_{ii} = 0$ occurs, its sign is defined to be opposite to that of $H_{i-1,i-1}$.

For instance, for $\lambda = 4$ in the matrix $\underline{A}$ of Equation (2-40)

** The suggestion for this method was made by Professor E. van Spiegel, Mathematics Dept., T.H., Delft, whom the author expresses his gratitude.

all the H_{ii} will alternate in sign, giving no eigenvalues larger than +4. For $\lambda = 0$ all the H_{ii} will be positive and thus all the eigenvalues will be larger than zero, as they should be.

At this point the lengthy calculations must be taken over by a computer, which is given the following instructions:

1) Determine the number of agreements a_1 for a certain λ_1.
2) Determine the number of agreements a_2 for $\lambda_1 - \Delta\lambda_1 = \lambda_2$ (where Δ is a multiplying factor, rather than an arithmetic increment, so as to give equal increments on a logarithmic scale).
3) Find $a_2 - a_1$ and repeat the process until $a_1 = N$, the order of the matrix.
4) Give the results converted into log τ_R values, where $\tau_R = 1/\lambda_1$.

For the Algol-program of this procedure see the Appendix.

As a result of such a calculation it was found that δ must be very small (10^{-3} to 10^{-6}) in order to affect significantly the spectrum obtained with the unmodified Rouse matrix. Clearly this result does not only apply to a chain with free ends, i.e. a matrix with 3's in the corners, but also to a chain with fixed ends, i.e. a matrix with 1's in the corners, containing such chain distortions as appear in Equation (2-40). For instance if $\delta = 0.1$, the change is so slight as to be undetectable by experiment. This result is of importance in the following sections, and an example is given in Chapter 5. It does not mean, however, that the overall mobility of the junctions is actually reduced a thousand or a million fold. This is physically unlikely because then they would resemble fixed points. The physical significance of small δ values will become clear in section 2-4.

2-3 Modification for crosslinked networks.

The ends of crosslinked chains are in fact not fixed in space. The line of reasoning in the preceding section must therefore be modified for cooperative motions of crosslinked or entangled molecules.

Duiser[16] has given a derivation for chemically crosslinked networks, with mobile crosslink points, which is repeated below.

Consider the system of four chains between five crosslinks, shown in Figure 2-2. A, B, C and D are fixed point crosslinks

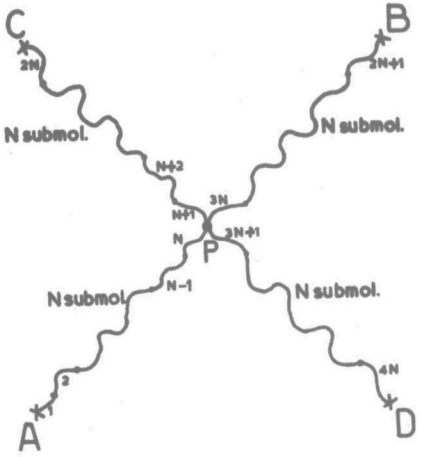

and P is a mobile crosslink halfway along AC and BD. Each chain contains N submolecules and the submolecules are numbered as follows:
from A to P: 1 to N, from P to C: N + 1 to 2 N, from B to P: 2 N + 1 to 3 N and from P to D: 3 N + 1 to 4 N.

Assume that the crosslink P has a reduced mobility B/2 because of the double mass associated with the junction. This value of B/2 is an estimate whose precision is of no consequence: B/3 or B/5 would yield the same result in the following treatment.

The velocity of back-diffusion in the x-direction at the point P is calculated as before. With all the junctions fixed except the (N - 1)th

$$(\dot{x}_N)_{N-1} = - B \left[\frac{\partial \mu}{\partial x_N} - \frac{\partial \mu}{\partial x_{N-1}} \right] \qquad (2\text{-}43)$$

and with all junctions fixed except the Nth

$$(\dot{x}_N)_N = - \frac{B}{2} \left[\frac{\partial \mu}{\partial x_N} - \frac{\partial \mu}{\partial x_{N+1}} + \frac{\partial \mu}{\partial x_{3N}} - \frac{\partial \mu}{\partial x_{3N+1}} \right] \qquad (2\text{-}44)$$

where μ is the chemical potential of the whole four chain system. The sum of these velocities gives $(\dot{x}_N)_D$

$$(\dot{x}_N)_D = - B \left[- \frac{\partial \mu}{\partial x_{N-1}} + \frac{3}{2} \frac{\partial \mu}{\partial x_N} - \frac{1}{2} \frac{\partial \mu}{\partial x_{N+1}} + \frac{1}{2} \frac{\partial \mu}{\partial x_{3N}} - \frac{1}{2} \frac{\partial \mu}{\partial x_{3N+1}} \right]$$

Similarly

$$(\dot{x}_{N+1})_D = - B \left[- \frac{1}{2} \frac{\partial \mu}{\partial x_N} + \frac{3}{2} \frac{\partial \mu}{\partial x_{N+1}} - \frac{\partial \mu}{\partial x_{N+2}} - \frac{1}{2} \frac{\partial \mu}{\partial x_{3N}} + \frac{1}{2} \frac{\partial \mu}{\partial x_{3N+1}} \right]$$

This result, expressed in a mobility coefficient matrix of order $4N$, gives

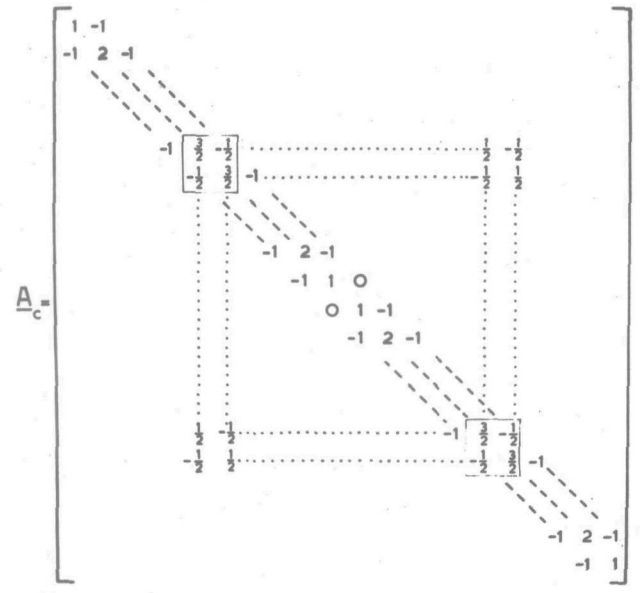

$$\underline{A}_c = \quad (2\text{-}45)$$

The characteristic equation $|\underline{A}_c - \lambda \underline{I}| = 0$ can be simplified as follows: The (2N)th row is added to the (2N+1)th, the (2N-1)th row is added to the (2N+2)th, etc. Then the 2Nth column is subtracted from the (2N-1)th, the (2N+1)th column is subtracted from the (2N-2)th, etc. The resulting determinant can then be split into a product of three determinants, of which the first corresponds to a chain of 2N submolecules between fixed points and the other two correspond to two chains of N submolecules between fixed points.

Thus the mathematical equivalence of this four-chain network with one mobile crosslink is as shown in Figure 2-3. Physically, this can be explained as follows: the chain AC can move with almost complete freedom. Once it has chosen a configuration, however, the point P appears to the chain BD as if it were fixed. The sections BP and PD then choose their own configurations independently of each other. The system of four chains therefore has three degrees of freedom instead of the commonly accepted four.

There seems to be no obvious reason why this physical interpretation should not also apply to a case where P is not at the center of the chains AC and BD, although it is not easy to prove this mathematically.

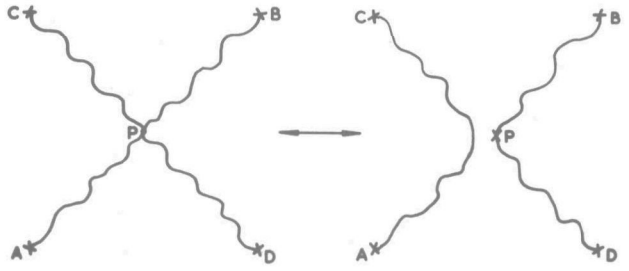

Fig. 2-3

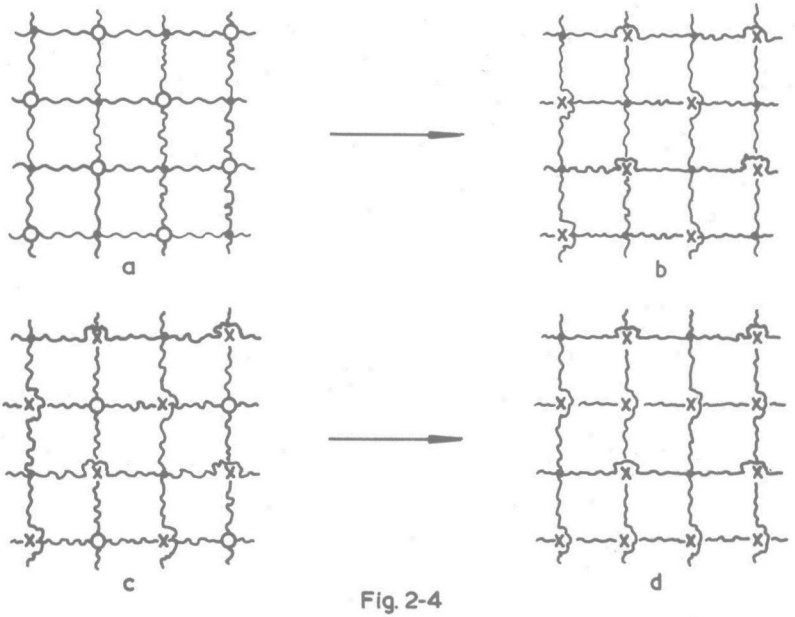

Fig. 2-4

The principle of this mathematical equivalence can be applied to a whole network[16]. To this end the network partly shown in Figure 2-4a is considered. The network is two-dimensional but can be regarded as the projection of a three-dimensional network. All the crosslinks are fixed and the ν_e chains between them are all N submolecules in length. Now, half the crosslinks are given a mobility, indicated by a circle, and application of

the above principle results in stage (b). Again, half the remaining fixed crosslinks are given a mobility, as shown in (c) giving (d). This process is repeated until only four fixed crosslinks are left at the outer boundary of the network. The relaxation spectrum of the final system of chains divided by ν_e is given by[16]

$$H_{perm.netw.} = \tfrac{1}{4} H(N) + \tfrac{3}{4} \sum_{k=1}^{\infty} \frac{1}{4^k} H(2^k N) \qquad (2\text{-}46)$$

where $H(2^k N)$ is the relaxation spectrum of a chain with fixed ends and of length $2^k N$ submolecules. It should be noted that the spectrum represented by Equation (2-46) is no longer a series of lines of equal height. This relaxation spectrum $H_{perm.netw.}$ has two important properties:

a) The slope of $-\frac{1}{2}$ of the $\log H$ —— $\log \tau$ plot (see Equation (2-30)) in the glass transition region is followed at higher τ by a slope of -1.

b) The number of infinite relaxation times of height kT is half the number of effective network chains ν_e in the initial network. This follows from Equation (2-46), because

$$\frac{1}{4} + \frac{3}{16} + \frac{3}{64} + \ldots = \tfrac{1}{2}$$

2-4 Modification for temporary or entanglement networks.

In concentrated solutions, chain entanglement occurs provided the molecular weight is high enough. These entanglements are of a complicated geometrical nature. Molecules of polymers with very different degrees of chain flexibility caused by steric hindrance, seem to become entangled to the same extent, indicating that an entanglement is not concentrated at one point on a chain. When devising a model, however, one has no choise but to concentrate the effect of entanglement coupling on infinitesimal points on the chain as is done in the model described below. The approximation does not seem serious, for theoretical and experimental results show a good fit. An essential requirement, however, is a large entanglement spacing along the molecule, i.e. the entanglement points should be separated

from each other by several (at least two) submolecules. The model is therefore not applicable to every undiluted polymer system, but only to those polymer systems, preferably diluted, which yield a maximum rubbery shear modulus $G(t)$ or $G'(\omega)$ of about 3×10^6 dynes/cm^2.

An entanglement network is assumed, having four-functional entanglement points, which are all equal and are randomly situated over the entire length of the molecule. All molecules contain the same number of submolecules (monodisperse polymer) and are assumed to have the same number of entanglements. The chains are assumed to slip slowly at their entanglement points. This slipping process must be much slower than the movement of a free submolecule if it is to explain the presence of a group of long relaxation times beyond the glass transition region.

First a two-chain system is considered, like that in Figure 2-2, where the point P now represents a mobile entanglement point, while A, B, C and D are fixed. It is assumed that, as in the case of a crosslink, the mobility is B/2 at the point P although there is some slip between the chains. With all junctions except the (N-1)th fixed, the velocity of back diffusion along the x_N coordinate becomes

$$(\dot{x}_N)_{N-1} = - B \left[\frac{\partial \mu}{\partial x_N} - \frac{\partial \mu}{\partial x_{N-1}} \right] \qquad (2\text{-}47)$$

With all junctions except the Nth fixed, it becomes

$$(\dot{x}_N)_N = - B/2 \left[\frac{\partial \mu}{\partial x_N} - \frac{\partial \mu}{\partial x_{N+1}} + (1 - 2\delta) \frac{\partial \mu}{\partial x_{3N}} - (1 - 2\delta) \frac{\partial \mu}{\partial x_{3N+1}} \right] \qquad (2\text{-}48)$$

where μ is the chemical potential of the whole system of two chains, and $(1 - 2\delta)$ accounts for the reduction in the forces due to slip in the second chain. δ is the slip parameter and, as mentioned above, must be much smaller than one. The factor 2 is included merely for mathematical convenience.

The resulting $(\dot{x}_N)_D$ and $(\dot{x}_{N+1})_D$ are:

$$(\dot{x}_N)_D = -B\left[-\frac{\partial \mu}{\partial x_{N-1}} + \frac{3}{2}\frac{\partial \mu}{\partial x_N} - \frac{1}{2}\frac{\partial \mu}{\partial x_{N+1}}\right]$$

$$-B\left[\left(\tfrac{1}{2}-\delta\right)\frac{\partial \mu}{\partial x_{3N}} - \left(\tfrac{1}{2}-\delta\right)\frac{\partial \mu}{\partial x_{3N+1}}\right] \qquad (2\text{-}49)$$

$$(\dot{x}_{N+1})_D = -B\left[-\frac{1}{2}\frac{\partial \mu}{\partial x_N} + \frac{3}{2}\frac{\partial \mu}{\partial x_{N+1}} - \frac{\partial \mu}{\partial x_{N+1}}\right]$$

$$-B\left[-\left(\tfrac{1}{2}-\delta\right)\frac{\partial \mu}{\partial x_{3N}} + \left(\tfrac{1}{2}-\delta\right)\frac{\partial \mu}{\partial x_{3N+1}}\right] \qquad (2\text{-}50)$$

The (4N)th order mobility coefficient matrix then becomes

$$\underline{A}_c = \qquad (2\text{-}51)$$

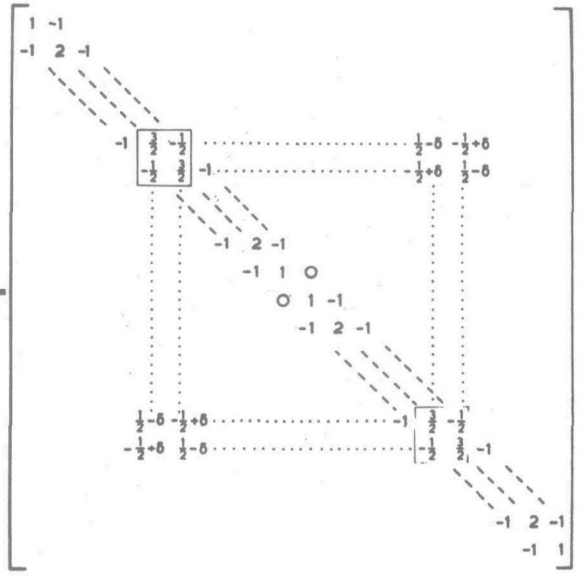

By applying the reduction previously applied to the characteristic Equation of the matrix in Equation (2-45), the determinant of (2-51) is reduced to a product of the two determinants:

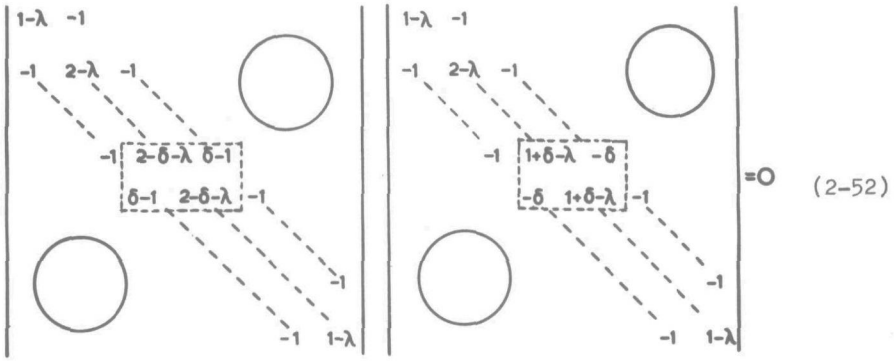

(2-52)

The results of section 2-2 should now be recalled. It was shown then that only a very small δ has an influence. To find the physical interpretation of Equation (2-52) the following cases must be examined for mathematical completeness:

a) δ is a large fraction, e.g. 1/3,

b) $\delta = 0$ or is very small,

c) $\delta = 1$ or almost = 1.

If δ is a large fraction, both determinants in Equation (2-52) reduce to the large δ case discussed in section 2-2. The eigenvalues then hardly differ from those of two independent chains between fixed points. Since, in practice, entanglements do have an influence on the relaxation spectrum, this case must be rejected.

If $\delta = 0$, Equation (2-52) reduces to the result of Duiser for a chemical crosslink, i.e. one long chain and two short chains between fixed points. If δ is very small, the left-hand determinant corresponds to the large δ case as above, but the right-hand determinant corresponds to a chain with 2N submolecules between fixed ends and with an increased friction coefficient in the middle.

If $\delta = 1$, Equation (2-52) also reduces to the result of Duiser, the roles of the determinants being reversed. If δ is almost = 1, the case with δ very small is repeated, again with the roles of the determinants reversed.

Thus the cases where δ is very small and almost one are physically identical, as can be seen from inspection of Equations (2-49) and (2-50). From these, it is clear that the

case where δ is almost one corresponds to the case where the segments DP and BP interchange their roles. Hereafter, δ is taken to be very small.

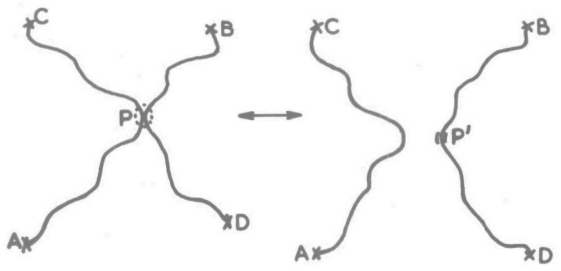

Fig.2-5

Thus the mathematical equivalence of the system of two chains between four fixed points, with one mobile entanglement, is as shown in Figure 2-5. On the right hand side one of the resulting chains (AC) is undisturbed, while the second (BD) of equal length posesses a lower mobility at the former point of contact P'. The mobility at such a "slow point" P' is equal to δB. Physically δB represents the ease of slipping of the entanglement point along one of the two chains. The small value of δ is now quite understandable, for this is now the mobility, not of the entanglement itself (as assumed in section 2-2) but of the slow point P' in the mathematical equivalent.

In order to apply this principle to an entanglement network, a fixed point network is first considered as shown in Figure 2-4a. All the chains between the fixed point crosslinks are of equal length (N submolecules) and the n primary molecules are also of equal length (m N submolecules).

Now each of these crosslinks is successively replaced by an entanglement of mobility B/2 and slip parameter δ , in such a manner that the four chain segments being considered are of the same length and terminate in a fixed point. As more and more crosslinks are transformed in this way, care must be taken that the remaining fixed points are symmetrically distributed in the network, so that the four chain segments under consideration contain the same number of slow points. Finally,

only four untransformed fixed points remain, which lie on the outside boundaries of the network.

Thus an entanglement network consisting of n molecules, each containing (m-1) entanglements, may be transformed to its mathematical equivalent, which is a system of:

n/4	molecules with	(m-1)	slow points
+ 3n/8	"	(m-1)/2	slow points
+ 3n/16	"	(m-1)/4	slow points
+ 3n/32	"	(m-1)/8	slow points, etc.

The relaxation spectrum for one molecule of this entanglement network may now be written:

$$H_{ent.} = \tfrac{1}{4} H[m-1] + \tfrac{3}{4} \sum_{k=1}^{\infty} \frac{1}{2^k} H\left[(m-1)/2^k\right] \qquad (2\text{-}53)$$

where $H[(m-1)/2^k]$ is the relaxation spectrum of a molecule (m N submolecules long) with $(m-1)/2^k$ slow points. Equation (2-53) like Equation (2-46) represents a discrete line spectrum in which the lines are not all of equal height.

The entanglement-network model for which Equation (2-53) was derived suffers from at least three imperfections, because in a real entanglement network:

1) The chain segments between entanglements are not of equal length.
2) The n primary molecules are not of equal length (i.e. the polymer is polydisperse).
3) The number of elastically effective chains is not exactly equal to the number of network chains.

The treatment outlined below to deal with these imperfections is also applicable to chemically crosslinked networks.

1. A real entanglement network is not made up of equal chain segments; the entanglements are almost randomly distributed along the molecules. From Figure 2-1 it can be seen that a chain regularly subdivided by (m-1) fixed points yields a spectrum with many maxima, including one maximum of (m-2) relaxation times at infinity. Likewise, a chain regularly subdivided by (m-1) slow points will exhibit a relaxation

spectrum with many maxima, including one group of (m-2) very large relaxation times. In contrast, a random distribution of the (m-1) slow points along the molecule will result in a much smoother spectrum.

Equations (2-45) and (2-51) indicate that the procedure for transformation to the mathematically equivalent networks is also valid if the matrices (2-45) and (2-51) are not only symmetric about their principal diagonal (i.e. each element $a_{ij} = a_{ji}$) but are also symmetric about the other diagonal i.e. each element $a_{ij} = a_{(N-j+1)(N-i+1)}$. This means that if two chains are entangled as shown in Figure 2-6a, where the chains are divided into two pairs of equal chain segments, they can be represented by their mathematical equivalent as in Figure 2-6a.

Fig. 2-6a

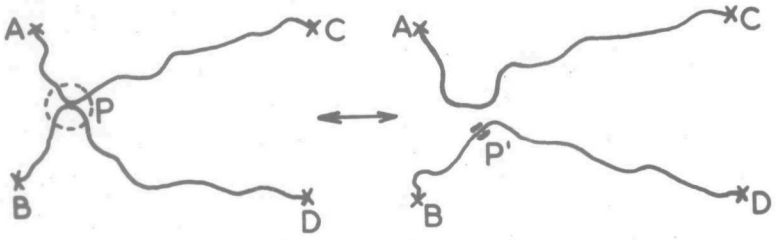

Fig. 2-6b

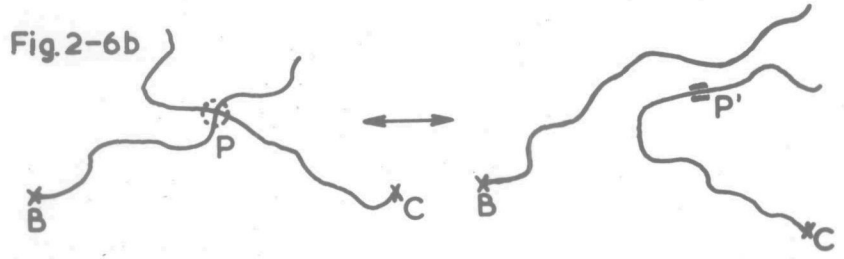

This also means that a mathematical equivalence may be found for two entangling chains containing only two fixed points and two free ends, as shown in Figure 2-6b, provided the entanglement divides the chains into two pairs of equal chain segments.

Making use of this principle it was found possible to construct a network containing different chain lengths between the fixed points, in such a way that an entanglement network is

obtainable by an unfixing process similar to that illustrated in Figure 2-4. Equation (2-53) is still valid for this special entanglement network, which is still not randomly entangled.

It is now assumed that the relaxation spectrum $H_{ent.}$ of an entanglement network with random distribution of chain lengths between entanglements, is also represented by Equation (2-53). This assumption is reasonable in the light of the physical interpretation made for the transformation in the case of a chemical crosslink. Each term $H\,[(m-1)/2^k]$ in this equation then represents an average of all possible entanglement distributions for a molecule with $(m-1)/2^k$ slow points. In practical calculations, however, for each term $H\,[(m-1)/2^k]$, one of the many possible distributions must be chosen and an average spectrum calculated from 5 or 10 such choices, depending on the accuracy which is desired.

The relaxation spectrum obtained in this fashion, plotted as $\log H_{ent.}$ vs. $\log \tau_R$ (where τ_R is defined as $\tau_R = 1/\lambda$) has the following properties:

a) In the short-time region, the spectrum is identical with the spectrum for a crosslinked network as derived by Duiser: The slope of $-\frac{1}{2}$ is followed by a slope of -1.

b) A rather low minimum in the curve is followed by a group of long relaxation times, the sum of whose heights is exactly equal to half the number of elastically effective chains (ν_e) in the entanglement network multiplied by kT.

c) Beyond the maximum in this group, the slope is practically constant and equal to $-\frac{1}{2}$ up to the highest relaxation time, as was already intuitively suggested by Ferry and coworkers[17]. Examples of these calculations will be given in Chapter 5.

2. Up to this point only a monodisperse polymer was being considered. Nevertheless, the calculated spectrum already showed a fairly good fit with the curves obtained from experiments on fractionated samples. For such samples, a $\bar{M}_w/\bar{M}_n$ ratio of 1.1 to 1.3 is usually found, depending on the fractionation conditions.

If the molecular weight distribution in the sample is approximately known, then instead of assuming a continuous

curve (like e.g. a Schulz-Flory distribution) the sample is assumed to have a distribution like, for instance, the step-curve shown in Figure 2-7.

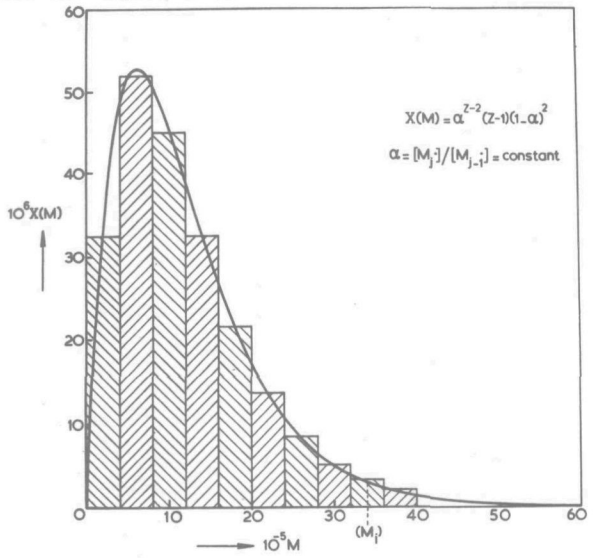

Fig. 2-7. Schulz–Flory distribution for a radically polymerized polymer with $\bar{M}_w = 1.8 \times 10^6$ and $\bar{M}_n = 1.2 \times 10^6$

The calculation of Equation (2-53) is carried out for each M_i, after which a weighted average is calculated from the resulting $H_{ent.}(M_i)$ values.

With this refinement, the resulting relaxation spectrum shows a much smoother curve. The slope of -1 mentioned above is limited to a narrow time region or may even disappear. Only the slopes of $-\frac{1}{2}$ will remain.

3. The third correction involves the calculation of the number of elastically effective network chains (ν_e). A treatment is given below in which the symbols differ from those used in Flory's derivation [18]. It applies equally to chemically cross-linked or entangled networks with 4-functional couplings.

Consider n primary molecules per unit volume, coupled in pairs by one crosslink per two molecules. This process will require $\frac{1}{2}n$ crosslinks. At this first stage the number of network chains (ν) and the number of effective network chains (ν_e) are both zero. [A network chain is defined as a chain which has a crosslink at both ends. An effective network chain is defined as one half of a closed circuit which must contain at

least two crosslinks. Both definitions are identical with those of Flory.]

Every intermolecular crosslink subsequently formed creates two network chains until a second stage is reached where all the molecules form one giant linear macromolecule. If the total number of crosslinks is C, then

$$\nu = 2(C - \tfrac{1}{2}n)$$

or

$$C = \tfrac{1}{2}\nu + \tfrac{1}{2}n \qquad (2\text{-}54)$$

At this second stage the number of network chains is equal to n-2, while the total number of crosslinks used is n-1.

Each new crosslink (evidently intramolecular) formed thereafter, produces two elastically effective network chains. If the number of effective crosslinks is C_e, then $C_e = \frac{1}{2}\nu_e$. Since the number of crosslinks used to reach the second stage is (n-1), the number of effective crosslinks is

$$C_e = C - (n-1)$$

or

$$\tfrac{1}{2}\nu_e = (\tfrac{1}{2}\nu + \tfrac{1}{2}n) - (n-1) = \tfrac{1}{2}\nu - \tfrac{1}{2}n + 1 \qquad (2\text{-}55)$$

Usually $n \gg 2$. Then Equation (2-55) reduces to

$$\nu_e = \nu - n \qquad (2\text{-}56)$$

Thus the correction term for ν is -n whereas Flory's deduction yields -2n. The difference is due to the quantity ν, which in Flory's treatment is defined +n higher than in the derivation described above.

2-5 Summary of Chapter 2.

The theory of Rouse is outlined. This proposes a free-draining model which can be modified for the effect of chemical crosslinks or entanglements through the "mobility coefficient matrix". With this model the relaxation spectrum of a free chain molecule is found to be equivalent to that of a set of Maxwell elements in parallel.

The theory of Duiser extends the Rouse model to the case of a permanent network. A mathematical consequence is that a

mobile crosslink which joins the centers of two equal chains, can be transformed into a fixed point at one of the centers, as shown in Figure 2-3. The physical interpretation appears plausibly extendable to chains crosslinked at any point along their length.

This principle is applied to an entanglement network theory where an expression is derived and assumed to apply for a randomly entangled molecule (Equation (2-53)). The terms in this expression are identical with the relaxation spectra of uncoupled molecules containing a number of "slow points". These spectra are obtained by the application of a property of the "Sturm sequence".

If the molecular weight distribution of a polymer is known, a correction procedure can be followed to account for the polydispersity.

The number of elastically effective chains was newly derived. The same correction is also required in the calculation of the number of entanglement points.

The spectra obtained from Equation (2-53) provide a means of determining the number (ν_e) of elastically effective chains in an entanglement network. This can be done by integrating the total area from the minimum to the highest relaxation time. This area is equal to $\frac{1}{2}\ \nu_e\ kT$.

References (Chapter 2)

1) P.E. Rouse, Jr.; J. Chem.Phys. 21, 1272 (1953).
2) N.W. Tschoegl & J.D. Ferry; Kolloid Z. 189, 37 (1963).
3) G. Harrison, J. Lamb & A.J. Matheson; J.Phys.Chem. 68, 1072 (1964)
4) B.H. Zim; J.Chem.Phys. 24, 269 (1956).
5) N.W. Tschoegl; J.Chem.Phys. 39, 149 (1963).
6) N.W. Tschoegl; J.Chem.Phys. 40, 473 (1964).
7) N.W. Tschoegl & J.D. Ferry; J.Phys.Chem. 68, 867 (1964).
8) J.E. Frederick, N.W. Tschoegl & J.D.Ferry; J.Phys.Chem. 68, 1974 (1964).
9) P. Debye; J.Chem.Phys. 14, 636 (1946).
10) F.T. Wall; J.Chem.Phys. 10, 132 (1942),
" " 10, 485 (1942).
11) J.A. Duiser & A.J. Staverman; in Physics of Non-Crystalline Solids, ed. J.A. Prins, North Holland Publ.Comp., Amsterdam (1965) p. 376 - 387.
12) J.D. Ferry; Viscoelastic properties of polymers, John Wiley & Sons, Inc., N.Y. (1961) p.157 ff.
13) F. Bueche; J.Applied Phys. 26, 738 (1955).
14) R.S. Marvin; Viscoelasticity-Phenomenological Aspects, ed. J.T. Bergen; Academic Press, N.Y. (1960), p. 27 ff.
15) J.H. Wilkinson; Numerische Mathematik 4, 362 (1962).
16) J.A. Duiser; Ph.D. thesis, Leiden (1965).
17) J.D. Ferry, R.F. Landel & M.L. Williams; J.Appl.Phys. 26, 359 (1955).
18) P.J. Flory; Chem.Reviews, 35, 67 (1944).

CHAPTER 3

PREPARATION AND CHARACTERIZATION OF THE POLYMERS

3-1 Anionic polymerization.

It has been pointed out in Chapter 1 that a polymer sample with a narrow molecular weight distribution is needed for an evaluation of the molecular theory of Chapter 2. Radical polymerization gives a rather broad distribution. At best, the ratio $\overline{M}_w/\overline{M}_n$ is about 1.5. Even after fractionation, the distribution in the fractions is by no means monodisperse.

In principle, a polymerization in which the termination process is absent can yield a very sharp distribution[1]. In practice, this is obtainable if the initiation rate is much greater than the propagation rate which in turn must be much greater than the termination or chain transfer rate. Then, after instantaneous initiation, the chains grow with equal probability of reaction and at the end, when all the monomer is consumed, they have about the same lengths. The molecules can continue to grow in length on addition of fresh monomer.

Vinyl monomers can be polymerized in this fashion by an anionic mechanism in a homogeneous phase[2], by the process

$$I^{\ominus} + M \rightarrow M_1^{\ominus} \quad ; \quad M_1^{\ominus} + M \rightarrow M_2^{\ominus}, \text{ etc.}$$

Szwarc[3] has described a method to prepare polystyrene by the above principles and has coined the term "living polymer" for the polymer grown in such a non-terminating reaction. The conditions necessary to the formation of a "living" polymer are: a) The organometallic initiator and the polymer must remain in solution, b) the polymer and counter-ion should be well solvated, c) the temperature of the solution must remain below the ceiling temperature (above which the degradation rate exceeds the polymerization rate), and d) electrophylic reagents must be absent to prevent termination.

It can be proved that this method gives a Poisson distribution of molecular weights[4], i.e. that

$$X(M_x) = \left[\exp(-\gamma) \right] \gamma^{x-1}/(x-1)! \qquad (3\text{-}1)$$

where $X(M_x)$ is the mole fraction of molecular weight M_x and $\gamma = \overline{Z}_n - 1$, where $\overline{Z}_n$ is the number-average degree of polymerization of the sample. For this distribution, it can be shown that

$$\overline{M}_w/\overline{M}_n = 1 + 1/\overline{Z}_n \qquad (3\text{-}2)$$

It is not possible to prepare poly-methyl acrylate (PMA) anionically using this principle, since the carbonyl group of the ester side chain can accept nucleophilic agents, according to the following mechanism

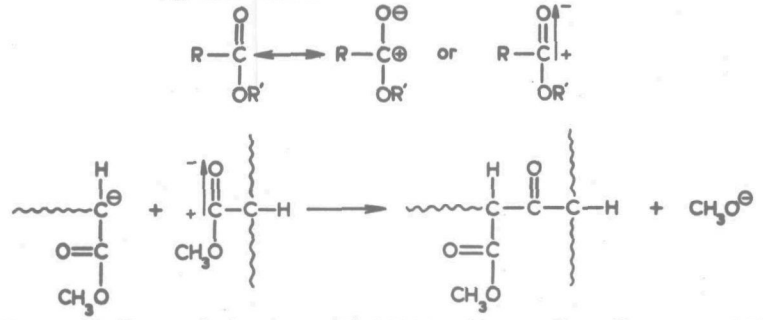

Thus, methyl acrylate is self-terminating under these conditions.

Surprisingly, methyl methacrylate can form a living polymer[5-6] which is even reasonably stable at room temperature[6]. If a model of this polymer (PMMA) is made from Stuart atomic models, and compared with a model of PMA, it is seen that in the former the carbon atom of the carbonyl group is sterically protected.

It was found possible to apply this principle to the polymerization of acrylate esters by using tertiary butyl acrylate as the monomer. The bulky tertiary butyl groups surrounded the polymer chain in such a way that the carbonyl carbon was again sterically protected, as could be seen from a model. Extra stability was given to the carbonyl carbon and to the tertiary hydrogen atom on the next carbon atom by the electron-releasing effect (+ I effect) of the tertiary butyl group.

The tertiary hydrogen atom is not sterically protected and can therefore take part in side reactions, causing chain-transfer.

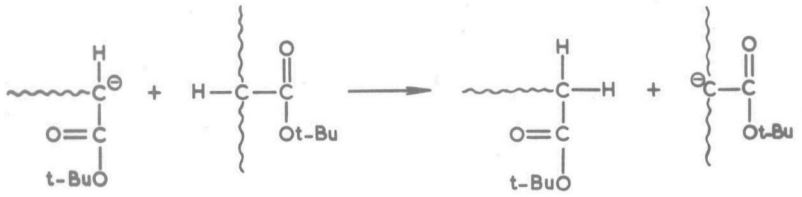

These side reactions form branched chains or may even lead to crosslinking. They must therefore be suppressed by polymerizing at very low temperature, where the propagation rate is still very high, while the chain transfer reaction rate, having a much higher activation energy, is greatly reduced.

The solvent must therefore have a low freezing point, as well as good solvating properties[7]. THF and ethylene glycol dimethyl ether have often been used in the preparation of living polymers and found satisfactory. Anionic polymerization in dimethyl ether (DME), however, has never been reported although there seems to be no reason why this should not be a good solvent. THF melts at -108°C while DME melts at -139°C. For this reason, and since it was assumed that it would also be a good solvent, DME was chosen rather than the more frequently used THF. Moreover, the low boiling point of DME (-24°C) facilitated distillation in the purification procedure.

The initiator to be used should be completely ionized in the solvent. Moreover, a monofunctional initiator is more suitable than a bifunctional, if a narrow distribution of molecular weights is required[8]. Rather arbitrarily, cumyl potassium, also used by Rempp and co-workers[9], was chosen.

The poly-tertiary butyl acrylate (PTBA), having been prepared, was then converted to PMA by alcoholysis.

3-2 Experimental procedure*

a) Preparation of cumyl potassium.

Methyl-cumyl ether was first prepared by a method described by Ziegler and Dislich[10]. The reaction consists of the addition of a molecule of methanol to a molecule of α-methyl styrene, with perchloric acid as catalyst, to form methyl cumyl ether.

* The author is very grateful to Mr. J.W.C. Adamse for the assistance given in the anionic polymerization experiments.

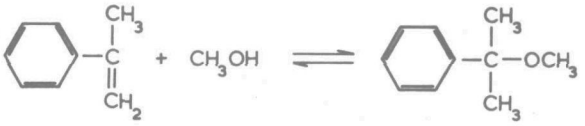

After a reaction time of 48 hours at 50°C, the reaction mixture was washed with a dilute solution of sodium hydroxide in water and distilled under reduced pressure. The distillate still contained some α-methyl styrene, which was converted to cumene by hydrogenation in solution in ethanol with hydrogen at atmospheric pressure and active platinum as catalyst. This reaction lasted 6 hours at room temperature. The mixture was filtered and distilled under reduced pressure. The fraction which boiled at 81°C and 20 mm Hg was collected and checked for the absence of α-methyl styrene by gas-liquid chromatography.

The methyl-cumyl ether was reacted in THF with a liquid sodium-potassium alloy, giving cumyl-potassium and potassium methylate, which are both soluble in THF.

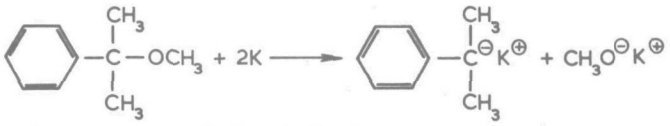

The reaction was carried out in the apparatus shown in Figure 3-1. All the vessels contained a magnetic stirrer. All glass joints were sealed with silicone grease and the whole apparatus was thoroughly cleaned by heating all parts with a flame under vacuum.

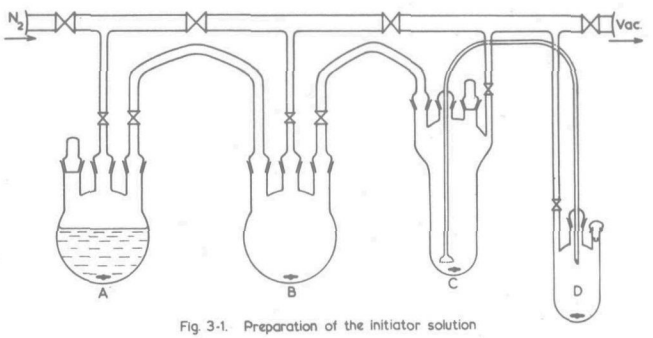

Fig. 3-1. Preparation of the initiator solution

Purified water-free THF was put in flask A and de-gassed under vacuum. In the de-gassing procedure, the solvent was frozen with liquid nitrogen. The vessel was then evacuated and the vacuum valve was closed. The THF was melted, releasing bubbles of gas, and was re-frozen. The vessel

was then re-evacuated and the process repeated a few times, until no more gas was liberated.

The vessel B contained sodium and naphthalene. It was evacuated and the THF was distilled from A to B by cooling B with alcohol and solid CO_2. After some time, the mixture in B turned green, indicating that the THF had reached a sufficient degree of purity. This THF was then distilled into vessel C, which contained a mixture of methyl cumyl ether and sodium-potassium alloy. The potassium immediately reacted with the methyl cumyl ether and the solution became dark red. After a certain amount of THF had been distilled into vessel C, the reaction was allowed to proceed for 2 hours. The concentration of cumyl potassium was then about 0.2 gmol/l which was determined by titration with an aqueous NaOH solution. The solution was syphoned into vessel D through the filter and stored until needed.

b) Preparation and purification of t-butyl acrylate.

The monomer is not commercially available and must therefore be prepared. The laborious synthesis from acryloyl chloride and t-butanol[11-12] was tried but gave a very low yield (less than 20 per cent referred to acryloyl chloride).

A much more elegant method has been proposed by McCloskey[13] et al., who applied it to the preparation of di-t-butyl malonate. The preparation is based on the reaction of carboxylic acids with iso-butene which with a suitable catalyst gives t-butyl esters.

The catalyst used by McCloskey, sulfuric acid, was found to be unsuitable for t-butyl acrylate. A boron trifluoride-phosphoric acid complex* gave satisfactory results. It was prepared by the method of Greenwood and Thompson[14]. A slow stream of BF_3 was passed through 100% H_3PO_4 until an increase in weight was reached corresponding to equal moles of H_3PO_4 and BF_3. The product was a liquid at room temperature.

About 3 g of this complex, together with 48 g of acrylic acid, 56 g of iso-butene and 66 g of methylene chloride, were placed in a small pressure vessel, and shaken for 17 hours at room temperature. The vessel was then cooled to $-50^{\circ}C$ and opened.

* The author is indebted to Prof. H.C. Beyerman, Laboratory for Organic Chemistry, T.H. Delft, for suggesting this catalyst.

The excess acid was neutralized with solid potassium carbonate and a small amount of hydroquinone was added for stabilization. The remaining liquid was distilled and the fraction with a B.P of 117° - 118°C at atmospheric pressure was collected. The yield was 59% referred to acrylic acid.

The purification of t-butyl acrylate was carried out in the apparatus shown in Figure 3-2. Each vessel contained a magnetic stirrer. This apparatus was cleaned and heated under vacuum as before. The parts from B to E were in one piece and contained no greased joints.

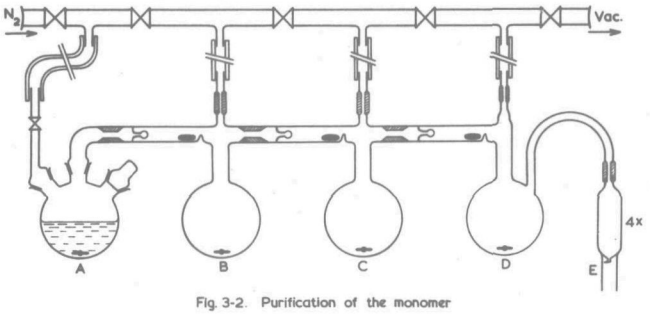

Fig. 3-2. Purification of the monomer

The monomer, thoroughly washed with a weak alkaline solution, dried and distilled through a long column, was placed in vessel A, where it was de-gassed under vacuum. The monomer was then distilled into vessel B, which contained some calcium hydride. The tube connecting A and B was sealed and the monomer was stored in B for one week. Then the monomer was distilled into flask C, which contained a sodium mirror, and was de-gassed under vacuum. Flask C was then heated to room temperature and kept between 20° and 30°C for about 1 hour until the liquid, through partial polymerization, had become viscous. Then the remaining monomer was quickly distilled into vessel D, which contained a small amount of calcium hydride, which seemed to have a stabilizing action on the monomer. From D, the monomer was carefully distilled into the ampulles E, which were then sealed at low temperature.

c) Purification of Nitrogen gas for use in the polymerization apparatus.

The nitrogen in the cylinder contained about 10 ppm oxygen, which was removed as shown in Figure 3-3. The gas was passed through a column B kept at 70°C and filled with pellets of BTS catalyst[15], supplied by the Badische Anilin und Soda-Fabrik,

Ludwigshafen, W. Germany. According to the literature on the subject, this step reduced the oxygen content to 0.1 ppm.

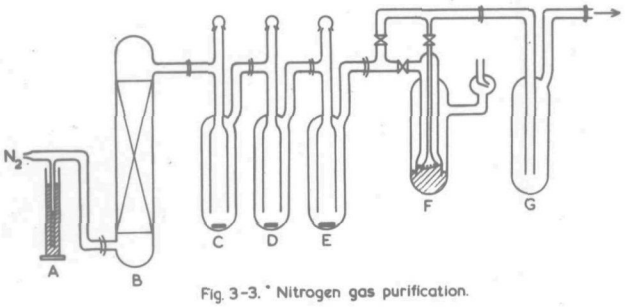

Fig. 3-3. Nitrogen gas purification.

The gas was then passed through the three washbottles C, D and E, which contained a green solution of sodium naphthalene in THF and were cooled to $-20^{\circ}C$ to prevent excessive evaporation of the solvent.

When the polymerization apparatus was under vacuum and had to be filled with nitrogen, the gas must flow gently through the purification vessels. The flow was regulated by the mercury valve F[16]. The vessel G was empty and A was a mercury safety valve.

d) Purification of DME and polymerization of t-butyl acrylate.

Both reactions were carried out in the apparatus shown in Figure 3-4, which was cleaned and heated under vacuum as before. The monomer ampulle G had already been attached to the vessel F and the monomer was kept frozen with liquid nitrogen. The vessels D and F contained nickel magnetic stirrers running on wheels.

The DME was received in a cylinder from Gerling, Holz & Co., Hanau/Main, W. Germany, and was fed into the apparatus at A. Vessel B contained a little solid sodium and naphthalene, and could be turned so that the contents dropped to the bottom of vessel C. About one third the amount of DME needed was then condensed in vessel C by cooling it in alcohol and solid CO_2. The solvent apparently still contained too many impurities, because the solution did not turn green. It was therefore de-gassed under vacuum and heated to $-24^{\circ}C$ (which was the B.P. at 1 atm.) after which an equal volume of a concentrated solution of sodium-naphthalene in THF was added. The solution then remained green. The remaining two-thirds of the DME was added and the green solution was stored at $-78^{\circ}C$ overnight. It was then de-gassed under vacuum and distilled into vessel D.

The apparatus was now filled with nitrogen at 1 atm. and the cumyl potassium solution was injected through the side tube M,

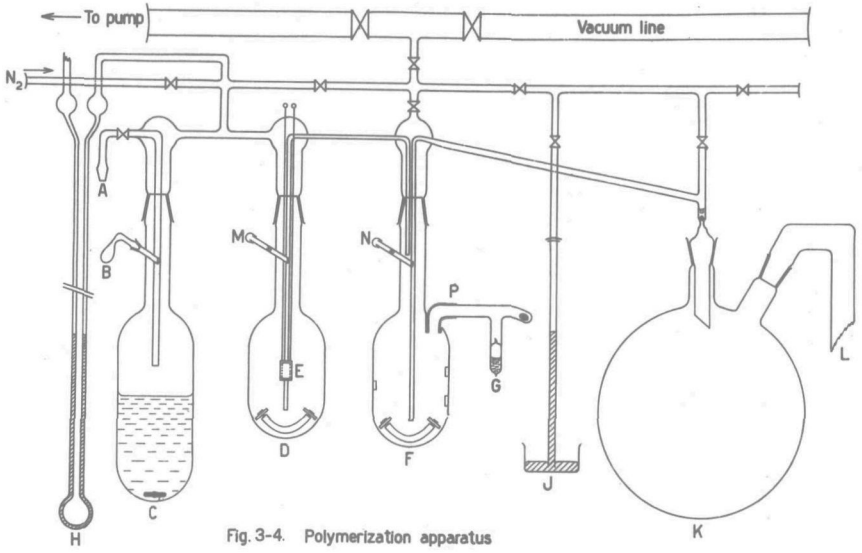

Fig. 3-4. Polymerization apparatus

which had a rubber serum-cap and a break-seal. The tube was sealed again, the initiator concentration was measured from the resistance of the solution between the platinum electrodes E[17] and the initiator solution (about 1 l) was syphoned into vessel F.

Here the solution was again de-gassed under vacuum, heated to -120°C (by surrounding the vessel with melting ethyl bromide) and the monomer from G (about 34 g) was slowly distilled into vessel F over one hour, while the solution was kept vigorously stirred. As it distilled over, the monomer immediately reacted and the red solution became colorless. The heating coil P prevented condensation in the connecting tube. The polymerization could be terminated either by injecting a terminating agent through the side-tube N (identical with M) or by syphoning the solution into vessel K, in which some solid CO_2 had been placed. L was an overflow to take care of any foaming. Each time a polymerization was performed as above, the yield was 100%. Several were carried out, and the apparatus was slightly improved between each one. The polymer from the last polymerization was caracterized after conversion to PMA.

e) Conversion of PTBA to PMA.

In acid solution, t-butyl esters are rather unstable and methyl esters are fairly stable. The alcoholysis was therefore carried out with dry HCl as catalyst.

About 3.5 g of PTBA were dissolved in 40 cm^3 of methylene chloride and 50 cm^3 of methanol were added. The solution was refluxed for 24 hours, while dry HCl gas was bubbled through. The polymer was then precipitated with excess methanol and vacuum-dried at 50°C.

The weight of the PMA indicates a quantitative conversion to the methyl ester. Titration of the polymer dissolved in dimethyl formamide with a tetramethylammonium hydroxide solution indicated the presence of 0.31% $\pm$ 0.01% acrylic acid monomer units on the chain. Quantitative analysis of the carbon and hydrogen contents showed a content of 99% $\pm$ 1% methyl acrylate monomer units; thus the alcoholysis had gone to completion.

3-3 Characterization of PMA polymers.*

The anionically polymerized PMA and a radically polymerized PMA were characterized side by side. The evaluation of the anionic PMA distribution was thus checked against that of the radical PMA, whose ratio $\bar{M}_w/\bar{M}_n$ was expected[18] to be between 1.5 and 2.0.

The latter polymer was prepared as follows. The inhibitor was removed from some methyl acrylate monomer by extracting with a dilute alkaline solution, after which the monomer was dried and distilled under reduced pressure. A quantity of this monomer was mixed with an equal volume of purified benzene, and the polymerization was carried out at 60°C, using azo-bis-isobutyronitrile as the initiator and triethylamine as a chain-transfer agent. After a 10% conversion was reached the reaction was stopped by adding a little inhibitor and cold methanol, which precipitated the polymer.

Several such polymerizations were made with different amounts of initiator and triethylamine. The intrinsic viscosities $[\eta]$ of the polymers defined by

$$[\eta] = \lim_{c \to o}(\eta_{sp}/c) = \lim_{c \to o}(\eta - \eta_s)/\eta_s c \qquad (3\text{-}3)$$

* A great deal of assistance with the characterization was given by Mr.J.D.Capel, to whom the author is very grateful.

were measured with a regular Ubbelohde viscometer. By suitable interpolation, a radical polymer could be prepared which had about the same intrinsic viscosity as the anionic polymer.

The values of the viscosities determined to obtain $[\eta]$ are plotted in Figure 3-5. The intrinsic viscosity $[\eta]$ and the viscosity-average molecular weight $\bar{M}_v$ are related by Staudinger's equation

$$[\eta] = K \bar{M}_v^a \qquad (3\text{-}4)$$

where K and a are constants. These have been determined for PMA in toluene at 30°C by Srinivasan et al.[21] Using their values of $K = 3.1 \times 10^{-2}$ and $a = 0.58$, the following molecular weights were calculated

anionic PMA: $\bar{M}_v = 1.60 \times 10^5$
radical PMA: $\bar{M}_v = 1.68 \times 10^5$

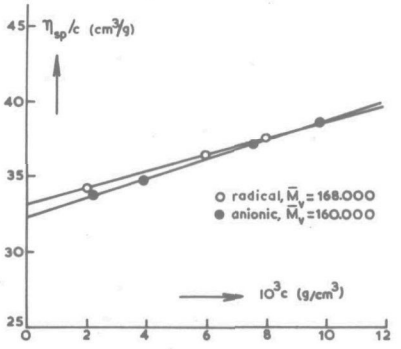

Fig. 3-5. Determination of $[\eta]$

The number average molecular weights $\bar{M}_n$ of the two samples were determined by osmometry in a toluene solution at 37°C using a membrane osmometer, model 502, made by Mechrolab, Inc., Mountain View, California. It can be shown[4] that the osmotic pressure π is related to $\bar{M}_n$ by the equation

$$\pi/RTc = 1/\bar{M}_n \qquad (3\text{-}5)$$

for an infinitely dilute solution. In real polymer solutions, the RMS of Equation (3-5) must be written in a power series in c on account of the non-ideal behavior of the solution. Thus the measurements must be extrapolated to c = o, as shown in Figure 3-6. This figure shows that the second virial coefficient is smaller for the anionic polymer than for the radical polymer. From these measurements, the following $\bar{M}_n$ values were calculated:

anionic PMA: $\bar{M}_n = 0.67 \times 10^5$
radical PMA: $\bar{M}_n = 0.79 \times 10^5$

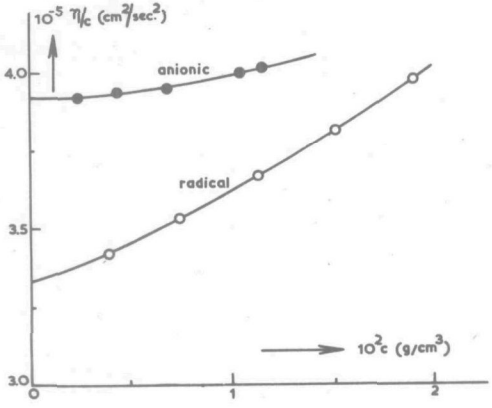

Fig. 3-6. Extrapolation of osmotic pressures to C=O.

The weight average molecular weights $\bar{M}_w$ were determined by sedimentation in dilute solutions with an ultracentrifuge. The Archibald method was used to calculate the $\bar{M}_w$. This method considers the mass transport in the immediate neighbourhood of the meniscus. It can be shown[19] that for an ideally dilute solution, the $\bar{M}_w$ is related to the concentration gradient at the meniscus $(\delta c/\delta x)_m$ by

$$\bar{M}_w = \frac{RT}{\omega^2 (1-\bar{v}\rho)} \left(\frac{\delta c/\delta x}{cx}\right)_m = \frac{RT}{\omega^2 (1-\bar{v}\rho)} \cdot \delta_m \qquad (3\text{-}6)$$

where δ_m is a constant for a given sample at a particular angular velocity ω and the subscript m denotes the meniscus. ρ is the density of the solution, $\bar{v}$ is the partial specific volume of the polymer and x is the distance to the center of rotation. The concentration gradient $\delta c/\delta x$ was calculated from dn/dx, where n is the refractive index. The refractive index gradient was obtained from a photograph of the light passed through a Schlieren-optical system. The concentration c was calculated at different times by a suitable integration of a $\delta c/\delta x$ vs. x plot.

The $\bar{M}_w$ at the meniscus decreases with time, and the solution does not behave ideally, so that the value of δ_m must be extrapolated to t = o and c = o. This is shown in Figures 3-7 and 3-8.

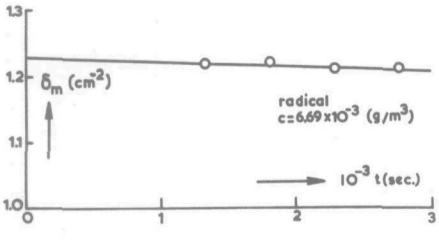

Fig. 3-7. Extrapolation of δ_m to t=O

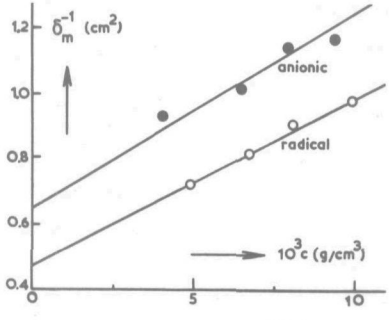

Fig. 3-8. Extrapolation of $(\delta_m)_{t=O}$ to c=O.

The sedimentations were performed in butanone at 25°C in a Model E Ultracentrifuge (Beckman-Spinco, Palo Alto, California) at 11270 r.p.m.

The values of the constants used in the calculation of $\bar{M}_w$ were:

$dn/dc = 0.0914$ (with c in g/cm^3), $\bar{v} = 0.8919\ cm^3/g$ and $\rho = 0.8013\ g/cm^3$. The extrapolated values for $(\delta_m)_{t=c=o}$ from Figure 3-8 are 1.53 and 2.12, which yield the results:

anionic PMA: $\bar{M}_w = 0.95 \times 10^5$

radical PMA: $\bar{M}_w = 1.32 \times 10^5$

Thus, with the values of $\bar{M}_n$ obtained previously, the heterogeneity indices were:

anionic PMA: $\bar{M}_w/\bar{M}_n = 1.42$

radical PMA: $\bar{M}_w/\bar{M}_n = 1.67$

These results indicate that the present technique for preparing PMA anionically via PTBA gives a polymer with a molecular weight distribution, which is not a significant improvement over that of a radically polymerized PMA.

There are several possible reasons for this. One possible cause may be the chain transfer reaction due to the tertiary hydrogen atoms on the main chain, which leads to branching. The molecular weight distribution in the anionic PMA, however, is a little narrower than in the radical PMA, showing that branching must have been slight. This effect could probably be suppressed by polymerizing at lower temperatures. However, lower temperatures might reduce the degree of dissociation of the initiator, which may be a second possible reason for the wide distribution.

The main reason for the wide molecular weight distribution, however, is probably the polymerization procedure itself. The propagation rates of acrylate monomers are generally so high that with the apparatus used, it was not possible to complete the mixing of all the initiator and monomer before any polymer had been formed. The alternative used of gradually condensing the monomer on the surface of the living polymer solution may introduce a rather wide molecular weight distribution by preventing an equal chance of reaction for every molecule at every moment[20].

The task of considering every one of these difficulties in detail was such as to require an effort out of proportion to the main rheological endeavor. It was therefore decided to use the more readily obtained radically polymerized PMA in the rheological experiments to be described in the last chapter.

To satisfy the requirement that the network should contain many entanglements, a sample of radical PMA was prepared with a very high molecular weight. The $\bar{M}_w$ was 1.8×10^6 and was determined by light scattering. The molecular weight distribution of this sample was assumed to follow a Schulz-Flory distribution function with a ratio $\bar{M}_w/\bar{M}_n$ of 1.5.

References (Chapter 3)

1) P.J. Flory; Principles of Polymer Chemistry; Cornell University Press, Ithaca, N.Y. (1953).
2) M. Szwarc; Nature 178, 1168 (1956).
3) M. Szwarc, M. Levy and R.Milkovich; J.Am.Chem.Soc. 78, 2656 (1956).
4) C. Tanford; Physical Chemistry of Macromolecules; John Wiley & Sons, Inc, N.Y. (1961).
5) P.H. van der Mey; private communication.
6) Y.Y. Tan; private communication.
7) M. Szwarc; Makromol.Chem. 35, 132 (1960).
8) M. Szwarc; private communication.
9) P. Rempp, V.I. Volkov, J.Parrod & Ch. Sadron; Bull.Soc.Chim., France 1960, 919.
10) K. Ziegler & H.Dislich; Ber. 90, 1107 (1957).
11) H.T. Neher; U.S. patent 2.117.349 (17 May 1938).
12) G.H. Stempel, R.P. Cross, R.P. Mariella; J.Am.Chem.Soc. 72, 2299 (1950).
13) A.L. McCloskey, G.S. Fonken, R.W. Kluiber & W.S. Johnson; Org.Syntheses, Coll. Vol. IV, p. 261 (1963).
14) N.N. Greenwood, A. Thompson; J.Chem.Soc. 1959, 3493.
15) M. Schütze; Angew.Chem. 70, 697 (1958).
16) J. Almond; J.Sci.Instr. 35, 70 (1958).
17) D.J. Worsfold & S.Bywater; J.Chem.Soc. 1960, 5234.
18) C.H. Bamford, W.G. Barb, A.D. Jenkins & P.F. Onyon; The Kinetics of Vinyl Polymerization by Radical Mechanisms, Butterworths Sci.Publ., London (1958).
19) H.K. Schachman; Ultracentrifugation in Biochemistry; Academic Press, N.Y. (1959).
20) R.V. Figini & G.V. Schulz; Z.Physik.Chem. N.F. 23, 233 (1960).
21) N.T.Srinivasan and M.Santappa;Makromol.Chem. 27, 61 (1958).

CHAPTER 4

THE RHEOMETER

4-1 General construction of the rheometer.

The rheometer was designed to measure directly the shearing force f, the shear deformation γ , and the phase angle δ between them. This permitted calculation of the real and imaginary components G' and G" of the complex shear modulus G^*.

This method was chosen rather than the indirect method which measures the mechanical impedance by means of an electro-mechanical transducer[1-4], because the polymer-solvent mixtures to be investigated were expected to show a wide range of moduli in changing from liquid to solid-like consistencies.

A resonance method[5-7] was rejected, since the resonance frequency is proportional to the reciprocal of the square root of the vibrating mass. This makes difficult the design of an apparatus with a wide frequency range.

The direct-measurement methods described in the literature tend to have rather elaborate and bulky designs[8-11], especially in the vibration exciters, and thus tend to make good temperature control difficult.

These difficulties were avoided by using ferro-electric titanate ceramics for the necessary electro-mechanical transformations, which permitted compact construction of the apparatus and operation over a wide range of frequencies. Only one other rheometer, based on this principle, has been reported[12], also applied to a direct measurement method.

When used as vibration exciters these ceramics have the disadvantage of rather small strain amplitudes. As force transducers, however, they have the advantage of infinitesimal displacement amplitude losses and large pressure ranges (≈ 6 decades). The ceramic is not suitable to D C. measurements.

The rheometer consisted basically of four parts.

a) Two coaxial cylinders, holding the sample in the annular space between them.

b) A ferro-electric ceramic vibration exciter.

c) A ferro-electric ceramic force-transducer.

d) A displacement transducer of an inductive type.

The so-called Pochettino geometry[13-14] consists of two coaxial cylinders having an annular space between them, which is filled with the sample. One of the cylinders is clamped and the other moves axially. In the present case the annular space was closed at the lower end with a "Teflon" foil, 5×10^{-2} mm thick. A disadvantage of this geometry is that the rheometer is difficult to fill, but this difficulty is minor when working with polymer solutions.

Having chosen piezo electric devices for the vibration exciter and force transducer, the first model of the rheometer was as shown in Figure 4-1, which is a vertical cross-section through the apparatus.

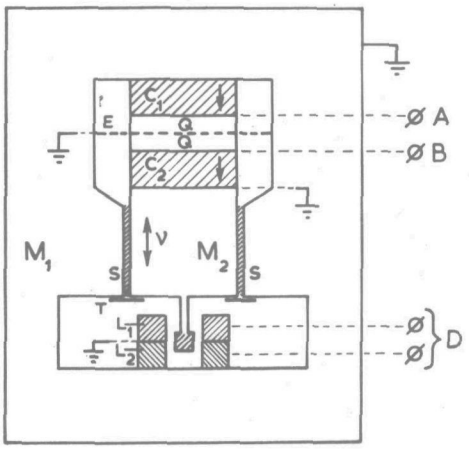

Fig. 4-1

M_1 is a heavy metal body with a much greater mass than the vibrating piston M_2. C_1 is the vibration exciter (the "driver") which gives the column consisting of Q, C_2 and M_2 a vertical harmonic motion and which is excited by a high voltage at A. The insulator Q is quartz-glass. E is a Faraday cage which shields C_2 from C_1. The output of the force transducer C_2 (the "pick-up") is measured at B.

C_2 acts, in fact, as a pressure transducer, since the signal at B depends on the horizontal cross sectional area of C_2.

The direction of polarization of C_1 and C_2 was chosen parallel to the direction of vibration.

The narrow gap S contains the polymer solution, which is sheared by the metal piston M_2. T is the "Teflon" foil, described previously.

The displacement of the piston relative to the body M_1 is measured at D by an inductive displacement transducer. Unlike the more common differential transformers with three coils, which have a fairly large zero signal, this displacement transducer has only two coils, with inductances L_1 and L_2 which form two arms of a Wheatstone impedance bridge fed by a 50 Kc/s AC voltage. With a suitable demodulating amplifier, one can easily obtain clear signals from displacement amplitudes of 10^{-4} to 1 mm at frequencies from 0 to 10 Kc/s.

The inductive type of transducer was chosen over the capacitive type, since the latter is very sensitive to dust particles and to changes in the dielectric constant of the atmosphere between the plates (due e.g. to the presence of solvent vapors and to changes in temperature).

The phase difference between B and D was measured with a phase angle meter. After calibrating for the effect of T and M_2, the angle δ and G' and G" could thus be calculated.

In order to simplify the design, it was decided to assemble the vibrating column by glueing the components (except the displacement transducer core and the Teflon foil) together with very thin layers of adhesive. After some experiments, Eastman 910 was chosen as the most suitable. This is α-cyano-methyl-acrylate monomer, which polymerizes anionically, traces of water on the surfaces to be joined acting as initiator.

In order to strain this glue layer as little as possible with changes of temperature, M_1, M_2 and E were made of invar whose coefficient of expansion is very close to that of the ceramics C_1 and C_2. (Linear coefficients of expansion of invar Λ_i and the ceramic PZT4 Λ_c are: $\Lambda_i = 0.9 \times 10^{-6}/^{\circ}C$ $\Lambda_c = 2.2 \times 10^{-6}/^{\circ}C$) The insulator Q was of amorphous quartz ($\Lambda_Q = 0.6 \times 10^{-6}/^{\circ}C$).

4-2 Deformation of the sample.

Figure 4-2 shows an axial cross-section of the gap between the two cylinders. The piston has moved a distance x from its equilibrium position under the influence of a vertical force f.

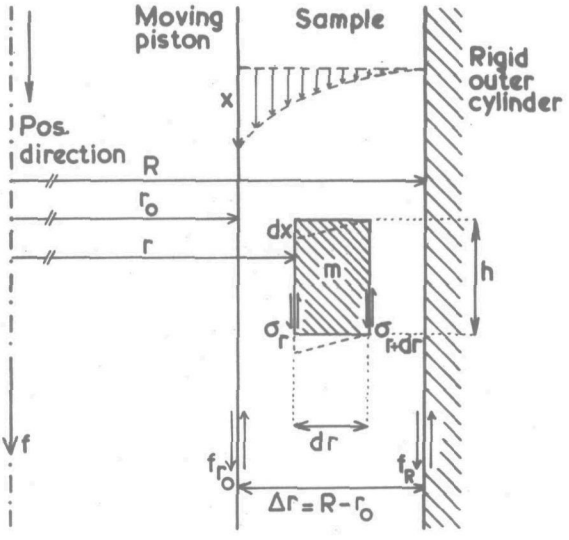

Fig. 4-2

Consider first the transient loading case and the constant deformation rate case. In these cases the material is not accelerated and $f = f_{r_o} = f_R = f_r$ at any coaxial cylindrical boundary, where f denotes the shearing force. The shear stress σ_r on a cylindrical element of height h, mass m and radius r causes a deformation dx/dr.

Then $\sigma_r = - G\, dx/dr$ in the case of a solid,

or $\sigma_r = - \eta\, d\dot{x}/dr$ in the case of a liquid,

where $\dot{x} = dx/dt$ and the negative sign is due to the negative dx/dr.

When the solid or liquid is viscoelastic, the quantities σ_r, G and η become functions of time.

Experimentally, the force, rather than the stress is measured, so that the following is the suitable derivation:

$$f_r(t)/2\pi r h = - G(t)\, dx/dr \qquad (4\text{-}1)$$

$$f_{r_o}(t) \int_{r_o}^{R} dr/r = - 2\pi h\, G(t) \int_{x}^{o} dx$$

$$f_{r_o}(t) = 2\pi h/\ln(R/r_o).G(t).x \qquad (4\text{-}2)$$

and similarly:

$$f_{r_o}(t) = 2\pi h/\ln(R/r_o).\eta(t).\dot{x} \qquad (4\text{-}3)$$

The factor $2\pi h/\ln(R/r_o) = b$ is the well known form factor for the Pochettino geometry[15]. If R and r_o are large compared with Δr so that $R/r_o \approx 1$, then $\ln(r/r_o)$ can be replaced by $\Delta r/r_o = (R-r_o)/r_o$.

Equation (4-1) shows that the strain dx/dr changes hyperbolically with r, so that the strain within Δr can only be taken as linear with r when Δr is very small compared with R.

Considering now the dynamic loading patterns, the quantity G(t) cannot be simply replaced by the complex modulus $G^* = G' + i\,G''$, because now the piston and sample are subjected to an acceleration and their masses must be taken into account. Then $f^*_{r_o} \neq f^*_R$ and the equation of motion for a volume element is obtained as follows (the superscript * denotes complex quantities):

$$f^*_r = - 2\pi G^* hr \frac{dx^*}{dr}$$

$$f^*_{r+dr} = 2\pi G^* hr \frac{dx^*}{dr} + \frac{\partial}{\partial r}(2\pi G^* hr \frac{\partial x^*}{\partial r})dr$$

$$f^*_r + f^*_{r+dr} = m\ddot{x}^* \longrightarrow 2\pi G^* h \frac{\partial}{\partial r}(r \frac{\partial x^*}{\partial r}).dr = 2\pi rh\rho\, \ddot{x}^* dr \qquad (4\text{-}4)$$

where ρ is the sample density and $\ddot{x}^*$ is the acceleration at the center of gravity of the volume element.

If $x^* = x_o \exp(i\omega t)$, then $\ddot{x}^* = - \omega^2 x^*$

$$\frac{G^*}{\rho\omega^2}(r \frac{\partial^2 x^*}{\partial r^2} + \frac{\partial x^*}{\partial r}) + x^* r = 0 \qquad (4\text{-}5)$$

and similarly

$$\frac{i\eta^*}{\rho\omega}\left(r\frac{\partial^2 x^*}{\partial r^2}+\frac{\partial x^*}{\partial r}\right)+x^* r=0 \qquad (4\text{-}6)$$

in accordance with

$$G^* = G' + i\,G'' = \omega\eta'' + i\omega\eta' = i\omega\eta^*$$

Equations (4-5) and (4-6) are Bessel differential equations whose solutions are obtainable but cumbersome. In the present case, practical exigencies lead to an apparatus design in which both $R/r_o \approx 1$ and $\Delta r < \lambda_r/10$, where λ_r is the shear wave length in the radial direction. Moreover, the force given by integration of Equation (4-4) represents at most a 5% correction to the main shearing force as given by Equation (4-2).

Thus precise solution of Equation (4-5) and (4-6) can be circumvented by assuming that $\partial^2 x^*/\partial r^2 = 0$ over the distance Δr. Then the treatment for the volume-element may be extended to the entire volume of the sample. It follows then from Equation (4-4) that the extra force which accelerates the sample of mass m becomes simply:

$$f^*_{r_o} + f^*_R = \pi(R^2-r_o^2)h.\rho.\ddot{x}^* = -\tfrac{1}{2}\pi h\rho\omega^2(R^2-r_o^2)x^* \qquad (4\text{-}7)$$

where $\ddot{x}^*$ is replaced by $-\frac{1}{2}\omega^2 x^*$ because the center of gravity of the sample moves only half the distance x^*.

Equation (4-7) gives the additional force for the acceleration of the sample, which must be added to the shearing force (Equation (4-2)). Then

$$f^*_{r_o} = 2\pi h.G^* x^*/\ln(R/r_o) - \tfrac{1}{2}\pi h\rho\omega^2(R^2-r_o^2)x^*$$

$$= \pi h[2\,G^*/\ln(R/r_o) - \tfrac{1}{2}\rho\omega^2(R^2-r_o^2)\,]\,x^* \qquad (4\text{-}8)$$

where h is now the height of the sample.

The second term in the brackets, which is the correction term, will be important only at low moduli and high frequencies.

4-3 The piezoelectric devices.

The ferroelectric material used for the driver and pick-up is PZT4, a lead-zirconium titanate ceramic made by the Brush Crystal Co. Hythe, Southampton, England. This ceramic is prepolarized in manufacture at high voltage and high temperature. (The Curie point is 320°C)

At low voltages, ferroelectric materials behave like piezoelectric crystals. At high fields, however, especially at resonance, they may become depolarized or counter-polarized. To avoid this, excitation field strengths over 1000 V/cm were never used, and the devices therefore always behaved purely piezoelectrically.

Unpolarized lead-zirconium titanate is isotropic. The relation between stress σ and strain γ in one dimension is then $\gamma = S\sigma$, where S is the compliance of the material. The relation between dielectric displacement D and electric field F in one dimension is $D = \varepsilon F$, where $\varepsilon = \varepsilon_0 \varepsilon_r$ is the dielectric constant of the material. ε_r = the relative dielectric permittivity of the medium.

Polarized PZT4 is anisotropic. The above relations must then be extended to three dimensions, while piezoelectric properties also appear[16].

PZT4 belongs to class C_{6v} of the Hexagonal system. This class has 5 elastic, 3 piezoelectric and 2 dielectric constants, which are given later. The z axis (subscript 3) is chosen parallel to the polarization direction, as usual.

The dielectric displacement and the electric field are related by the second order tensor equation

$$\begin{Bmatrix} D_1 \\ D_2 \\ D_3 \end{Bmatrix} = \begin{bmatrix} \varepsilon_{11} & \varepsilon_{12} & \varepsilon_{13} \\ \varepsilon_{21} & \varepsilon_{22} & \varepsilon_{23} \\ \varepsilon_{31} & \varepsilon_{32} & \varepsilon_{33} \end{bmatrix} \begin{Bmatrix} F_1 \\ F_2 \\ F_3 \end{Bmatrix} \qquad (4\text{-}9)$$

or $$D_i = \sum_k \varepsilon_{ik} \cdot F_R \quad (i \text{ and } k = 1, 2 \text{ or } 3) \qquad (4\text{-}9a)$$

This tensor is symmetric i.e. $\varepsilon_{ik} = \varepsilon_{ki}$. Equation (4-9) is equivalent to three equations, each with three terms on the right hand side.

The stresses and strains are also second order tensors,

which for simplicity are written:

$$\underline{\sigma} = \begin{bmatrix} \sigma_{11} & \sigma_{12} & \sigma_{13} \\ & \sigma_{22} & \sigma_{23} \\ & & \sigma_{33} \end{bmatrix} \quad \text{and} \quad \underline{\gamma} = \begin{bmatrix} \gamma_{11} & \gamma_{12} & \gamma_{13} \\ & \gamma_{22} & \gamma_{23} \\ & & \gamma_{33} \end{bmatrix}$$

The other coefficients below the main diagonal are equal to their mirror images and are left out for convenience.

In piezoelectric materials the dielectric polarization $\underline{P}$ and the stress $\underline{\sigma}$ are related by the third order tensor equation

$$\begin{Bmatrix} P_1 \\ P_2 \\ P_3 \end{Bmatrix} = \sum_l \begin{bmatrix} d_{11l} & d_{12l} & d_{13l} \\ d_{21l} & d_{22l} & d_{23l} \\ d_{31l} & d_{32l} & d_{33l} \end{bmatrix} \begin{Bmatrix} \sigma_{1l} \\ \sigma_{2l} \\ \sigma_{3l} \end{Bmatrix} \tag{4-10}$$

$$\text{or} \quad P_i = \sum_k \sum_l d_{ikl}\sigma_{kl} \quad (i, k \text{ and } l = 1, 2 \text{ or } 3) \tag{4-10a}$$

This is called the direct piezoelectric effect, and d_{ikl} is called the piezoelectric strain coefficient. This tensor is also symmetric, i.e. $d_{ikl} = d_{kil}$. Equation (4-10) is equivalent to three equations each with nine terms on the right hand side.

The dielectric polarization $\underline{P}$ is related to the dielectric displacement $\underline{D}$ and the field $\underline{F}$ by

$$\underline{P} = \underline{D} - \varepsilon_o\underline{F} = (\underline{\varepsilon}_r - \underline{1})\varepsilon_o\underline{F}$$

where $\underline{\varepsilon}_r - \underline{1} = \underline{\varkappa}$, the electric susceptibility of the medium, or, in tensor notation $P_i = \sum_j \varkappa_{ij}\ \varepsilon_o F_j$

Similarly the strain $\underline{\gamma}$ in the piezoelectric materials is related to the electric field $\underline{F}$ by the third order tensor equation

$$\begin{Bmatrix} \gamma_{1l} \\ \gamma_{2l} \\ \gamma_{3l} \end{Bmatrix} = \begin{bmatrix} d_{11l} & d_{21l} & d_{31l} \\ d_{12l} & d_{22l} & d_{32l} \\ d_{13l} & d_{23l} & d_{33l} \end{bmatrix} \begin{Bmatrix} F_1 \\ F_2 \\ F_3 \end{Bmatrix} \tag{4-11}$$

$$\text{or} \quad \gamma_{kl} = \sum_i d_{ikl}F_i \quad (i, k \text{ and } l = 1, 2 \text{ or } 3) \tag{4-11a}$$

This is called the inverse piezoelectric effect. Equation (4-11) is equivalent to nine equations, each with three terms on the right hand side.

The stresses σ_{kl} and strains γ_{ij} are related by the fourth order tensor equation

$$\begin{Bmatrix} \gamma_{1j} \\ \gamma_{2j} \\ \gamma_{3j} \end{Bmatrix} = \sum_{1} \begin{bmatrix} S_{1j1l} & S_{1j2l} & S_{1j3l} \\ S_{2j1l} & S_{2j2l} & S_{2j3l} \\ S_{3j1l} & S_{3j2l} & S_{3j3l} \end{bmatrix} \begin{Bmatrix} \sigma_{1l} \\ \sigma_{2l} \\ \sigma_{3l} \end{Bmatrix} \qquad (4\text{-}12)$$

or $$\gamma_{ij} = \sum \sum S_{ijkl}\sigma_{kl} \quad (i,j,k \text{ and } l = 1,2 \text{ or } 3) \qquad (4\text{-}12a)$$

This tensor is also symmetric i.e. $S_{ijkl} = S_{jikl} = S_{klij} = S_{lkij}$. Equation (4-12) is equivalent to nine equations, each with nine terms on the right hand side.

Because of the symmetry of the tensors, an abbreviated notation can be used instead of the full notation used above. The short notation suffers the disadvantage that with it, no coordinate axis transformation can be carried out. In the short notation double suffices are replaced by single suffices. For instance the second order stress tensor

$$\begin{bmatrix} \sigma_{11} & \sigma_{12} & \sigma_{13} \\ & \sigma_{22} & \sigma_{23} \\ & & \sigma_{33} \end{bmatrix} \quad \text{becomes} \quad \begin{bmatrix} \sigma_1 & \sigma_6 & \sigma_5 \\ & \sigma_2 & \sigma_4 \\ & & \sigma_3 \end{bmatrix}$$

and Equations (10a) and (11a) become

$$P_i = \sum_j d_{ij}\sigma_j \qquad (4\text{-}13)$$

and

$$\gamma_j = \sum_i d_{ij}F_i \qquad (4\text{-}14)$$

$(i = 1,2 \text{ or } 3 \text{ and } j = 1,2,\ldots 6)$

Equation (4-14) applies to a stress-free crystal. Similarly Equation (4-13) applies to a field-free, open-circuit situation.

In cases where these conditions are not present, Equations (4-13) and (4-14) must be extended as follows

$$P_i = \sum_j d_{ij}\,\sigma_j + \sum_k \varkappa^{\sigma}_{ik}\,\varepsilon_o F_k \qquad (4\text{-}15a)$$

(i and k = 1, 2, 3 and j and l = 1, 2 ...6)

$$\gamma_j = \sum_i d_{ij}\,F_i + \sum_l S^{F}_{jl}\,\sigma_l \qquad (4\text{-}15b)$$

The superscripts σ and F have the following meaning:

$$\varkappa^{\sigma}_{ik}\,\varepsilon_o = \left(\frac{\partial P_i}{\partial F_k}\right)_{\sigma} \quad \text{and} \quad S^{F}_{jl} = \left(\frac{\partial \gamma_j}{\partial \sigma_l}\right)_{F}$$

$$\text{Similarly: } d_{ij} = \left(\frac{\partial P_i}{\partial \sigma_j}\right)_{F} = \left(\frac{\partial \gamma_j}{\partial F_i}\right)_{\sigma} \qquad (4\text{-}16)$$

This means that the direction of the polarization associated with a given strain is always the same, whether strain and polarization are due to mechanical forces or to an impressed electric field[16]. This result is of importance in section 4-6.

In the present case, the piezoelectric ceramics were to be glued into the vibrating column. A precise calculation of their behavior according to Equations (4-15a) and (4-15b) would have been very laborious and the approximations represented by Equations (4-13) and (4-14) were therefore used. For this class of crystal (C_{6v} hexagonal), Relation (4-13) can be written

	σ_1	σ_2	σ_3	σ_4	σ_5	σ_6
P_1	0	0	0	0	d_{15}	0
P_2	0	0	0	d_{15}	0	0
P_3	d_{31}	d_{31}	d_{33}	0	0	0

(4-17)

since, from symmetry considerations, $d_{24} = d_{15}$ and $d_{32} = d_{31}$. Relation (4-14) can be written similarly.

The values of these piezoelectric coefficients for PZT4 are[17]:

$d_{31} = -130 \times 10^{-12}$ Coulombs/Newton
$d_{33} = +300 \times 10^{-12}$ Coulombs/Newton
$d_{15} = +450 \times 10^{-12}$ Coulombs/Newton

Equation (4-12) for C_{6v} crystals can be written (using the short notation for the elastic constants):

	γ_1	γ_2	γ_3	γ_4	γ_5	γ_6
σ_1	S_{11}	S_{12}	S_{13}	0	0	0
σ_2	S_{12}	S_{11}	S_{13}	0	0	0
σ_3	S_{13}	S_{13}	S_{33}	0	0	0
σ_4	0	0	0	S_{44}	0	0
σ_5	0	0	0	0	S_{44}	0
σ_6	0	0	0	0	0	$2(S_{11}-S_{12})$

(4-18

The values of these compliances for PZT4 are[17]:

$S_{11} = 12 \times 10^{-12}$ m^2/Newton
$S_{12} = -3.7 \times 10^{-12}$ "
$S_{13} =$ —— "
$S_{33} = 15 \times 10^{-12}$ "
$S_{44} = 39 \times 10^{-12}$ "

The relative dielectric permittivities ε_r of PZT4 are:

$$\varepsilon_{22}/\varepsilon_o = \varepsilon_{11}/\varepsilon_o = 1360 \; ; \quad \varepsilon_{33}/\varepsilon_o = 1200$$

and $\varepsilon_o = 9.10^{-12}$ Coul/Vm

With these parameters in mind, the practical performance of the ceramics can be estimated.

For the driver, the fields F_1 and F_2 are zero. Application of F_3 therefore results in the strains:

$$\gamma_1 = \gamma_2 = d_{31}F_3 \quad \text{and} \quad \gamma_3 = d_{33}F_3$$

γ_3 is the strain of interest in the deformation of the sample. If a displacement of 0.3 microns (3×10^{-7}m) is required,

$$\gamma_3 = \Delta l/l = 3x10^{-7}/l$$

where l is the thickness of the driver. The electric field F_3 inducing the strain is $F_3 = \Delta V/l$, where ΔV is the applied voltage.

Therefore $\Delta l/l = d_{33} \cdot \Delta V/l$

and $\Delta V = 3\times10^{-7}/3\times10^{-10} = 10^3$ Volts

As mentioned previously, the electric field must be kept below 1000 Volts/cm. Consequently, the thickness of the driver was made one centimeter. The effects of the perpendicular strains γ_1 and γ_2 are discussed later in this chapter.

For the pick-up crystal, if all stresses except σ_3 are assumed to be zero, the only equation that remains of Equation (4-17) is

$$P_3 = d_{33}\,\sigma_3$$

ε_r has such a large value for PZT4 (≈ 1200) that $\varepsilon_r \approx \kappa$ and

$$P_3 \approx D_3 = \varepsilon_o\,\varepsilon_r F_3$$

so that

$$F_3 = \left(d_{33}/\,\varepsilon_o\,\varepsilon_r\right)\sigma_3 = g_{33}\,\sigma_3 \qquad (4\text{-}19)$$

where $g_{33} = 28.3\times10^{-3}$ Vm/Newton.

Equation (4-19) shows that for maximum voltage from the pick-up the thickness of the pick-up should be large and its cross-section small. However, the smaller the cross-section, the larger the stress on the glue joints, while a large thickness influences considerably the resonance frequencies of the whole column.

A compromise was found by making the thickness of the pick-up equal to that of the driver, namely one centimeter, and the diameter of the column three centimeters.

The length of the piston M_2 was chosen to be 4.5 cms. The total length of the column, including insulating spacers, became 7 cm.

4-4 Operating limits.

The following physical limitations of the design will impose limits on the modulus and frequency ranges that can be covered.

a) The bending and longitudinal vibrations in the column
b) The dimensions of the sample
c) The frequency limits of the electronic apparatus
d) The finite modulus of the piston
e) The sensitivity of the force transducer

a) Resonance of the column vibrating as a cantilever must be avoided. The resonance frequency ν_o of such a cylindrical rod is given by[15)]

$$\nu_o = \frac{r_o}{\pi L^2} \sqrt{\frac{E_c}{B_n \rho_i}} \qquad (4\text{-}20)$$

where L = length of the rod = 0.07 m
r_o = radius of the rod = 0.015 m
E_c = average Young's modulus at the base of the rod = 7×10^{10} Newton/m^2
(The moduli of quartz glass and of PZT4 are almost equal to this average value.)
ρ_i = average density of the rod = 8×10^3 Kg/m^3
(The densities of invar and PZT4 are almost equal to this average.)
B_n is a numerical constant, which, for the lowest harmonic, is equal to 0.974.

With these values ν_o is found to be = 2.9×10^3 c/s. This resonance frequency was increased by boring out the center of the invar piston and a further increase is obtained by the damping effect of the sample. As a result of these effects, cantilever resonance was not observed below 5000 c/s.

At high frequencies, phase differences can occur between the displacement at the force transducer and at the bottom of the piston. The combined lengths of these should therefore be small compared to the longitudinal wavelength λ_a, which is independent of the presence of polymer;

λ_a is given by $\lambda_a = \frac{\sqrt{(E_i/\rho_i)}}{\nu_a}$ (4-21)

where E_i = Young's modulus of invar = 2.0×10^{11} N/m^2.

At 4000 c/s λ_a is then 1.25 m. The distance from the pick-up to the displacement transducer core was 6.5 cm, or about $\lambda_a/20$. This is equivalent to a phase difference of 18^o, which was assumed to be the upper limit at which a correction for this phenomenon can still be made.

b) For reasons similar to those cited just above, the thickness of the sample must be kept smaller than one tenth of the shear wavelength λ_r through the polymer solution. Since the gap between the cylinders was chosen to be 0.3 mm, the shortest wavelength allowed was 3 mm. The shear wavelength λ_r is approximately given by

$$\lambda_r = \frac{\sqrt{(G'/\rho)}}{\nu_r} \quad (4\text{-}22)$$

where ρ = density of polymer solution $\approx 10^3$ kg/m^3.

Since $G' = \rho \lambda_r^2 \nu_r^2$ it follows that, at ν_r = 100 c/s, the minimum allowable G' is 90 Newton/m^2 and at $\nu_r = 10^4$ c/s the minimum allowable G' is 9×10^5 Newton/m^2.

c) The impedance Z_{c1} of the driver limits the frequency range of the power amplifier. The capacity of the driver was calculated to be 765 pF, to which must be added the capacity of the feed cable, estimated at 250 pF. The impedance of this combination is then

$$Z_c = 1/(j\omega C) \approx -j/(\omega \times 10^{-9}) \ \Omega$$

The current at 1000 V and 5000 c/s is then about 32 mA. The high fidelity power amplifier purchased to meet this requirement had a lower frequency limit of 10 c/s.

d) With a polymer solution of very high modulus, the piston will be compressed so that the displacement will be different at the two ends of the piston.

Assuming that the stress gradient in the piston is still linear when these displacements differ by 20%, the modulus of the polymer can still be measured by introducing a correction.

At this limit

$$f/A = E_i . \Delta L_i/(k.L_i) \qquad (4\text{-}23)$$

where ΔL_i, the change in length of the piston, is 20% of the displacement amplitude, which has a maximum value of 0.3 microns and E_i = the Young's modulus of invar = 2.0×10^{11} N/m^2.
A = cross sectional area of the piston = 7.07×10^{-4} m^2
L_i = length of the piston = 4.5×10^{-2} m^2
k = 0.55, a correction factor for the effective length of the piston, to take account of the fact that the stress in the piston decreases linearly and is zero at the free end.

The maximum allowable force on the piston is then, from Equation (4-23):

$$f_{max} = 337 \text{ N}$$

Equation (4-8) without correction term gives

$$G^* = f^*/(b.x^*) \quad \text{or} \quad G' = f_o \cos\delta /(b\, x_o) \qquad (4\text{-}24)$$

where $b = 2\pi h/\ln(R/r_o)$, the form factor for the Pochettino geometry and f_o and x_o are the amplitudes of f^* and x^*, h = the height of the polymer = 4×10^{-2} m which gives b = 12.7 m.
If $x_o = 0.3 \times 10^{-6}$ m and $f_o = 3.37 \times 10^2$ N and $\cos\delta \approx 0.7$
Equation (4-24) gives

$$G'(max) = 6.2 \times 10^7 \text{ N/m}^2$$

e) Assuming that the minimum measurable signal from the pick-up is 1 mV, Equation (4-19) gives a minimum measurable force of 2.5×10^{-3} N.

From Equation (4-24), assuming the same $\cos\delta$ and x_o, the lower limit of the polymer shear modulus becomes

$$G'(min) = 4.6 \times 10^2 \text{ N/m}^2$$

The limits discussed above are illustrated in Figure 4-3, where they are labelled according to above paragraphs.

Fig. 4-3

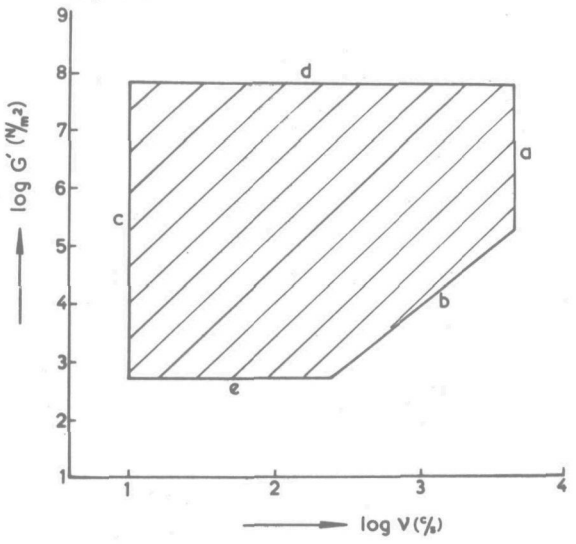

4-5 Calibration of the pick-up.

Consider the forces acting on the pick-up. They can be expressed by

$$f_t^* = bx^* G^* + kx^* + m_e \ddot{x}^* \qquad (4\text{-}25)$$

where f_t^* = the total force.

$bx^*G^* = f^*$ = the force due to the presence of the polymer

kx^* = the force due to the Teflon foil T.

$m_e\ddot{x}^*$ = the force required to accelerate the parts of the column below and including the pick-up.

The mass m_e is the sum of the effective masses of these parts, where the effective mass of the pick-up is one half its real mass. The superscript * denotes complex quantities.

If $x^* = x_o \exp(i\omega t)$ then $f_t^* = f_{t,o}^* \exp(i\omega t)$, where $f_{t,o}^*$ is a complex quantity because G^* is generally complex. Inserting this in Equation (4-25) yields

$$f_{t,o}^* = b\, x_o(G' + i\, G'') + k\, x_o - m_e\, \omega^2 x_o \qquad (4\text{-}26)$$

Calibration of the pick-up is thus possible by vibrating the rheometer in the absence of polymer and "Teflon" foil. Vibrating the rheometer with only the "Teflon" foil in place, permits determination of the elastic constant k, after which the polymer can be put in and $f^*_{t,o}$ measured. G' and G" can then be calculated from

$$f^*_{t,o}/x_o = (b\,G' - m_e\omega^2 + k) + i\,b\,G'' =$$

$$= |f^*_{t,o}/x_o|\,(\cos\varphi + i\,\sin\varphi) \qquad (4\text{-}26a)$$

Because of the change in the piezoelectric constants with temperature, the calibration must be carried out at all temperatures at which the viscoelastic properties are to be measured.

4-6 Mechanical coupling between the driver and the pick-up.

Early experiments with the apparatus shown in Figure 4-1 indicated the need for an improvement. The lateral strains γ_1 and γ_2 of the driver mentioned in section 4-3 would have no effect if the material between driver and pick-up had an infinite rigidity.

In fact, two undesired vibration modes are imparted by the driver to the column and induce very large unwanted signals at the pick-up. The first of these is the simple transmission of the strains γ_1 and γ_2 in transverse waves along the surface. The second is due to the fact that the driver is glued to two pieces which are not equally flexible. The result is that, for instance if γ_1 and γ_2 are positive, the driver C_1 tends to assume a shape as shown in Figure 4-4, where a and b are the undeformed and deformed states. The arrows indicate the direction of pre-polarization.

The two modes make contributions to the disturbance at the pick-up which are unknown in magnitude but opposite in phase for the following reasons. In the first mode, a positive γ_1 and γ_2 at the driver will induce a positive γ_1 and γ_2 at the pick-up, giving a signal in phase with that at A according

Fig. 4-4
(not to scale)

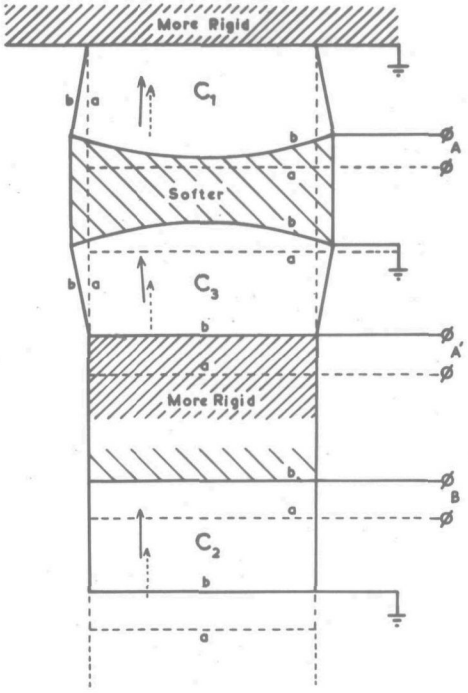

to Equation (4-16). In the second mode, a positive γ_1 and γ_2 will impart a convex curvature to the driver (as in Figure 4-4) which will in turn induce a concavity in the pick-up, giving a signal opposite in phase with that at A again according to Equation (4-16). To eliminate the resulting effect on the pick-up, it is then necessary to weaken the stronger of the two modes.

Both modes can be compensated by the introduction in the column of a third ceramic C_3 (the "compensator") as shown in Figure 4-4. The compensation of the first mode clearly requires a voltage on A' which is opposite in phase with that at A. The manner in which the compensator eliminates the effect of the second mode is shown in Figure 4-4, where the voltage at A' must clearly be in phase with that at A. Thus a suitable voltage at A' should, by weakening the stronger mode and strenghtening the weaker, lead to complete compensation of the disturbing signal at C_2.

These considerations were not verified individually. The only support of their validity is the fact that it was found possible to adjust the voltage at A' so as to give a signal at C_2 less than 1 mV at low frequencies. Since this voltage had to be in phase with that at A, it was supplied from a voltage divider circuit between A and ground.

In the empty rheometer, the only signal remaining is then due to $(-m\omega^2 + k)x^*$.

This construction worked satisfactorily at room temperature but at low temperatures (below $-60^{\circ}C$), the glue layer tends to become brittle. The stresses set up by the opposite curvatures

of C_1 and C_3 then caused failure of the joints. This problem was overcome by the use of ceramics in which a cylindrical hole was drilled out of the center, reducing the cross-sectional area by about one half. The three solid ceramics were thus replaced by three tubes of the same outside dimensions and a wall thickness of about 4 mm.

The construction with hollow ceramics gave more reproducible results and required much lower voltages at A' ($\approx$ 0.07 of A) to suppress the effects of the two disturbing deformation modes. Even so, use of glued vibrating columns sets limits to the operating temperatures that can safely be used. Measurements were made at -80° to $+30^{\circ}$ without causing failure of the joints, but it was felt that lower temperatures might lead to fracture and time consuming repairs. The upper limit could probably be increased to $+80^{\circ}$ if the need arose.

4-7 Additional details.

The glued construction of the column made impossible the use of the usual deposited-silver electrodes. It was found necessary to have all parts of the column ground optically plane-parallel and to use thin invar plates glued to the ceramics as electrodes.

Minute sparks across the edges of the ceramics and the electrodes were observed at high voltages (>800 V). These were satisfactorily suppressed by smearing a fluorocarbon grease (Kel F90, 3M Company, Minnesota) on the spark sites.

Since the rheometer was to be suitable for measurements on dilute gels as well as on polymer solutions, the sample gap must contract with decreasing temperature, in order to prevent the sample from becoming detached from the wall. Assuming an average volume expansion coefficient for the samples of $10^{-3}/^{\circ}C$, the gap was found to expand by the same amount if the outer cylinder was made of brass.

To fill the sample gap with a polymer solution which was very viscous, it was found necessary to inject the solution through a hole in the brass cylinder using a hypodermic syringe fitted with a nozzle which screwed into the hole.

The temperature at the center of the rheometer was measured

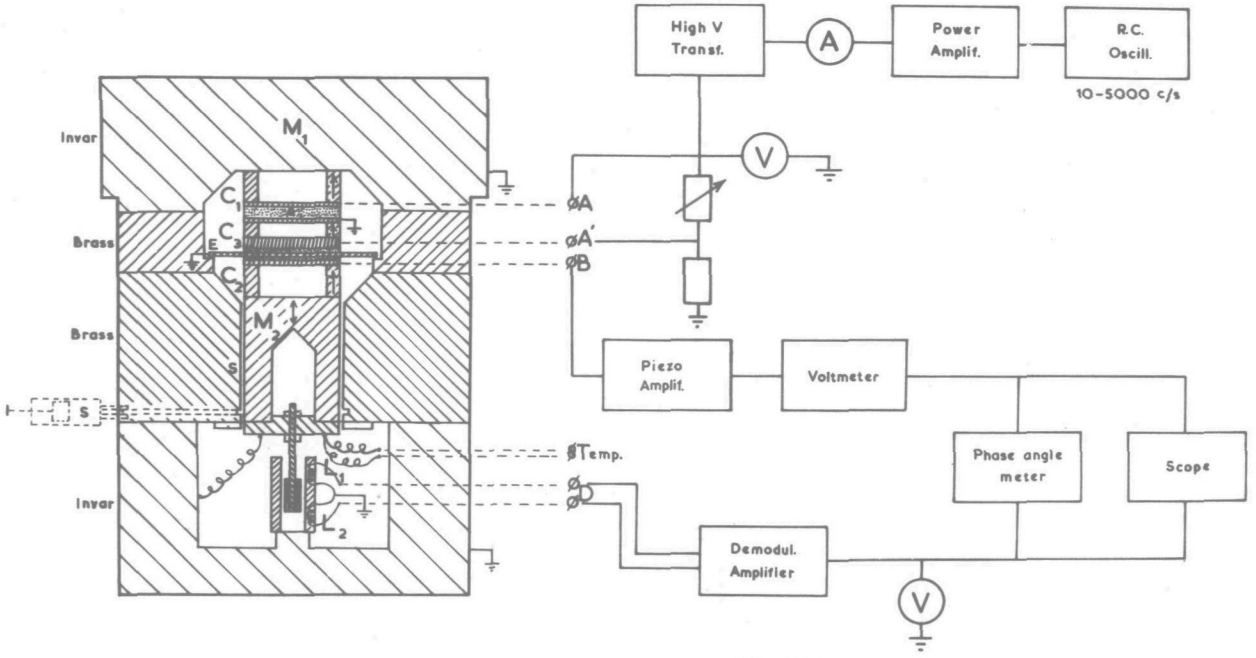
High V Transf.
A
Power Amplif.
R.C. Oscill.
10-5000 c/s
V
Invar
Brass
Brass
Invar
M1
M2
C1
C3
C2
E
S
øA
øA'
øB
øTemp.
Piezo Amplif.
Voltmeter
Phase angle meter
Scope
Demodul. Amplifier
V

Fig. 4-5

with a copper-constantan thermocouple, attached to the lower end of the piston.

A detailed drawing of the rheometer is included at the end of this thesis.

4-8 Electronic components.

Figure 4-5 is a diagram of the final form of the rheometer and of its auxiliary circuitry.
The following is a detailed list of the electronic parts.
R.C. Oscillator: A Hewlett-Packard low frequency oscillator, model 202C with a frequency range of 1 c/s to 100 Kc/s.
Power Amplifier: A Unitran N.V. (Weesp, Holland) 100-W high fidelity power amplifier, with a range of 10 c/s to 20 Kc/s. The output was fed to a high-ratio, 100-W transformer, also suitable from 10 c/s to 20 Kc/s.

The capacitive load C_1 on the transformer output was balanced by a variable inductance across the input, which was adjusted at each frequency in order to minimize the amplifier output current.
Piezo Amplifier: Because of the high output impedance of the pick-up ceramic, a special 10^{14}-ohm input impedance piezo amplifier was used (Type TA-1/B, Vibro-meter Corp., Fribourg, Switzerland). This amplifier had a frequency range of 0 -150 Kc/s, an output impedance of 50 ohms, and a maximum output of 1 V. The amplification, controlled by an attenuator was 2.25 in the most sensitive range.

Traces of water or other conducting impurities tended to condense on the surface of the pick-up when the apparatus was cooled. These were successfully removed by electrolizing with a 300 V DC. voltage applied for several hours before measuring.
Voltmeter Amplifier: The signal from the piezo amplifier was measured with a Rohde & Schwarz (München) type UVN millivolt-meter amplifier, having a maximum amplification of 1000. The output at full scale deflection on the meter was 1 V. The frequency range was from 10 c/s to 100 Kc/s.
The demodulating Amplifier and the inductive displacement pick-up were both made by Hottinger Messtechnik GMBH, Darmstadt.

The displacement pick-up (Type W1E/3) had a sensitivity of

70 mV/V/mm displacement. Its working temperature range was from -100° to $+150^{\circ}$C. It was fed with a 5V - 50 Kc/s excitation current from the Demodulating Amplifier, which made it possible to measure vibration displacements with frequencies from 0 to 10 Kc/s.

The Demodulating Amplifier (Type KWS II/50) has, in the most sensitive position a high frequency output noise of 22 mV. In this position, a 0.5 micron displacement gave an output of 4 V. Thus, accurate measurement of displacement amplitudes as small as 0.1 microns was possible.

Phase angle meter and oscilloscope. The amplified force and displacement signals were fed to an AD-YU phase angle meter, Type 405L(AD-YU Electronics, Passaic, N.J.) and to a Hewlett-Packard, Type 130C oscilloscope in parallel.

The phase angle meter had a frequency range of 1 c/s to 40 Kc/s and required two input signals of at least 0.3V. The accuracy was $\pm$ 15'.

The oscilloscope was only used for inspection of the wave-form and of the sign of the phase angle, although it could have been used for phase angle measurements also, but to a lower accuracy.

4-9 Low temperature bath.

The rheometer was cooled or heated to the required temperature by enclosing it in a waterproof brass enclosure, which was immersed in an alcohol bath. The bath was heat insulated with a thick layer of polystyrene foam and was cooled to -77°C by dropping chopped solid CO_2 into the alcohol. Further cooling could be achieved by blowing liquid nitrogen through copper coils in the liquid, which was meanwhile kept gently stirred. The bath temperature could be raised by means of a 22-ohm electric heating coil.

References (Chapter 4)

1) T.L. Smith, J.D. Ferry & F.W. Schremp;
J. Applied Phys. 20, 144 (1949)
2) E.R. Fitzgerald; Phys. Rev. 108, 690 (1957)
3) M.H. Birnboim & J.D. Ferry; J. Applied Phys. 32, 2305 (1961)
4) W. Philippoff; J. Applied Phys. 34, 1507 (1963)
5) J.H. Dillon, I.B. Prettyman & G.L. Hall;
J. Applied Phys. 15, 309 (1944)
6) E.A.W. Hoff; J.Polymer Sci. 9, 41 (1952)
7) H.C. Rorden & A. Grieco; J.Applied Phys. 22, 842 (1951)
8) W. Philippoff; J.Applied Phys. 24, 685 (1953)
and 25, 1102 (1954)
9) H. Goldberg & O. Sandvik; Ind.Eng.Chem.Anal.Ed. 19, 123 (1947)
10) J.W.A. Labout; Rheologica Acta 1, 186 (1958)
11) B. Vinzelberg; Rheologica Acta 3, 55 (1963)
12) D.O. Miles; J.Applied Phys. 33, 1422 (1962)
D.O. Miles & G.C. Knollman; J.Applied Phys. 35, 2549 (1964)
13) A. Pochettino; Nuovo Cimento 8, 77 (1914)
14) T.G. Fox & P.J. Flory; J.Am.Chem.Soc. 70, 2384 (1948)
15) J.D. Ferry; Viscoelastic Properties of Polymers, John Wiley
& Sons Inc., N.Y. (1961), p 107 and 132
16) W.G. Cady; Piezoelectricity, McGraw Hill, Comp. (1946)
17) Landolt Börnstein; (6th edition) II Band, Volume 6,
Electrical Properties I, p 414 ff. (1959)

CHAPTER 5

EXPERIMENTS AND RESULTS

In this chapter, the theory of Chapter 2 is checked against some detailed results on a poly-n-octyl methacrylate fraction, published by Ferry and co-workers[1-4]. Results are then given of measurements on a solution of poly-methyl acrylate in toluene, made with the rheometer described in Chapter 4.

5-1 Examples of computations of H[m-1].

The treatment given in section 2-2 is illustrated by the following examples. A hypothetical molecule was chosen, with a length of 1879 submolecules and whose motion was restricted by 72 slow points. Then $N = 1879$ and $m = 73$. The computer instructions outlined in section 2-2 were then programmed in ALGOL 60[5].

The program is given in the Appendix, together with an example of the type of input data used for the molecule. The third number in the first row is λ_1, the fourth number is δ, and the fifth is the square of the relative machine precision. The remaining 73 numbers represent distances (in numbers of submolecules) between consecutive slow points. These 73 numbers were randomly chosen and represent only one of the many possible distributions of slow points along the chain.

The calculations were carried out by a Telefunken TR4 computer. The output consisted of a table giving the number of relaxation times in each interval $\Delta \log \tau_R$, where $\tau_R = 1/\lambda$. This number is equal to 2.303 H[72], where H[72] is the discrete relaxation spectrum of one molecule with 72 slow points and where each line in the spectrum has unit height.

This calculation was repeated with four other distributions of slow points, and the average of these five spectra was obtained. Figure 5-1 shows the results of the above process for four different values of δ, converted into continuous spectra.

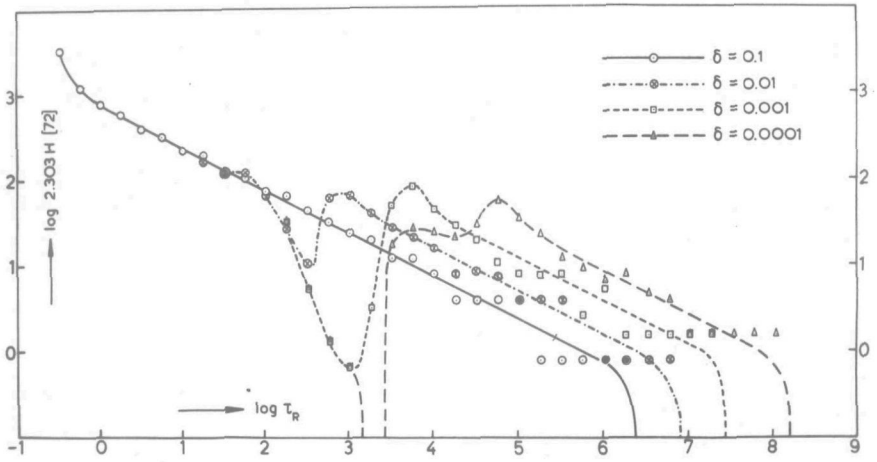

Fig. 5-1. Relaxation spectrum 2.303 H [72] for one molecule containing 1879 submolecules and 72 slow points.

It can be seen that the larger values of δ do not alter the Rouse spectrum, as already reported in section 2-2.

5-2 Calculations with poly-n-octyl methacrylate (POMA).

The preparation and fractionation of the sample used by Ferry and co-workers is described by Chinai et al.[1]. The relaxation spectrum was obtained partly from dynamic and partly from transient-loading experiments[2-4] for the fraction with $\bar{M}_w = 3.62 \times 10^6$. The $\bar{M}_n$ of the fraction is not known but it is shown below that this quantity is not critical.

It follows from section 5-1 that to compare the theory with Ferry's results, the latter must be divided by nkT (to give the spectrum for one molecule with lines of unit height) and multiplied by 2.303 (to change the abscissa from $\ln\tau$ to $\log\tau$). For an undiluted polymer nkT can be replaced by $\rho RT/\bar{M}_n$, where ρ is the density of the polymer.

In section 2-4 it was shown that: $\nu_e = \nu - n$. For a single molecule, this equation reduces to: $\nu_{eR} = \nu_R - 1$.

For a rough estimate of n, the $\bar{M}_n$ was chosen as 2.71×10^6. Then the resulting reduced relaxation spectrum $2.303\ H_R$ for one molecule is as given in Table 5-I. A plot of $2.303\ H_R$ vs. $\log\tau$ can now be drawn and the area under the hump measured. This area is equal to $\frac{1}{2}\nu_{eR}$ lines. The integration yields $\frac{1}{2}\nu_{eR} = 31$ lines,

Table 5-I

Calculation of the degree of polymerization between entanglement points of poly-n-octyl methacrylate at 100°C, for $\bar{M}_w/\bar{M}_n = 1.336$.

Log τ	log H(dyn/cm^2)	log(2.303 H_R)	2.303 H_R	
-5.0	6.06	2.39	245	
-4.0	5.54	1.87	74.1	
-3.0	5.00	1.33	21.4	
-2.0	4.60	0.93	8.51	
-1.5	4.41	0.74	5.50	<...(min)
-1.0	4.37	0.70	5.01	
-0.5	4.47	0.80	6.31	
0	4.56	0.89	7.76	
0.5	4.68	1.01	10.23	
1.0	4.79	1.12	13.18	
1.5	4.58	0.91	8.13	
2.0	4.35	0.68	4.79	
2.5	4.09	0.42	2.63	
3.0	3.73	0.06	1.15	
3.5	3.39	-0.28	0.52	

$\bar{M}_w = 3.62 \times 10^6$; $\bar{M}_n = 2.71 \times 10^6$; $M_o = 1.98 \times 10^2$.

$\rho RT/\bar{M}_n = 1.07 \times 10^4$ dyn/cm^2.

$\log(2.303) - \log(1.07 \times 10^4) = -3.67$

$$\int_{-1.25}^{\infty} 2.303 H_R \, d \log\tau = 30.98 \approx 31 \text{ lines with unit height.}$$

$\nu_{eR} = 62 \longrightarrow \nu_R = 63 \longrightarrow$ 64 entangl/mol $\longrightarrow$ m = 65.

$\bar{Z}_n = 2.71 \times 10^6/198 = 1.37 \times 10^4 \equiv 570$ submolecules (each 24 monom.)

$\bar{Z}_e = 1.37 \times 10^4/65 = 211$ (at 100°).

Table 5-II

Calculation of the degree of polymerization between entanglement points of poly-n-octyl methacrylate at 100°C, for $\bar{M}_w/\bar{M}_n = 1.075$

log τ	log H(dyn/cm^2)	log(2.303 H_R)	2.303 H_R	
-5.0	6.06	2.49	309	
-4.0	5.54	1.97	93.3	
-3.0	5.00	1.43	26.9	
-2.0	4.60	1.03	10.72	
-1.5	4.41	0.84	6.92	...(min)
-1.0	4.37	0.80	6.31	
-0.5	4.47	0.90	7.94	
0	4.56	0.99	9.77	
0.5	4.68	1.11	12.88	
1.0	4.79	1.22	16.60	
1.5	4.58	1.01	10.23	
2.0	4.35	0.78	6.03	
2.5	4.09	0.52	3.31	
3.0	3.73	0.16	1.45	
3.5	3.39	-0.18	0.66	

$\bar{M}_w = 3.62 \times 10^6$; $\bar{M}_n = 3.37 \times 10^6$; $M_o = 1.98 \times 10^2$.

$\rho RT/\bar{M}_n = 0.86 \times 10^4$ dyn/cm^2.

$\log(2.303) - \log(0.86 \times 10^4) = -3.57$.

$\int_{-1.25}^{\infty} 2.303\, H_R \, d \log \tau = 39.29 \approx 39$ lines with unit height.

$\nu_{eR} = 78 \longrightarrow \nu_R = 79 \longrightarrow 80$ entangl/mol $\longrightarrow m = 81$.

$\bar{Z}_n = 3.37 \times 10^6/198 = 1.705 \times 10^4 \equiv 710$ submolecules (each 24 monom)

$\bar{Z}_e = 1.705 \times 10^4/81 = 211$ (at 100°C).

whence $\nu_R = 63$. Thus there are 64 entanglements per molecule and m = 65. With a monomer molecular weight of $M_o = 198$, the number average degree of polymerization between entanglements is

$$\bar{Z}_e = \frac{2.71 \times 10^6}{198 \times 65} = 211 \quad (\text{at } 100^\circ\text{C})$$

When $\bar{M}_n$ was chosen as 3.37×10^6, $\bar{Z}_e$ was again found to be 211 (see Table 5-II). The method is therefore not sensitive to the accuracy of the molecular weight determination.

This value of $\bar{Z}_e$ compares well with those obtained by other methods[4], which range from 250 to 580 monomer units.

If, for POMA, one submolecule is chosen to be 24 monomer units long, then an $\bar{M}_n$ of 2.71×10^6 is equivalent to 570 submolecules, while an $\bar{M}_n$ of 3.37×10^6 is equivalent to 710 submolecules.

These two cases are considered below. The relaxation spectrum $H_{ent.}(570)$ for a molecule having 570 submolecules and 64 entanglement points was calculated as follows. Each term in Equation (2-53) was obtained by a procedure like that in section 5-1, with a δ value of 8×10^{-6}, which was chosen for the best fit of the final spectrum with the experimental data. The summation was carried out up to the term in H[1], i.e. until k log2 = log(m-1). H[1] was chosen as the penultimate term. The last term was then taken to be H[0] and was given a coefficient such as to make the sum of all the coefficients in the series equal to unity. Equation (2-53) then became

$$H_{ent.}(570) = \tfrac{1}{4}.H[64] + 3/8.H[32] + \ldots + 3/256.H[1] + 3/256.H[0] \qquad (5\text{-}1)$$

where the last term in the series is clearly the spectrum of a Rouse molecule. The calculation of the spectrum for one slow point distribution for H[32] is given as an example.

Table 5-III gives the input data and Table 5-IV gives the output from the computer. For the evaluation of the series, 36 such operations were carried out. Figure 5-2 is the averaged H[32] spectrum converted to a continuous curve.

A similar spectrum was obtained for each term in the series and Figure 5-3 is the curve of $H_{ent.}(570)$ obtained by the summation in Equation (5-1). Since $H_{ent.}$ and $2.303\ H_R$ are equivalent

Table 5-III

Input data for the calculation of H[32].

```
= = a 6,
u = 20, r = 2,
+ 33, + 570, + 4, + 8 10-6, + 10-20,
+ 14, + 22, + 12, + 6, + 10, + 24, + 10, + 16, + 15, + 17, + 12,
+  8, + 11, + 14, + 7, + 13, + 25, + 13, + 15, + 19, +  3, + 11,
+ 16, + 20, + 21, + 9, + 23, + 18, + 28, + 26, + 32, +  9, +  5;
```

Table 5-IV

Output data for the spectrum H[32]

$\log\tau_R$			2.303 H_R	$\log\tau_R$			2.303 H_R
-0.60206	to	-0.35164	245	2.90382	to	3.15424	0
-0.35164	"	-0.10122	94				
-0.10122	"	+0.14920	58	5.15760	"	5.40802	0
+0.14920	"	+0.39962	41	5.40802	"	5.65844	4
0.39962	"	0.65004	31	5.65844	"	5.90886	7
0.65004	"	0.90046	20	5.90886	"	6.15928	8
0.90046	"	1.15088	16	6.15928	"	6.40970	2
1.15088	"	1.40130	15	6.40970	"	6.66012	4
1.40130	"	1.65172	9	6.66012	"	6.91054	0
1.65172	"	1.90214	7	6.91054	"	7.16096	2
1.90214	"	2.15256	3	7.16096	"	7.41138	2
2.15256	"	2.40298	0	7.41138	"	7.66180	0
2.40298	"	2.65340	0	7.66180	"	7.91222	0
2.65340	"	2.90382	0	7.91222	"	8.16264	0
				8.16264	"	8.41306	2

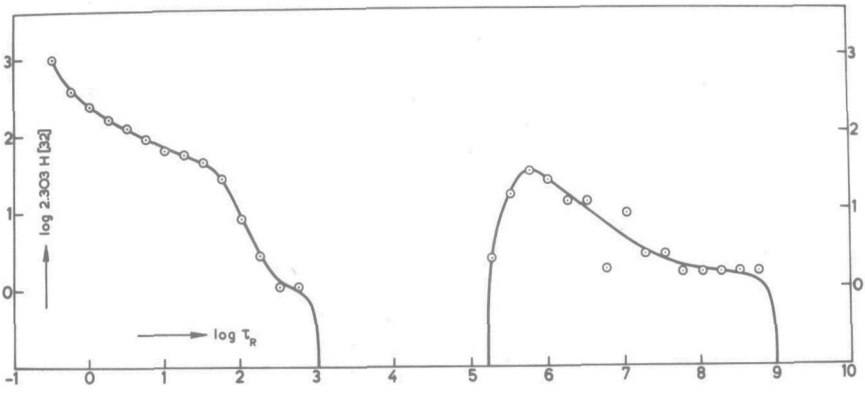

Fig. 5-2. Relaxation spectrum for one molecule of 570 submolecules containing 32 slow points. The slip parameter $\delta = 8 \times 10^{-6}$.

the experimental values calculated in Table 5-I are also plotted in Figure 5-3.

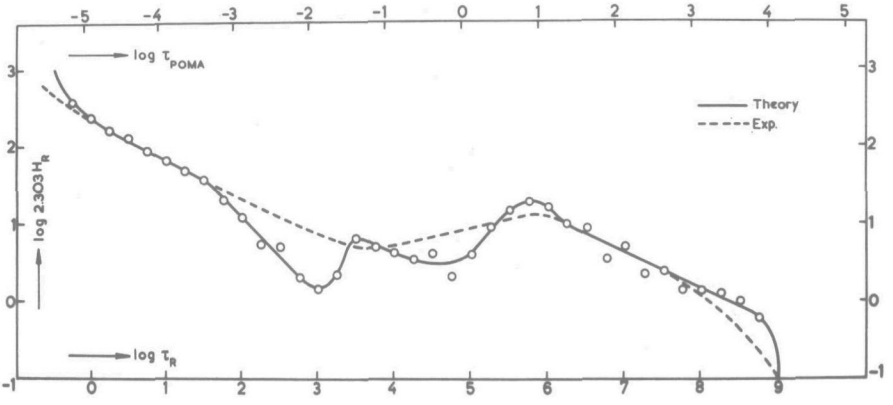

Fig. 5-3. Relaxation spectrum of POMA compared with a hypothetical monodisperse polymer containing 570 submolecules and 64 entanglements per molecule. The slip parameter δ is chosen as 8×10^{-6}

It can be seen that the value of $\delta = 8 \times 10^{-6}$ causes the curves to coincide in both the right and the left hand regions where the slopes are $-\frac{1}{2}$. This value of δ was arrived at as follows: a few spectra were calculated as in Figure 5-3 for different values of δ, and the slopes of $-\frac{1}{2}$ on the left, which all coincided were made to fit with that of the experimental curve. The value of δ for the best fit on the right could then

be found either by interpolation or by use of the property that the horizontal shift of the right hand side is approximately proportional to -log δ.

The left region with slope of $-\frac{1}{2}$ is the glass-rubber transition region and is not affected by the above modification for entanglements. Therefore this part of the curve must coincide with the spectrum predicted by the Rouse treatment which is characterized by the parameters a and ζ_o as calculated by Ferry[4]. From Equation (2-24b)

$$\tau_{POMA} = a^2q^2 \zeta_o \tau_R/6kT = D.\tau_R \qquad (5-2)$$

which gives the position of the relaxation times of the experimental curve with respect to the τ_R values. Substituting Ferry's values in Equation (5-2) the value of logD is found to be -4.9, which is also found on inspection of the two ascissae of Figure 5-3.

The relaxation spectrum $H_{ent.}(710)$ of a molecule having 710 submolecules and 80 entanglements with a δ value of 8×10^{-6} was also calculated, and is given in Figure 5-4. The left and right regions of slope $-\frac{1}{2}$ still coincide with the experimental spectrum in Table 5-II.

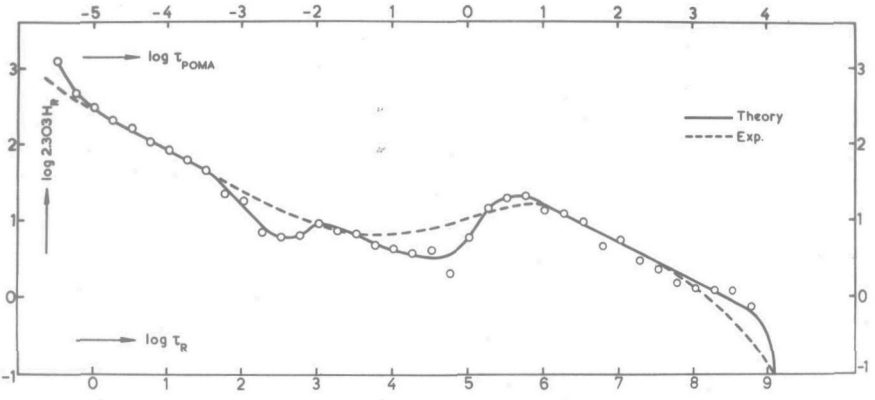

Fig. 5-4. Relaxation spectrum of POMA compared with a hypothetical monodisperse polymer containing 710 submolecules and 80 entanglements per molecule. The slip parameter δ is chosen as 8×10^{-6}

It is not possible to make a comparison of the experimental curve with a theoretical spectrum in which the molecular weight distribution is taken into acccunt, since the latter is not known. However, to show the effect of a finite molecular weight distribution, a hypothetical blend of four molecular weights, was considered. The blend is described in Table 5-V, where the first column gives the mole fractions and the second column the length of the molecules in number of submolecules.

Table 5-V

Composition of a hypothetical blend of 4 monodisperse samples.

n_i	M_i	$n_i M_i$	$n_i M_i^2$
0.2 mol.	850 submolec.	170	144500
0.3 "	710 "	213	151230
0.3 "	570 "	171	97470
0.2 "	430 "	86	36980

$$\bar{M}_n = \left[\sum_i n_i M_i\right] \Big/ \sum_i n_i = 640$$

$$\bar{M}_w = \left[\sum_i n_i M_i^2\right] \Big/ \sum_i n_i M_i = 672$$

$$\bar{M}_w / \bar{M}_n = 1.05$$

This rather narrow distribution has a $\bar{M}_w/\bar{M}_n$ ratio of 1.05. The spectrum $\langle H_{Mn} \rangle$ of this hypothetical sample was then the weighted average of the individual spectra, given by

$$\langle H_{Mn} \rangle = \sum_{i=1}^{4} n_i . H_{ent}(M_i) \qquad (5\text{-}3)$$

and is plotted in Figure 5-5.

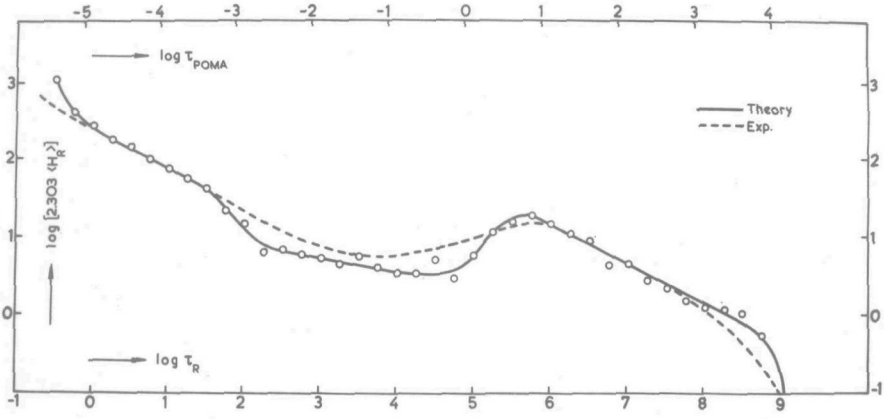

Fig. 5-5. Relaxation spectrum of POMA compared with a hypothetical blend of 4 molecular weights. The number average chain length is chosen as 640 submolecules and $\bar{M}_w/\bar{M}_n = 1.05$. The slip parameter δ is chosen as 8×10^{-6}

5-3 Conclusions from the results for POMA

Figures 5-3 to 5-5 show that the theoretical curves give a reasonable fit with experimental data. A precise fit cannot be expected for the monodisperse cases of Figures 5-3 and 5-4 since in practice, a sample must always have a finite molecular weight distribution. The strong effect on the theoretical relaxation spectrum of even a slight broadening of the distribution is illustrated in Figure 5-5. It is clear from the figure that for a test of the theory, a narrow fraction should be used, since a broad distribution tends to smooth out the important features (minimum and maximum) of the spectra. Even for such a narrow fraction, the molecular weight distribution must be known.

The spectrum for a broader distribution of molecular weights can be predicted from the theory, provided the distribution and, in addition, the parameters $\bar{Z}_e$ and δ are known.

The number of entanglements per unit chain length found from the experimental curve seems to be independent of the total chain length, provided the molecular weight is very high, as it is in the case considered.

A proof of the validity of the calculations performed by the computer is found in the slopes of $-\frac{1}{2}$ yielded by the calculations for the glass-rubber transition region of the

spectrum, and in the horizontal position of this part of the curve relative to the experimental spectrum. This position is fixed by Equation (5-2), where the molecular parameters a and ζ_0 have been calculated by Ferry.

The value of δ found by fitting the theoretical and experimental spectra is a constant which is independent of the arbitrarily chosen length of the submolecule. By changing this length the position of the maximum in the theoretical spectrum can be shifted along a line with a slope of $-\frac{1}{2}$. An estimate of the actual length of a submolecule can thus be obtained by suitably adjusting the position of this maximum.

5-4 Measurements with poly-methyl acrylate.

The rheometer described in Chapter 4 was assembled with the Teflon foil in position. A driving voltage was applied and the voltage at A' was adjusted so as to compensate not only for the unwanted modes but also for the additional signal kx^* due to the elasticity of the Teflon foil. For this adjustment, the voltage at A' was 6.43 per cent of the voltage at A.

The empty rheometer was then cooled to several temperatures, and at each one a set of measurements of force, displacement and phase angle (Φ_1) was made over the entire frequency range. These were the "zero measurements".

Since force and displacement were found to be exactly proportional, the force readings were all converted to a standard displacement signal of 1 V. These converted force signals (f_1) were plotted on log-log plots against frequency of which two examples are given in Figure 5-6. Except at very low frequencies, the plots were straight lines all with a slope of 2, in accordance with Equation (4-26).

From this curve, the sensitivity of the force transducer was readily obtained by making the proper substitutions in the relation:

$$f_o = - 4\pi^2 \nu^2 m_e x_o$$

where m_e is the effective vibrating mass and f_o and x_o the force and displacement amplitude at the frequency ν. The mass m_e was 0.2501 Kg and x_o was 1.25×10^{-7} m, giving a signal of 1 Volt. At 100 c/s, f_o was then 1.235×10^{-2} Newton, which on the graph was equivalent to 8.7 mV. The conversion factor C of the force

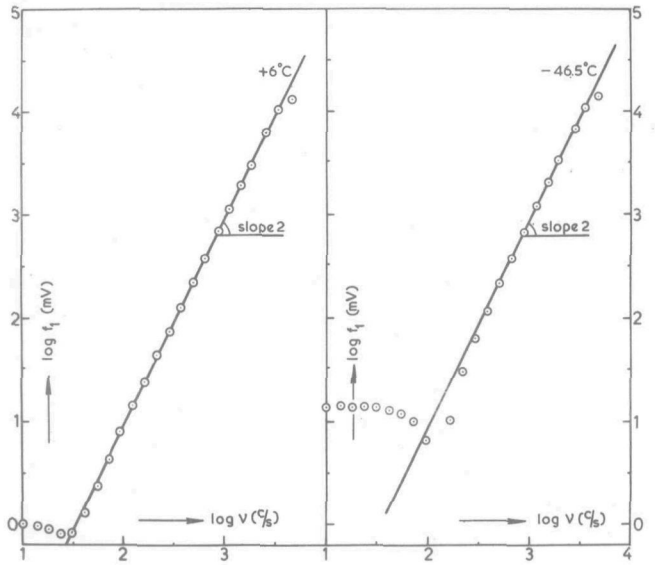

Fig.5-6. Pick-up calibration curves at +6°C and at -46.5°C.

transducer was therefore

$$1 \text{ mV} = 1{,}42 \times 10^{-3} \text{ N.} = \text{C}$$

This sensitivity was found to be almost independent of temperature.

The measured phase angle Φ_1 was not equal to the actual phase angle between the force vector f_1 and the displacement, but contained also a phase shift contributed by the electronic components of the amplifiers, which is dependent on frequency. This contribution (Φ_3) could be eliminated for those points in Figure 5-6 which lay on the straight line, since for them, the actual phase angle must be exactly 180°. For the points deviating from the straight line, the actual direction of zero phase angle was obtained from a second set of measurements where the Teflon foil was replaced by an elastic steel foil.

The molecular weight distributions of the polymers prepared by the anionic polymerization technique and by radical polymerization were not very different. The more easily prepared radically polymerized polymer was therefore used, whose $\bar{M}_w$, determined by light-scattering was 1.8×10^6.

This polymer was dissolved in toluene to a concentration of 14 per cent (by weight), after which the solution was slowly evaporated to a concentration of 25.5 per cent. The solution was injected into the rheometer by means of a hypodermic syringe, as described in Chapter 4.

The alcohol bath was cooled to - 77°C with solid CO_2 and the rheometer was allowed to reach equilibrium at this temperature over a 6-hour period. After the first set of force, displacement and phase angle measurements at this temperature, the bath was heated to the other pre-determined temperatures and the measurements were repeated.

These force measurements were also converted to a standard displacement signal of 1 Volt. The converted force signals (f_2) made a phase angle Φ_2 with the displacement. The suffix 2 was assigned to the "polymer measurements". The phase angles Φ_2 were also not equal to the actual phase difference between force and displacement.

Before the zero measurements could be subtracted vectorially from the polymer measurements, the phase shift Φ_3 must be subtracted from Φ_1 and Φ_2. If

$$\Phi_1 - \Phi_3 = \varphi_1$$

and $$\Phi_2 - \Phi_3 = \varphi_2,$$

the components of f_1 are $f_1 \cos \varphi_1$ and $f_1 \sin\varphi_1$ and the components of f_2 are $f_2 \cos \varphi_2$ and $f_2 \sin\varphi_2$.

Then $$f^* \cos \delta = f_2 \cos \varphi_2 - f_1 \cos\varphi_1$$

and $$f^* \sin \delta = f_2 \sin \varphi_2 - f_1 \sin\varphi_1$$

are the two components of the remaining electrical signal due only to the presence of the polymer, which is proportional to the complex modulus. These electrical signals were converted into Newtons by means of the conversion factor C obtained earlier.

The storage and loss moduli G' and G" were then calculated from

$$G' = (C.f^* \cos \delta)/bx = 1.119 \times 10^3 f^* \cos \delta$$

$$G'' = (C.f^* \sin \delta)/bx = 1.119 \times 10^3 f^* \sin \delta$$

and are shown in Figures 5-7 and 5-8. At high frequencies, determination of G" becomes increasingly inaccurate, since it is obtained from the subtraction of two almost co-linear vectors. For this reason, only G' values were plotted at the high frequencies, whereas the G" values at frequencies above 1600 c/s were discarded.

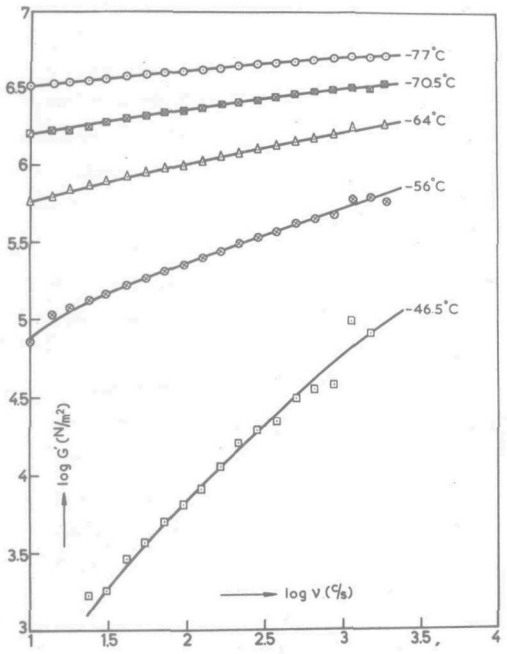

Fig. 5-7. Storage modulus of a PMA solution in Toluene.

These curves, obtained at different temperatures, must be converted into two master curves at a reference temperature T_o, before the relaxation spectrum could be obtained. This was done by shifting the curves horizontally until they formed two continuous curves G' and G". The amount each curve was shifted was log a_T . Since the same log a_T should apply to both the G' and G" curves, an average log a_T was taken.

It was assumed that the WLF equation[6]

$$\log a_T = - c_1(T - T_o)/(c_2 + T - T_o) \qquad (5\text{-}4)$$

applied for this polymer system. The constants c_1 and c_2 were obtained by plotting $(T_o - T)$ log a_T against T taking T_o as -46.5°C, and were found to be c_1 = 26.7 and c_2 = 133.6.

It must be noted that these values, in Equation 5-4, represent an unusually strong temperature dependence of the modulus. It was therefore not possible to use the modified WLF equation, in which a reference temperature T_s is assumed, where T_s is about 50 degrees above the glass transition temperature.

The values of c_1 and c_2 obtained from the plot were substituted in Equation (5-4) which permitted calculation of the

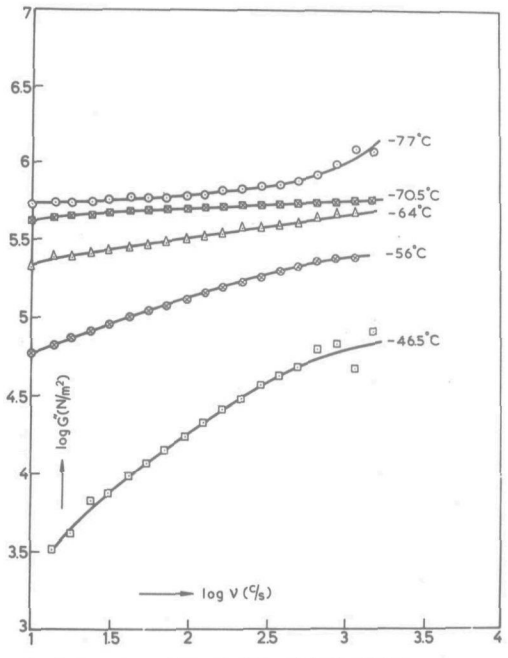

Fig. 5-8. Loss modulus of a PMA solution in Toluene.

log a_T values at the temperatures of the measurements. By plotting log G' and log G" vs. log(ωa_T), the master curves at the reference temperature of -46.5°C were obtained. These are shown in Figure 5-9. The loss tangent at -46.5° obtained from these curves is shown in Figure 5-10.

There are several approximation methods described in the literature[4] for calculating the relaxation spectrum from the components of the complex modulus. The method of

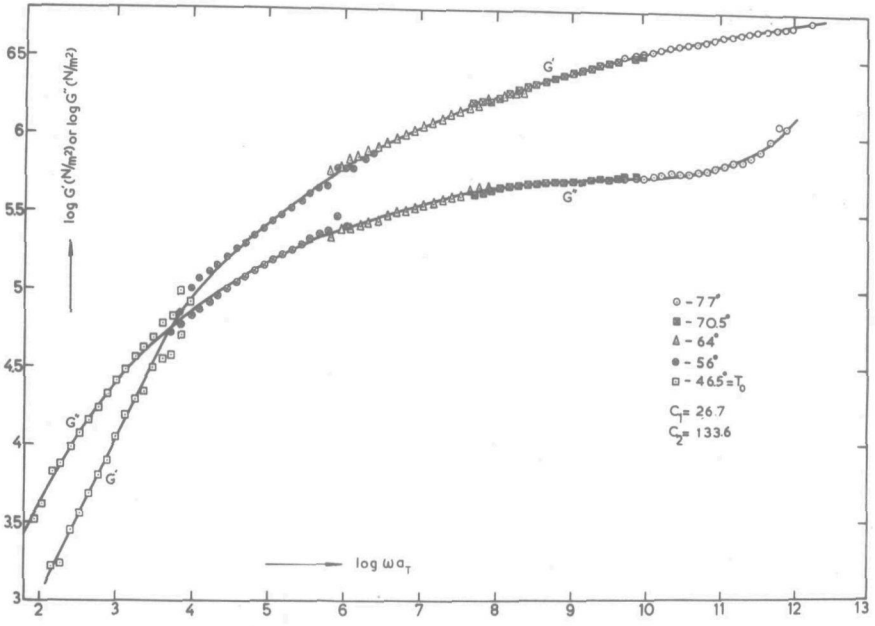

Fig. 5-9. Master curves of the storage modulus and loss modulus of a PMA solution (25.5%) in Toluene. Reference temperature T_0=-46.5°C

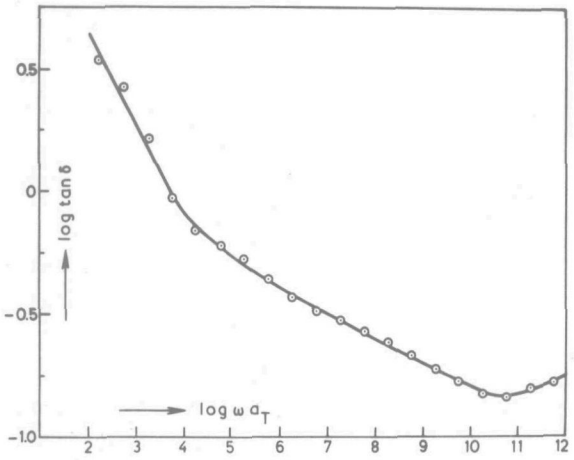

Fig. 5-10. Loss tangent for a PMA solution (25.5%) in Toluene. Reference temperature $T_0 = -46.5°C$.

Ninomyia and Ferry[7] was arbitrarily chosen. With this method, the slopes of the master curves are not measured directly, but are calculated from values of the ordinates in the vicinity of the point considered using the formulae

$$H(\tau) = \frac{G'(a\omega) - G'(\omega/a)}{2 \ln a} - \frac{a^2}{(a^2-1)^2} \cdot \frac{G'(a^2\omega) - G'(\omega/a^2) - 2\,G'(a\omega) + 2\,G'(\omega/a)}{2 \ln a}\Bigg|_{\tau=1/\omega} \qquad (5\text{-}5)$$

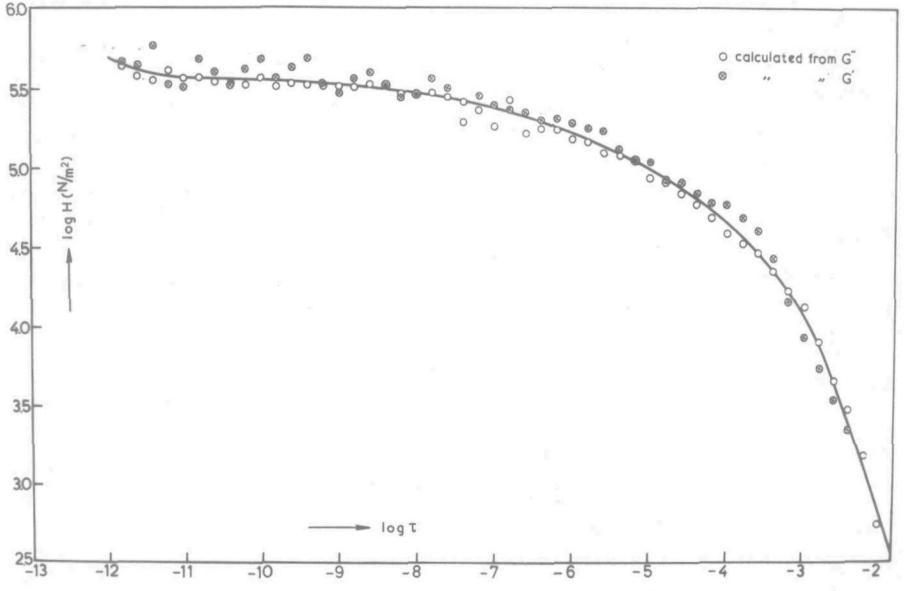

Fig. 5-11. Relaxation spectrum of a PMA solution (25.5%) in Toluene, Reference temperature $T_0 = -46.5°C$

$$H(\tau) = \frac{2\,G''(\omega)}{\pi} - \frac{2a}{\pi(a-1)^2}\left[G''(a\omega) + G''(\omega/a) - 2\,G''(\omega)\right]\Bigg|_{\tau=1/\omega} \qquad (5\text{-}6)$$

The spectra obtained from G' and G" should be identical. Points from both obtained with log a = 0.2 are plotted together in Figure 5-11, where the agreement appears reasonable.

5-5 Conclusions from the results for PMA

In general, the results of the measurements indicated that the rheometer worked very well. The compensator ceramic eliminated not only unwanted signals from the disturbing modes but also the need to account for the effect of the Teflon foil. This reduced the number of calculations required.

The calibration curves with the empty rheometer were not only very accurate, but since they provided an absolute means of calibration, avoided the use of standard viscosity samples. Moreover, the sensitivity of the pick-up was practically independent of temperature in the range in which it was used.

The only disadvantage of the design, as indicated in section 5-4, is the inaccuracy in the measurement of G" at high frequencies. The temperature control of the rheometer appears satisfactory, although the time required for reaching temperature equilibrium (about 2 hours) occupies the greater portion of the measuring time.

The results, however, indicated that the polymer exhibited unexpected mechanical behavior. It has already been mentioned that the sensitivity of the moduli to temperature was unusually high. This resulted in master curves which were spread over more than ten decades for only the rubbery and flow regions (Figure 5-9).

It was also found that the moduli in the rubbery region were about 100 times higher than was to be expected from similar experiments found in the literature[4], while the minimum value of the loss tangent was not as low as would be expected for a diluted rubber. Moduli of the magnitude found have not been previously reported for the rubbery regions of amorphous, uncrosslinked polymers, but rather approach the level of the rubbery region for filled or crystalline polymers.

As a result of these high moduli, the relaxation spectrum also has an unusually high plateau region without the expected

minimum. This high plateau region and the high value of G' in the rubbery region would indicate an impossibly short chain length between neighbouring temporary crosslinks. For this reason, the theory of Chapter 2 is not applicable.

In order to explain the anomalous behavior, a mechanism was required which would account for both the high moduli and their strong temperature dependence. Dipole-dipole forces between the chains were considered but these alone cannot be responsible for the phenomenon, since it is not observed in the undiluted polymer. Crystallization was rejected, since it could not explain the strong temperature dependence. It was finally found that the polymer solution became cloudy when cooled below $-25^{\circ}C$. This could only be attributed to phase separation, which on account of the high viscosity and the high concentration of the polymer, would occur on a microscopic scale. The extent of the phase separation would progress as the temperature was lowered producing more regions of higher polymer concentration. These must have a much higher modulus and may even tend to the glassy state. The formation of these regions thus gives rise to a spurious temperature dependence. The stiffening of the polymer by this process can be compared to the stiffening of a rubbery polymer by crystallization.

References (Chapter 5)

1) S.N. Chinai, A.L. Resnick & H.T. Lee; J.Polymer Sci. 33, 471 (1958).

2) W. Dannhauser, W.C. Child Jr. & J.D. Ferry; J.Colloid Sci. 13, 103 (1958).

3) J.W. Berge, P.R. Saunders & J.D. Ferry; J.Colloid Sci. 14, 135 (1959).

4) J.D. Ferry; Viscoelastic properties of polymers, John Wiley & Sons Inc., N.Y. (1961) pp. 63 ff. 75, 76, 197, 258, 289, 377, 457.

5) E.W. Dijkstra; A primer of Algol 60 programming, Academic Press, London (1962).

6) M.L. Williams, R.F. Landel & J.D. Ferry; J.Am.Chem.Soc. 77, 3701 (1955).

7) K. Ninomiya and J.D. Ferry; J.Colloid Sci. 14, 36 (1959).

SUMMARY

The linear viscoelastic behavior of polymers is reviewed, with particular attention to dynamic experiments in shear deformation.

A molecular theory is developed to describe quantitatively the mechanical behavior of entanglement networks of linear, randomly coiling molecules. The theory is based on the model of Rouse for a single molecule and is an extension of the theory of Duiser and Staverman for chemically crosslinked networks. The extensive calculations required for application of the theory make the use of a computer necessary. A computer program has been devised, which, using a property of the Sturm sequence, calculates the continuous relaxation spectrum from the "mobility coefficient matrix" of a molecule containing a number of "slow points", caused by the entanglements.

Application of the theory to experimental data will yield the number of elastically effective network chains of the entanglement network by integration of the area under the curve in the long-time region of the relaxation spectrum. This, in turn, yields the degree of polymerization between entanglement points, which is found to be almost independent of the accuracy with which the molecular weight of the sample is determined. The theory cannot yet account, however, for the dependence on molecular weight of the rheological properties.

A new molecular parameter δ, the "slip parameter", is introduced, which is a constant for a given sample, since its value is not dependent on the chosen length of a submolecule. As δ tends to zero the formulae reduce to those of the theory of Duiser & Staverman for chemically crosslinked networks.

The above theory has been successfully applied to the data for a poly-n-octyl methacrylate fraction published by Ferry and co-workers. A very good fit has been achieved between experimental

and theoretical relaxation spectra. It has been found both necessary and possible to take a molecular weight distribution quantitatively into account. This is a significant difference from previous treatments which considered only monodisperse samples.

Since the theory can best be checked with a monodisperse polymer sample, an attempt has been made to prepare a Poisson-distribution sample of poly-methyl acrylate by the Szwarc "living polymer" technique. This can be achieved by using tertiary-butyl acrylate as the monomer and by polymerization at very low temperatures, followed by alcoholysis to convert the tertiary-butyl ester groups into methyl ester groups. An apparatus has been constructed in which batch polymerization was carried out using di-methyl ether as a solvent. The initiator used was cumyl-potassium and the reaction was conducted at $-120^{\circ}C$. Although a 100 per cent conversion was obtained, indicating no unwanted termination, the resulting polymer had an unsatisfactory molecular weight distribution. The reason probably lies in an insufficiently refined polymerization technique, rather than in failure of the principle. An efficient procedure has been developed to convert the poly-t-butyl acrylate into poly-methyl acrylate by using hydrochloric acid as catalyst and a mixture of methylene chloride and methanol as a solvent. The yield was almost quantitative.

In order to investigate experimentally the linear viscoelastic behavior of polymers, a Pochettino-type rheometer has been made which is suitable for solutions or diluted networks. It directly measures sinusoidally varying stress and strain together with the phase angle between them. The design makes use of the piezoelectric properties of titanate ceramics for both the "driver" and the "pick-up". Thanks to these, the rheometer is rather compact, and temperature control is greatly simplified. The sample is located in a narrow gap (0.3 mm) between two coaxial cylinders. The very small displacements (0.1 microns) are measured with a high-resolution inductive displacement transducer. An important feature of the design is a "compensator" ceramic, between the driver and the pick-up, which eliminates secondary modes of motion generated by the driver. The rheometer is calibrated by an absolute method

which avoids the use of standard viscosity samples. The instrument can measure moduli from 500 to 6 x 10^7 N/m^2. The frequency range - not yet fully exploited - is from 10 to 3500 c/s. The temperature limits are not yet known, but measurements have been made between -80°C and + 30°C.

With the above rheometer, the relaxation spectrum of a 25.5 per cent solution of poly-methyl acrylate in toluene was obtained. Values of the components of the dynamic modulus obtained at several temperatures were reduced to master curves at -46.5°C by means of the WLF equation. From these, the relaxation spectrum was calculated using the approximation method of Ninomiya and Ferry. The observed behavior differed considerably from the expected pattern. The temperature dependence of the moduli was greater than any value previously reported. The moduli in the rubbery region were also anomalously high. The cause has been traced to phase separation in the sample. This hardening effect due to phase separation appears not to have been previously reported in the literature. The effect can be explained qualitatively by comparison with the stiffening effect of crystallization in a rubbery polymer.

LIST OF SYMBOLS

a	root mean square (or R.M.S.) end-to-end distance per square root of number of monomer units, or an interval on the logarithmic frequency scale
a_1	number of eigenvalues larger than λ_1
a_T	ratio of relaxation times at two different temperatures
a_{ij}	element in the i-th row and in the j-th column of a matrix
b	sample coefficient or form factor
b_i, b_i'	elements in a tridiagonal matrix
c	concentration (g polymer per cm^3 solution)
c_1, c_2	coefficients in the WLF equation referred to To as reference
c_i	elements in the main diagonal of a tridiagonal matrix
d	piezoelectric coefficient (charge output coefficient)
e	base of natural logarithms
f	chain parameter relating s_i to n_i, or driving force in the piston
f_r	shearing force at radius r
f^*	complex driving force to shear a sample
f_t^*	total complex driving force in the piston
g	piezoelectric coefficient (voltage output coeffcient), or chain parameter relating s_i to n_i
h	height of a sample
i, j	imaginary unit ($\sqrt{-1}$)
k	Boltzmann's constant, or spring constant of the "Teflon" foil
l	thickness of a ceramic
m	number of sections of a molecule separated by slow points or entanglements, or mass of a sample
m_e	effective mass
n	number of molecules per unit volume, or index of refraction
n_i	number of molecules in the unperturbed state, or number of molecules with molecular weight M_i
p	summation index

q	number of monomer units per submolecule
r	radius from the center of the piston
r_o	radius of the piston
$\langle r_o^2 \rangle^{\frac{1}{2}}$	R.M.S. end-to-end distance of a macromolecule (unperturbed)
$\langle r_s^2 \rangle^{\frac{1}{2}}$	R.M.S. end-to-end distance of a submolecule
s	running time variable
s_i	number of molecules in the perturbed state
t	time
u_p, v_p, w_p	transformed coordinates of a submolecule
$\dot{\underline{u}}_L, \dot{\underline{v}}_L, \dot{\underline{w}}_L$	components of the velocity gradient of a liquid
$\bar{v}$	partial specific volume of a polymer
x	distance to the center of rotation, or shear displacement, or linear displacement
x_o	shear displacement amplitude
x^*	complex shear displacement
x_j, y_j, z_j	coordinates of a submolecule
z	complex quantity ($p + i\,Q$)
A	cross sectional area
$\underline{A}_{ii}, \underline{A}_c, \underline{A}_e$	mobility coefficient matrix
B	translational mobility coefficient of a submolecule
B_n	numerical constant at the resonance frequency
C	number of crosslinks, or capicity, or conversion factor of the pick-up
C_e	number of effective crosslinks
D	conversion factor to reduce the experimental relaxation time to τ_R, or dielectric displacement
E	tensile modulus
E_c	tensile modulus of ceramic
E_i	tensile modulus of invar
F	linear relaxation spectrum (shear), or electric field
G^*	complex dynamic shear modulus
G'	shear storage modulus
G''	shear loss modulus

G_e	equilibrium shear modulus
G_i	spring constant in the i-th Maxwell element
G_g	glasslike shear modulus
$G(t)$	shear relaxation modulus
H	logarithmic relaxation spectrum (shear)
H_{ii}	sub-determinant in the Sturm sequence
H_R	relaxation spectrum reduced to one molecule
$H_{ent}(M_i)$	relaxation spectrum of one molecule in an entanglement network with molecular weight M_i
$\langle H_{Mn} \rangle$	relaxation spectrum of one molecule in a polydisperse entanglement network
$H(2^k N)$	relaxation spectrum of a chain with $2^k N$ submolecules between fixed ends
$H[(m-1)/2^k]$	relaxation spectrum of a molecule with free ends and containing $(m-1)/2^k$ slow points
$\underline{I}$	unit matrix
K	proportionality constant in Staudinger's equation
L	total length of the vibrating column
L_i	length of the invar piston
M_o	molecular weight per monomer unit
M_x	molecular weight of a molecule with a degree of polymerization x
$\bar{M}_n$	number average molecular weight
$\bar{M}_v$	viscosity average molecular weight
$\bar{M}_w$	weight average molecular weight
$[M_j.]$	concentration of growing radical molecules with weight M_j
N	number of submolecules in a macromolecule
N_o	Avogadro's number
P	rate of input of free energy per unit volume, or dielectric polarization
P_1	rate of input of free energy per molecule in $d\phi_i$
R	gas constant, or outer radius of Pochettino rheometer
$\underline{R}$	orthogonal matrix
Re	real part of a complex quantity
S	elastic compliance
T	absolute temperature
T_o	reference temperature

V	volume
$\underline{V}_L$	velocity gradient of a liquid
$X(M_i)$	mole fraction of molecules with weight M_i
Z	degree of polymerization, or electrical impedance
$\overline{Z}_e$	average degree of polymerization between entanglement points
$\overline{Z}_n$	number average degree of polymerization
α	constant in the relaxation function, or kinetic parameter in radical polymerization
β	constant in the relaxation function, or parameter in the Gaussian distribution function
γ	shear strain, or $\overline{Z}_n - 1$
$\dot{\gamma}$	rate of shear strain, or velocity gradient
γ^*	complex dynamic shear strain
γ_o	shear strain amplitude
$\dot{\gamma}_o$	velocity gradient amplitude
δ	slip parameter, or phase angle between sample strain and stress
δ_m	sample constant at the meniscus of a solution
δ_{pq}	Kronecker delta
ε	total dielectric constant
ε_o	dielectric constant in vacuum
ε_r	relative dielectric constant
ζ_o	monomeric friction coefficient
η^*	complex dynamic shear viscosity
η'	real part of complex viscosity
η''	imaginary part of complex viscosity
η_e	steady flow viscosity
η_i	viscosity of the dashpot in the i-th Maxwell element
η_s	viscosity of a solvent
η_{sp}	specific viscosity
$[\eta]$	intrinsic viscosity
$\eta(t)$	time dependent shear viscosity
$\varkappa$	electric susceptibility
λ	wave length, or eigenvalue

λ_1 highest eigenvalue (+4)
λ_a longitudinal wave length (axial direction)
λ_p p-th eigenvalue
λ_r shear wave length (radial direction)
μ chemical potential
ν number of molecules, or
number of network chains, or
frequency (cycles per second)
ν_a frequency in axial direction
ν_e number of effective network chains
ν_o cantilever resonance frequency
ν_r shear wave frequency in radial direction
π osmotic pressure
ρ density of a sample or of a solution, or
density of points in configuration space
ρ_i density of invar
ρ_o equilibrium density of points in configuration space
σ shear stress
σ_r shear stress at radius r
σ^* complex dynamic shear stress
σ_o shear stress amplitude
τ relaxation time
τ_i relaxation time of a Maxwell element
τ_R dimensionless reduced relaxation time ($1/\lambda$)
φ time derivative of the relaxation function, or
measured phase angle
ω angular velocity (radians per second)
Δ differencing symbol
Λ coefficient of linear expansion
$\underline{\Lambda}$ diagonal matrix (of eigenvalues)
Φ relaxation function
Ψ probability density function of configurations
Δl change in thickness of a ceramic
Δr width of a sample in the rheometer
ΔF elastic free energy change in volume V
ΔV voltage across the electrodes of a ceramic
$d\emptyset_i$ 3N-dimensional volume element

APPENDIX

```
==a2,
'begin' 'comment' relaxation spectrum, m, n, delta;
        'integer' m, i, a1, a2, m1, n, l, k, q, m2;
        'real' gu, lambda, y, q1, p1, norm, delta, t,
        dt, t2, gamma, r;
        read (m, n, gu, delta, gamma);
   'begin'  'integer' 'array' w[1:m];
            'array' p, c, b[1:n];

            'procedure' sturm  sequence;
      'begin'  p1:=o; q1:=1; a1:=o;
               'for' i:=1 'step' 1 'until' n 'do'
         'begin' y:= (c[i]-lambda)*q1-p[i]*p1;
                 p1:= q1; q1:=y;
                 'if' p1 'not less' o 'equiv' q1
                 'not less' o 'then' a1:= a1 + 1
         'end';
                 'if' q1 'equal' o 'and' p1 'greater' o 'then'
                 a1: = a1 - 1
      'end';
                 c[1]:= c[n]:= 3; k:= 1;
                 b[n]:= o; m2:= o;
                 read(w);
                 l:= 1; q:=w[1];
l1:              'for' i:= l 'step' 1 'until' q 'do'
                 c[i+1]:= 2;
                 'for' i:= l 'step' 1 'until' q + 1 'do'
                 b[i]:= -1;
                 'if' q 'not greater' n - 3 'then'
         'begin' c[q+2]:= c[q+3] := 1 + delta;
                 b[q+2]:= -delta
         'end';
```

```
==a6,
u=40,
r=10,
+73, +1879, +4, +0.0001, +10-12,
+23, +35, +16, +29, +14, +21, +11, +28, +19, +32,
+17, +27, +20, +33, +18, +21, +8, +19, +40, +22,
+48, +23, +24. +17, +52, +20, +16, +31, +13, +26,
+19, +37, +34, +23, +20, +3, +27, +44, +15, +21,
+31, +25, +28, +42, +18, +23, +25, +15, +36, +22,
+13, +24, +32, +17, +21, +6, +26, +24, +16, +20,
+30, +22, +12, +27, +25, +30, +22, +14, +26, +38,
+10, +18, +29;
```

```
                l:= q + 3; k:= k + 1;
                'if' k 'not greater' m 'then'
        'begin' q:= l + w[k]-1;
                'go to' l1
        'end';
                norm:= abs(c[1])+ abs(b[1]);
                'for' i:= 2 'step' 1 'until' n 'do'
        'begin' r:= abs(b[i-1]) + abs(c[i]) + abs(b[i]);
                'if' r 'greater' norm 'then' norm:= r
        'end';
                p[1]:= o;
                'for' i:= 1 'step' 1 'until' n-1 'do'
        'begin' 'if' b[i] 'equal' o 'then'
                p[i+1]:= gamma*norm*norm 'else'
                p[i+1]:= b[i]*b[i]
        'end';
l2:             lambda:= gu;
                sturm  sequence;
                a2:= a1;
                lambda:= gu-0.78*gu/1.78;
                sturm  sequence;
                m1:= a1 - a2;
                t:= ln(1/gu)/ln(10);
                dt:= ln(1/lambda)/ln(10);
                test(1/gu,1/lambda);
                print(''interval='', t,''till'', dt, ''h='',
                                                m1, ''s'');
                m2:= m2 + m1;
                'if' m2 'less' n 'then'
        'begin' gu:= lambda;
                'go to' l2
        'end'
  'end'
'end';
```

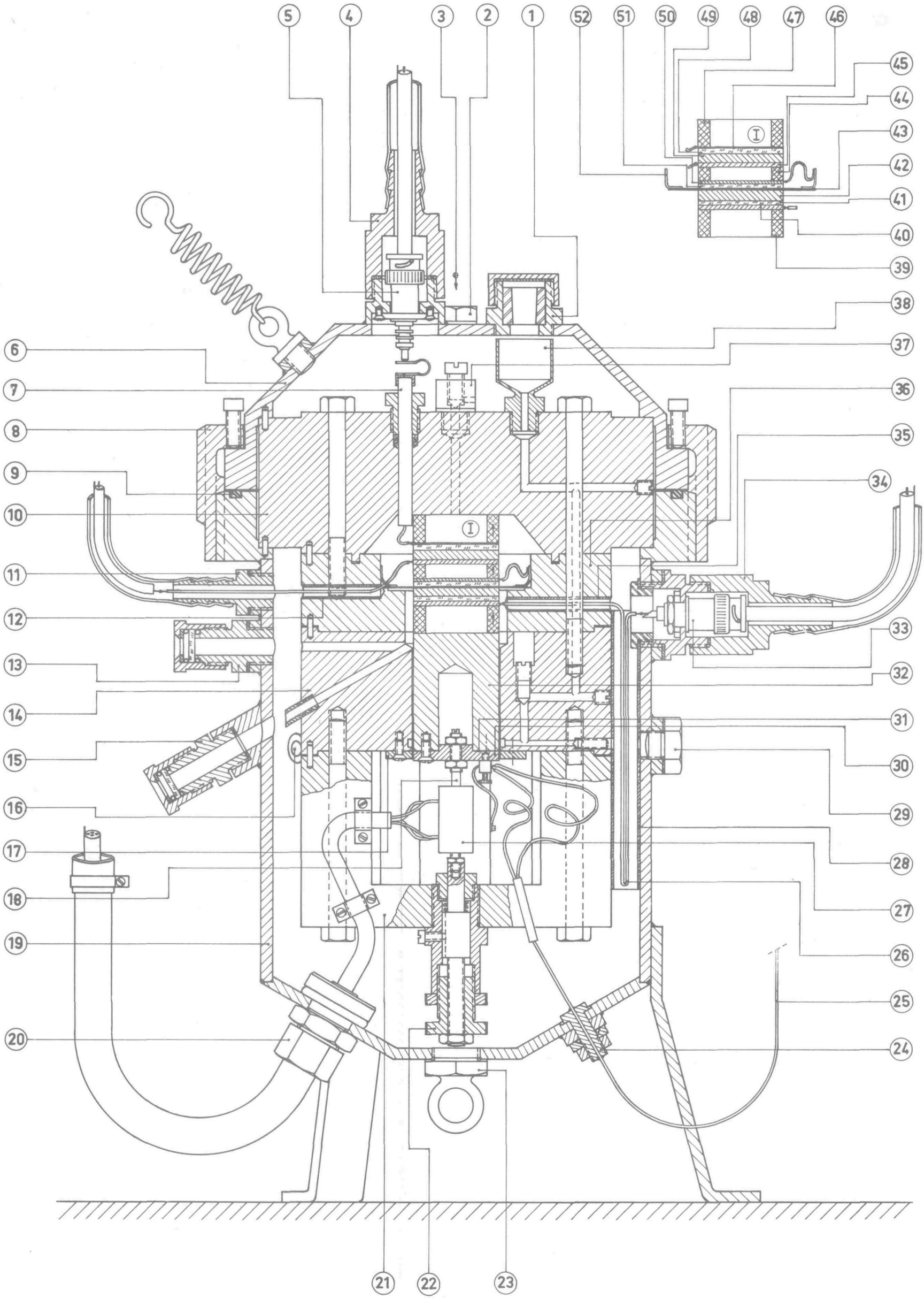
1
2
3
4
5
6
7
8
9
10
11
12
13
14
15
16
17
18
19
20
21
22
23
24
25
26
27
28
29
30
31
32
33
34
35
36
37
38
39
40
41
42
43
44
45
46
47
48
49
50
51
52
I
I

STELLINGEN

1. De relaxatiespectra die door Tobolsky worden weergegeven, suggereren een oplossend vermogen dat onmogelijk met de hedendaagse apparatuur te verwezenlijken is.

   A.V.Tobolsky ; Properties and Structure of Polymers, John Wiley Sons, Inc.(New York) 1960, p.316 .

   A.J.Staverman & F.Schwarzl ; Die Physik der Hochpolymeren, IV , ed.H.A.Stuart;Springer Verlag (Berlin)1956,p.46.

2. Hatfield en Rathmann hebben vergelijkingen opgesteld voor de adhesie van viscoelastische materialen aan een harde ondergrond. Met behulp van de door hen bepaalde molecule-parameters is de temperatuurafhankelijkheid van de critische onthechtingskracht te berekenen.De hiermee gevonden afhankelijkheid is dermate klein, dat de juistheid van bovengenoemde vergelijkingen betwijfeld moet worden.

   M.R.Hatfield & G.B.Rathmann; J.Phys.Chem.60, 957, (1956) .

3. Gedurende copolymerisatie van multicomponent-systemen verandert gewoonlijk de samenstelling van het zich vormende polymeer. Indien men de relatieve reactiviteitsverhoudingen en de gemiddelde snelheidsconstante van de polymerisatie kent, kan men een zodanige continue voeding van monomeren berekenen, dat bovengenoemde drift in de samenstelling volkomen wordt opgeheven.

   T.Alfrey Jr.,J.J.Bohrer & H.Mark; Copolymerization, Interscience Publ.Inc. (New York) 1952, p.156 .

4. De vergelijking die Bamford, Jenkins en Johnston hebben voorgesteld ter vervanging van de semi-empirische Q-e-relatie van Alfrey en Price, is niet in staat een betere voorspelling te geven van de relatieve radicaalreactiviteiten dan de eenvoudiger vergelijking van Alfrey en Price.

   C.H.Bamford, A.D.Jenkins & R.Johnston; Trans. Faraday Soc. 55, 418, (1959).

   T.Alfrey & C.C.Price; J.Polym.Sci. 2 , 101, (1947).

   J.C.Bevington ; Radical Polymerization ; Academic Press (London) 1961 , p. 86-89.

5. De opvatting van Kraus en Moczvgemba over de structuur van polymeernetwerken berust op een principiële vergissing.
G.Kraus & G.A.Moczvgemba ; J.Polym.Sci.A , 2 , 277 , (1964).

6. De voor geconcentreerde polymeeroplossingen uitgevoerde berekeningen van Kelley en Bueche, die gebaseerd zijn op de additiviteit van het vrije volume, kunnen beter vervangen worden door die van Fujita en Kishimoto.
F.N.Kelley & F.Bueche; J.Polym.Sci. 50 , 549 , (1961).
H.Fujita & A.Kishimoto; J.Polym.Sci. 28 , 547 , (1958)
en J.Chem.Phys. 34 , 393 , (1961).

7. De door Patton opgestelde empirische relatie voor alkydharsen ter berekening van de hardheid van een aan de lucht gedroogde vernisfilm, wekt ten onrechte de indruk, dat de veresteringsgraad niet van invloed is.
T.C.Patton ; Alkyd Resin Technology , Interscience Publishers (New York) 1962 , p. 179 .
R.Bult ; Offic.Dig.Federation Socs.Paint.Technol. 33, 1594(1961).

8. Het door Carmichael en Kinsinger voorgestelde model ter berekening van de ongestoorde dimensies van polymeren, waarbij aan alle mogelijke minima van de rotatiepotentiaal rond de ketenbindingen een gelijke potentiaal wordt toegekend, is weinig zinvol daar bovengenoemde veronderstelling tot grote fouten aanleiding geeft.
J.B.Carmichael J.B.Kinsinger; J.Polym.Sci.A , 1 , 2459 (1963).

9. Het centrum van een verstrengeling van ketens, zoals die zich manifesteert in het rheologisch gedrag van een macromoleculaire stof, kan men aanduiden met het woord "warpunt".